

Center for Integrative Physiology and Molecular Medicine
Theoretische Medizin und Biowissenschaften bzw. Klinische Medizin
der Medizinischen Fakultät
der Universität des Saarlandes, Homburg/Saar

**Murine optic nerve glial cell changes in the cuprizone
multiple sclerosis model and the impact of oligodendroglial
GABA_B receptor loss**

Dissertation

zur Erlangung des Grades eines Doktors der Medizin

**der Medizinischen Fakultät
der Universität des Saarlandes**

2023

Vorgelegt von: Alina Trumann
Geb. am: 31.12.1996 in Bremen

Betreuer: Prof. Dr. Frank Kirchhoff
Co-Betreuerin: Dr. Anja Scheller

Tag der Promotion: 05.11.2024

Dekan: Univ. -Prof. Dr. med. dent. Matthias Hannig

Berichterstatter: Prof. Dr. Frank Kirchhoff

Prof. Dr. Tobias Hartmann

Gewidmet meinem Vater

Table of Contents

Zusammenfassung	VI
Abstract	VIII
List of Figures	X
List of Tables	XII
Abbreviations	XIV
1. Introduction	1
1.1 Multiple Sclerosis.....	2
1.1.1 Epidemiology.....	2
1.1.2 Pathophysiology.....	2
1.1.3 Clinical Course	4
1.1.4 Optic Neuritis.....	7
1.1.5 Therapy and prognosis.....	8
1.2 Myelin and Oligodendrocytes	10
1.3 Cuprizone as a toxin-based Model of Demyelination	12
1.4 GABA _B Receptors	14
2. Materials and Methods	16
2.1 Materials.....	16
2.1.1 Chemicals	16
2.1.2 Consumables	17
2.1.3 Kits and Mixes.....	18
2.1.4 General Buffers and Solutions.....	18
2.1.5 Dyes and additional chemical substances	20
2.1.6 Primers for Genotyping	21
2.1.7 Antibodies	22
2.1.7.1 Primary Antibodies for Immunohistochemistry and Western blot	22
2.1.7.2 Secondary Antibodies for Immunohistochemistry	22
2.1.8 Mouse lines.....	23

2.1.8.1	TgH (NG2-Cre ^{ERT2}) NG2-Cre ^{ERT2} x TgH (Rosa26-CAG-lox/Stop/lox-GCaMP3) GCaMP3	23
2.1.8.2	TgH (GABA _B -floxed) GABA _B ^{fl/fl} x TgH (NG2-Cre ^{ERT2}) NG2-Cre ^{ERT2} x TgH (Rosa26-CAG-lox/Stop/lox-GCaMP3) GCaMP3	24
2.1.9	Animal maintenance.....	24
2.1.9.1	Ethics statement.....	24
2.1.9.2	Cuprizone food.....	24
2.1.9.3	Mice administration	25
2.1.9.4	Tamoxifen treatment.....	25
2.1.10	Software and Devices	25
2.2	Methods	27
2.2.1	Genotyping.....	27
2.2.1.1	Tail samples	27
2.2.1.2	DNA extraction	27
2.2.1.3	Polymerase chain reaction (PCR)	27
2.2.1.4	Agarose gel electrophoresis	28
2.2.2	Experimental design of tamoxifen and cuprizone treatment.....	28
2.2.3	Tissue sampling	30
2.2.4	Immunohistochemistry	31
2.2.4.1	Vibratome slices.....	31
2.2.4.2	Cryostat slices.....	31
2.2.4.3	Immunostainings	31
2.2.4.4	Zeiss Axioscan.Z1	32
2.2.4.5	Immunofluorescence measurements.....	33
2.2.5	Western blot analysis	33
2.2.6	Statistics.....	34
3.	Results	35
3.5	Optic nerve investigations of cuprizone induced myelin protein changes and astroglial activation during demyelination phase.....	35
3.5.1	Immunohistochemistry analyses revealed no changes in myelin proteins	36

3.5.2	Western blot analyses revealed high variability in myelin levels and astroglial activation.....	38
3.6	Immunohistochemical analyses investigating the effects of cuprizone treatment and GABA _B receptor loss on protein expression changes during the remyelination phase in the optic nerve.	42
3.6.1	Knockout mice revealed increased myelination	42
3.6.2	Immunohistochemistry revealed cuprizone treated mice with astroglial activation.....	46
3.7	Western blot analyses investigating the effects of cuprizone treatment and GABA _B receptor loss on protein expression changes during the remyelination phase in the optic nerve.....	50
3.8	Corpus callosum and other brain areas reveal astroglial and microglial activation two weeks after cuprizone treatment.....	53
4.	Discussion	61
4.5	Myelin gain after oligodendroglial GABA _B receptor loss and strong variability of myelin values after cuprizone powder food diet	62
4.6	Astrocyte and microglia activity after cuprizone treatment and loss of oligodendroglial GABA _B receptors	72
4.7	Corpus callosum and other brain areas reconfirming neuronal changes with astroglial and microglial activity	79
4.8	Further insights of the experimental design	82
4.8.1	Conditional inducibility of the GABA _B receptor knockout.....	82
4.8.2	Gender distribution	82
5.	Conclusion	84
	References	85
	Supplementary Figures.....	107
	Appendix.....	110
	Acknowledgements.....	119

Zusammenfassung

Multiple Sklerose (MS) ist eine chronische neuroinflammatorische und demyelinisierende Erkrankung des zentralen Nervensystems (ZNS), die häufig anfänglich den Sehnerv betrifft. Obwohl die Demyelinisierung bei MS Patienten seit Jahrzehnten bekannt ist, sind die molekularen Mechanismen, die letztendlich zum Absterben der Oligodendroglia und damit zum axonalen Myelinverlust führen, nach wie vor nicht abschließend geklärt. Bis heute basiert unser Verständnis der Ätiopathogenese hauptsächlich auf einem durch Tiermodellen erlangten Wissen. Dabei kann ein einzelnes Tiermodell nie das gesamte Spektrum klinischer Ausprägungen und pathologischer Merkmale der Erkrankung abdecken. Es erwiesen sich daher unterschiedliche Tiermodelle als äußerst wertvoll, um verschiedene Aspekte oder Targets der De- und Remyelinisierung zu untersuchen. Eines der am häufigsten angewandten Modelle ist dabei die Toxin-induzierte Demyelinisierung im Cuprizin Modell. Die orale Verabreichung von Cuprizin führt zur Apoptose von Oligodendrozyten und spiegelt dabei vor allem grundlegende Charakteristika des progressiven MS Verlaufs wider. Für dieser Arbeit wurde ein modifiziertes Cuprizin Modell entwickelt dessen Effizienz insbesondere im Hinblick auf Veränderungen des Sehnervs untersucht werden sollte.

Darüber hinaus lag der Fokus auf dem oligodendrogliale GABA_B-Rezeptor und der Frage, ob dessen Verlust beziehungsweise Knockout einen Einfluss auf die De- und Remyelinisierungsfähigkeit und die nachfolgende Interaktion von Gliazellen hat. Aktuelle Daten deuten bereits darauf hin, dass die oligodendroglialen GABA_B-Rezeptoren eine Rolle bei der Myelinmodifikation spielen könnten. Es wurde daher eine spezifische Mauslinie entwickelt, die diesen zellspezifische konditionalen GABA_B-Rezeptor-Knockout trägt. Diese Mauslinie wurde erzeugt durch die Kreuzung der GABA_B^{fl/fl}-Maus mit der NG2-CreERT2xGCaMP3-Treibermauslinie für Oligodendrozyten-Vorläuferzellen (OPCs).

Für diese Arbeit wurden zwei große Gruppen untersucht, wobei beide dem gleichen Cuprizin Protokoll unterzogen wurden. In der ersten Gruppe wurde der GABA_B Rezeptor knockout nicht induziert (*Non-induced_{clt}* Gruppe). Die Mäuse wurden unmittelbar nach der Cuprizin-Behandlung untersucht, und der Fokus lag allein auf dem Effekt der Cuprizin Behandlung. Die zweite Gruppe hingegen, mit induziertem GABA_B Rezeptor Knockout (*GABA_{knockout}* Gruppe), wurde erst zwei Wochen nach Beendigung der Cuprizin-Behandlung untersucht und sowohl auf die Cuprizin Effekte als auch auf die Auswirkungen des GABA_B Rezeptor Knockouts analysiert. Basierend auf aktuellen Studien wird angenommen, dass sich die *Non-induced_{clt}* Mäuse in der frühen Demyelinisierungsphase befinden, während die *GABA_{knockout}* Mäuse bereits in den frühen Stadien der Remyelinisierung sind.

In dieser Studie zeigten insbesondere die Astrozyten im Sehnerv zwei Wochen nach der Behandlung mit Cuprizon eine erhöhte Aktivität welches auf ein Geschehen auf Ebene der Gliazellen hindeutet. Der GABA_B-Rezeptor hingegen zeigte primär in der Abwesenheit von Cuprizon eine Myelin unterstützende Funktion.

Um die Ergebnisse am Sehnerv in einen größeren Kontext zu stellen, wurden in dieser Arbeit zusätzlich verschiedene Hirnregionen der Mäuse untersucht. Die bereits in vielen Studien nachgewiesenen Veränderungen im Gehirn durch Cuprizon sollen hier repräsentativ im Corpus callosum, Cortex, Striatum und Thalamus für unsere modifizierte Cuprizon Diät aufgezeigt werden.

Insgesamt unterstützen unsere Ergebnisse die bisherige Literatur und bestätigen, dass die modifizierte Cuprizon Diät ein bewehrtes Modell für die Auslösung von glialen Veränderungen darstellt. Weitere Untersuchungen des Cuprizon Modells am Sehnerv sind jedoch notwendig, um die molekularen Mechanismen zu untersuchen, die mit dem Verlust oligodendroglialer GABA_B-Rezeptoren während des Myelinisierungsprozesses verbunden sind.

Abstract

Multiple Sclerosis (MS) is a chronic neuroinflammatory and demyelinating disease of the central nervous system (CNS). The optic nerve is therefore often the first to show symptoms. Although demyelination in MS patients has been known for decades, the molecular mechanisms involved in oligodendroglial death and thus axonal demyelination remain unclear. Currently, the comprehension of the etiopathogenesis of MS is mainly based on insights gained via animal models. However, one animal model can never encompass the entire spectrum of clinical courses and pathological features of the disease. Therefore, various mouse models have proven highly valuable for investigating distinct aspects of de- and remyelination. One of the most commonly used animal models in MS research is the cuprizone model, which induces demyelination through toxin exposure. Oral administration of cuprizone results in oligodendrocyte apoptosis, which reflects the fundamental traits of the progressive course of MS. The objective of this study was to evaluate the effectiveness of a modified cuprizone model for the optic nerve.

Furthermore, focus was set on the oligodendroglial GABA_B receptor and whether its loss or rather knockout would affect myelination and the subsequent interaction of glial cells. Recent data suggest that the oligodendroglial GABA_B receptors may indeed play a role in myelin modification. To further investigate the influence of this receptor loss, a specific mouse line was established. The cell-specific conditional GABA_B receptor knockout mouse line was generated by crossing the GABA_B^{fl/fl} mouse with the NG2-CreERT2 x GCaMP3 driver mouse line for oligodendrocyte progenitor cells (OPCs).

Consequently, two major groups were studied for this work, both subjected to the same cuprizone protocol. In the first group, the GABA_B receptor knockout was not induced (*Non-induced_{ctrl}* group). The mice were examined immediately after the cuprizone treatment and therefore the focus was solely on the effect of the cuprizone treatment. The second group with an induced knockout (*GABA_B^{knockout}* group) was examined two weeks after the end of cuprizone treatment. Here, both cuprizone effect and the impact of GABA_B receptor knockout were analyzed. Based on recent studies, it is thought that the *Non-induced_{ctrl}* mice are in the early demyelination phase whereas the *GABA_B^{knockout}* mice are already in the early stages of remyelinating.

In this study, astrocytes in the optic nerve showed an increased activation two weeks after ending cuprizone treatment, suggesting an event at the glial level. The GABA_B receptor, on the other hand, showed a myelin-supporting function, particularly in the absence of cuprizone.

In order to put the results on the optic nerve in a broader context, this study additionally examined different regions of the mice's brains. The changes in the brain caused by cuprizone, have already been demonstrated in several studies. However, the effect of the modified cuprizone treatment were investigated in a representative manner in the corpus callosum, cortex, striatum and thalamus for the modified cuprizone diet.

Taken together, these results support previous literature and confirm that the modified cuprizone diet is a proven model for inducing glial changes. However, further studies of the cuprizone model in the optic nerve are needed to investigate the molecular mechanisms associated with the loss of oligodendroglial GABA_B receptors during the myelination process.

List of Figures

Figure 1.	Pathophysiology of the autoimmune pathway in MS.....	4
Figure 2.	Scheme courses of the four main subtypes of Multiple Sclerosis.....	6
Figure 3.	Optic neuritis via fundoscopy and MRI.....	8
Figure 4.	Schematic of the mechanisms by which cuprizone causes demyelination.....	12
Figure 5.	Schematic drawing of the GABAB receptor in OPCs.....	14
Figure 6.	Construct of the NG2-CreERT2xGCaMP3 mouse line.....	23
Figure 7.	Construct of the GABAB x NG2-CreERT2 x GCaMP3 mouse line.....	24
Figure 8.	Tamoxifen injection and cuprizone treatment protocol of GABABfl/fl x NG2-CreERT2 x GCaMP3 mice.....	29
Figure 9.	Schematic representation of optic nerve tissue.....	30
Figure 10.	No change of protein level in CPZ treated cohorts.....	37
Figure 11.	No change of protein level in CPZ-treated cohorts. CPZ-treated mice show high variability.....	40
Figure 12.	Comparison of MBP and dMBP expression level.....	43
Figure 13.	Increase of MBP expression level in knockout mice of cuprizone control cohorts.....	45
Figure 14.	Comparison of GFAP and Iba1 expression level. (A) Construct of GABABfl/fl x NG2-CreERT2 x GCaMP3 mice.....	47
Figure 15.	Increase of GFAP expression in genetic control mice after cuprizone treatment.....	49
Figure 16.	No change of protein level measurable in CPZ treated or knock-out cohorts.....	51
Figure 17.	Areas analyzed for de-myelination processes, corpus callosum (CC), cortex, striatum and thalamus.....	53
Figure 18.	No change in MBP levels. Tendencies of decreased myelin levels after CPZ treatment.....	55
Figure 19.	Significant increase of astroglial activity (GFAP) in knockout and genetic control mice after CPZ diet in areas of corpus callosum (CC), cortex and thalamus.....	57
Figure 20.	Increase of microglia (Iba1) activation in knockout and genetic control after CPZ diet in the corpus callosum (CC).....	59
Figure 21.	Unmyelinated optic nerve head (ONH) and myelinated optic nerve proper (ONP).....	73
Figure 22.	Optic nerve tubulin unedited Western blot gel documentary for GABA _{knockout}	107

Figure 23. Optic nerve MBP unedited Western blot gel documentary for GABA _{knockout}	107
Figure 24. Optic nerve GFAP unedited Western blot gel documentary for GABA _{knockout}	107
Figure 25. Optic nerve tubulin unedited Western blot gel documentary for Non-induced _{ctl} ...	108
Figure 26. Optic nerve MBP unedited Western blot gel documentary for Non-induced _{ctl}	108
Figure 27. Optic nerve GFAP unedited Western blot gel documentary for Non-induced _{ctl} ...	108
Figure 28. Nitrocellulose membrane showing Ponceau S staining.....	109

List of Tables

Table 1.	List of chemicals.....	16
Table 2.	List of consumables and their producers.....	17
Table 3.	List of kits.....	18
Table 4.	List of buffers and solutions with components.....	18
Table 5.	List of dyes and additional chemical substances.....	20
Table 6.	List of PCR primers used for genotyping.....	21
Table 7.	List of primary antibodies used for immunohistochemistry and Western blot.....	22
Table 8.	List of secondary antibodies used for immunohistochemistry.....	22
Table 9.	Utilized mouse lines and corresponding abbreviations.....	23
Table 10.	List of devices and their producers with the corresponding application.....	26
Table 11.	Descriptive statistical analyses for MBP fluorescence intensity in GABA _{knockout} group.....	110
Table 12.	Descriptive statistical analyses for dMBP fluorescence intensity in GABA _{knockout} group.....	110
Table 13.	Descriptive statistical analyses for GFAP fluorescence intensity in GABA _{knockout} group.....	111
Table 14.	Descriptive statistical analyses for Iba1 fluorescence intensity in GABA _{knockout} group.....	111
Table 15.	Descriptive statistical analyses for MBP Western blot analyses in GABA _{knockout} group.....	112
Table 16.	Descriptive statistical analyses for GFAP Western blot analyses in GABA _{knockout} group.....	112
Table 17.	Descriptive statistical analyses for MBP fluorescence intensity in Non-induced _{ctl} group.....	113
Table 18.	Descriptive statistical analyses for dMBP fluorescence intensity in Non-induced _{ctl} group.....	113
Table 19.	Descriptive statistical analyses for MBP Western blot analyses in Non-induced _{ctl} group.....	113
Table 20.	Descriptive statistical analyses for GFAP Western blot analyses in Non-induced _{ctl} group.....	114
Table 21.	Descriptive statistical analyses of the brain for MBP fluorescence intensity in GABA _{knockout} group.....	114
Table 22.	Descriptive statistical analyses of the brain for GFAP fluorescence intensity in GABA _{knockout} group.....	115

Table 23. Descriptive statistical analyses of the brain for Iba1 fluorescence intensity in GABA _{knockout} group.....	117
---	-----

Abbreviations

(v/v)	Percent by volume
(w/v)	Percent by mass
ATP	Adenosine triphosphate
BBB	Blood-brain barrier
Bp	Base pair
C3d	Complement component C3
CC1	Adenomatous polyposis coli clone 1
cKO	Conditional knockout
ctl	Control
cDNA	Complementary desoxyribonucleic acid
CIS	Clinically isolated syndrome
CNS	Central nervous system
CIPMM	Center for Integrative Physiology and Molecular Medicine
CPZ	Cuprizone; Bis(cyclohexanone)oxaldihydrazone
CSPG4	Chondroitin sulfate proteoglycan 4
DAPI	4',6-diamidino-2-phenylindole
DNA	Desoxyribonucleic acid
ddH ₂ O	Double distilled water
dMBP	Degraded myelin basic protein
DTT	Dithiothreitol
EAE	Experimental autoimmune encephalomyelitis
EBV	Epstein-Barr virus
EDSS	Expanded Disability Status Scale
f.c.	Final concentration
FI	Fluorescence Intensity
fl	Floxed
g-ratio	The ratio of the inner axonal diameter to the total outer diameter
GABA	Gamma-aminobutyric acid
GAD	Glutamic acid decarboxylase
GFAP	Glial fibrillary acid protein
GFP	Green fluorescent protein
HCl	Hydrochloric acid
HS	Horse serum
Iba1	Ionized calcium-binding adaptor molecule 1

IgG	Immunoglobulin G
IHC	Immunohistochemistry
IF	Immunofluorescence
kDa	Kilodalton
LED	Lighted-emitting diode
LPC	Lysophosphatidylcholine
LFB	Luxol Fast Blue
MAO	Monoamine oxidase
MBP	Myelin basic protein
MgCl ₂	Magnesium chloride
MOG	Myelin oligodendrocyte glycoprotein
mRNA	Messenger ribonucleic acid
MS	Multiple Sclerosis
NaCl	Sodium chloride
NaHCO ₃	Sodium hydrogen carbonate
NaOH	Sodium hydroxide
NG2	Neural/glial antigen 2
Olig2	Oligodendrocyte transcription factor 2
ONH	Optic nerve head
ONP	Optic nerve proper
OPC	Oligodendrocyte precursor cell
PBS	Phosphate buffered saline
PCR	Polymerase chain reaction
PDGFR α	Platelet-derived growth factor receptor alpha
PFA	Paraformaldehyde
PLP	Proteolipid protein
PPMS	Primary progressive Multiple Sclerosis
qRT-PCR	Qualitative real-time polymerase chain reaction
RNA	Ribonucleic acid
ROI	Region of interest
RRMS	Relapsing-remitting Multiple Sclerosis
RT	Room temperature
SD	Standard deviation
SDS	Sodium dodecyl sulfate
SEM	Standard error mean
SPMS	Secondary progressive Multiple Sclerosis

TAE	Tris-acetate-EDTA
TAM	Tamoxifen
TgH	Transgenic mouse generated by homologous recombination
Tris	Tris(hydroxymethyl)aminomethane
Tween® 20	Polyoxyethylene sorbitan monolaurate
UV	Ultraviolet
V	Volt
WB	Western blot
WPC	Weeks post cuprizone
WT	Wilde type
ZNS	Zentrales Nervensystem

1. Introduction

“Every five minutes, someone, somewhere in the world is diagnosed with MS.” (The Multiple Sclerosis International Federation, 2020)

Multiple sclerosis can present itself in many ways. One of the usual first signs may be heightened discomfort during eye movement, possibly accompanied by reduced visual clarity or acuity within a few days. These symptoms can be initially worrying, but they may not necessarily warrant concern besides getting examined by an ophthalmologist. If an inflammation or rather optic neuritis had been diagnosed, it would not be unlikely that an otherwise healthy young woman would have to be prepared for the possible development or diagnosis of MS. Based on current data, approximately 43% of individuals diagnosed with clinically isolated optic neuritis are considered to have a potential preliminary diagnosis of MS. It should be stressed, however, that many more criteria need to be met before a diagnosis can be made, and that indeed the clinical course can be quite variable. (Langer-Gould, 2014; The Multiple Sclerosis International Federation, 2020; Wilhelm & Schabet, 2015)

1.1 Multiple Sclerosis

1.1.1 Epidemiology

Encephalomyelitis disseminata, also known as Multiple Sclerosis (MS) is a chronic inflammatory disease of the central nervous system (CNS) (Noseworthy, 1999; World Health Organization, 2008). It is one of the most prevalent neurological diseases worldwide. At the current time, more than 2.8 million people are diagnosed with MS worldwide, with an ever-increasing prevalence (GBD, 2016; The Multiple Sclerosis International Federation, 2020). Looking at the latest epidemic studies, more than 280 000 people in Germany were affected in 2019, which implies a rising prevalence from 0.27 % (2012) to 0,34 % (2019) (Daltrozzo, Hapfelmeier, Donnachie, Schneider, & Hemmer, 2018; J. Holstiege et al., 2022). Worldwide, there are at least twice as many women affected by MS than men, in some regions (e.g. Western Pacific, Egypt) females have even three up to four times higher diagnosis rates. Even though, MS can occur in any age group, average age of diagnosis is 32 years (Browne et al., 2014; The Multiple Sclerosis International Federation, 2020). In Germany, there is a gradual increase in prevalence with a maximum between the ages of 45. and 54. Again, strong prevalence differences were found between men and women in all age groups, with the clearest relative differences occurring in the 20-24 age group (Jakob Holstiege, Steffen, Goffrier, & Bätzing, 2017).

1.1.2 Pathophysiology

The etiology of MS remains unknown. However, several genetic and environmental factors have been discussed. These include the pathology of specific antigens, in particular the Epstein-Barr virus (EBV), which induces a detectable autoreactivity (Agostini et al., 2018). Recent studies support the hypothesis that EBV is not only a risk factor but also a cause of MS. Showing that EBV antibody seroconversion in diagnosed patients was extremely high with 97 % compared to the control group where seroconversion was only detected in 57 % (Bjornevik et al., 2022).

At this point, two hypotheses for MS triggering pathophysiology are discussed which in short are both different mechanisms leading to the primary demyelination:

- Autoimmunity

Demyelination is evoked by an inflammatory auto-reaction where myelin-specific T-cells get focally primed and activated by myelin epitope-expressing cells those as macrophages and dendritic cells (Matute & Pérez-Cerdá, 2005; Nakahara, Aiso, & Suzuki, 2010).

This irritation activates and permeabilizes the blood-brain barrier (BBB) (Brown and Sawchenko, 2007), allowing additional T cells to enter the CNS and come into contact with activated endothelial cells and reactivate local antigen-presenting cells (Bartholomäus et al., 2009). Thus, myelin destruction, secondary loss of oligodendrocytes, and overall axonal damage occur directly through toxin-releasing T-cells or indirectly through induced toxins from activated macrophages and microglia (Ferguson et al., 1997; Trapp et al., 1998). Simultaneous remyelination processes counteract the inflammatory events (Buzzard et al., 2017).

- Oligodendroglipathy

Lucchinetti et al. already described oligodendrocyte apoptosis as a common feature in the early stages of MS (Lucchinetti et al., 2000). Exceeding this, studies show that oligodendroglial decline may even be the primary cause of the early structural change in newly formed MS lesions. The apoptosis is validated by an increased extracellular glutamate level (Goldberg & Ransom, 2003), oxygen radical released by viruses or virus-related products (Liu, Cai, & Zhang, 2003), or other reactive toxins (Matute & Pérez-Cerdá, 2005). In an affected area, the lesion is developing in three different time-dependent stages:

- I. Oligodendrocyte apoptosis (~ 17 hours) (Barnett & Prineas, 2004)
- II. Phagocytosis of the damaged oligodendrocytes by microglia, leading to myelin sheath destruction (~ 1-2 days)
- III. Phagocytosis of the damaged myelin by macrophages (Long-term modification)

However, after the oligodendrocyte apoptosis, an inflammatory response was seen, which could be explained by a microglial activation just as an infiltration with activated immune cells. (Matute & Pérez-Cerdá, 2005). Either way, both hypotheses include an inflammatory pathway as well as the decline of oligodendrocytes in the CNS.

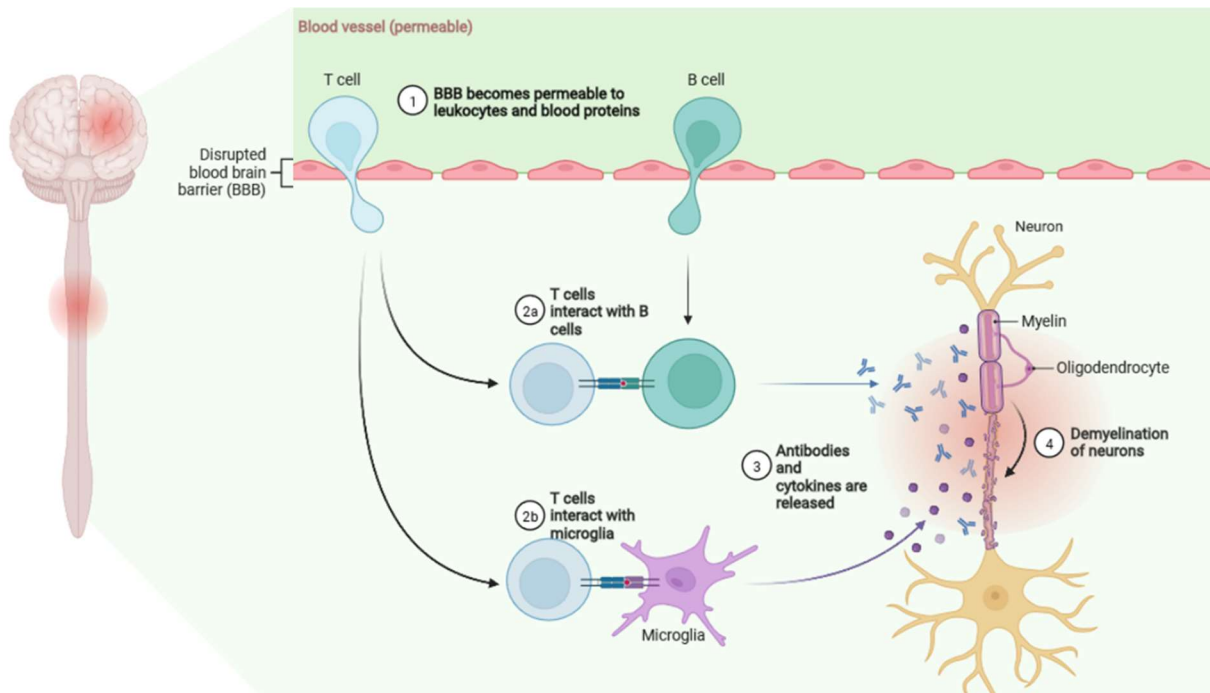


Figure 1. Pathophysiology of the autoimmune pathway in MS. MS as an autoimmune disease of the central nervous system, illustrates the inflammatory pathway. As MS progresses, it attacks myelin, the protective sheath of the axons, causing inflammation and general damage. Activated T-cells cross the BBB (1), followed by infiltration and recruitment of immune cells (2a), activation of microglia (2b), release of toxins and finally death of oligodendrocytes and clearance of damaged tissue (3). Modified from “Pathogenesis of MS”, by BioRender.com (2022). Retrieved from <https://app.biorender.com/biorender-templates>.

1.1.3 Clinical Course

On a short- or long-term basis, MS will lead to spreading focal areas of demyelination in white and grey matter effecting a global decline of neuronal tissue and concomitant neuronal cell death (Lassmann, Brück, & Lucchinetti, 2007).

Therefore, symptoms mostly start monosymptomatic and relapsing, which would be described as a relapsing-remitting MS accompanied by a clinically isolated syndrome. It is typical for the first outbreak and mostly occurs in the following:

- Optic neuritis with a following visual defect showing blurred, veil, or fog vision
- Motoric disorder which occurs in premature fatigue of the legs and as a gait disorder

- Sensory dysfunction with paraesthesia, which can manifest as the typical sensation of ants crawling across the skin.

These initial symptoms are often followed by a period of complete or partial resolution of the neurological deficits. The symptoms that develop during the clinical course are determined by the demyelination process and the associated slowed or absent axonal conduction in the CNS, with the location of the lesion determining the neurological symptoms. Multiple sclerosis therefore inevitably leads to physical and mental disability. Long-term affected regions and consequences can be seen (Faiss, 2011):

- Optic neuritis with pain during eye movement and several reductions of the eyesight
- Motoric disorders like central paresis causing spasticity
- Sensible symptomatic as paraesthesia, hypesthesia, or dysesthesia
- Disorder of the cranial nerves, in particular N. trigeminus and N. facialis
- Brain stem symptoms, often appearing in internuclear ophthalmoplegia
- Cerebellar symptoms like intentional tremors and dysarthria
- Ataxia
- Pain – Up to 50 % are suffering from some kind of acute or subacute pain, mostly concomitant of the previously named symptoms
- Vegetative dysfunction those as bladder, intestine, and especially sexual dysfunction
- Psychological and cognitive disorder with recurring cognitive and physical exhaustion (fatigue), depression, and memory disorder as well as intellectual restriction which affects up to 50 % of MS patients

These symptoms do not necessarily occur in waves or as an expression of a new relapse; endogenous or exogenous factors can also trigger a short-term appearance of symptoms (Faiss, 2011).

Generally, the clinical course is classified into three subtypes (it was first described as four stages in 1996 and later reduced to three) based on the frequency and duration of relapses and the lasting or reversible consequential damage, which was first established in 1996 by the US National MS Society (NMSS) Advisory Committee on Clinical Trials in MS (Fred D. Lublin & Reingold, 1996; F. D. Lublin et al., 2014):

- Relapsing-Remitting (RRMS)

At the time of diagnosis, the majority of the affected (85 %) showed an RRMS. Marked by the occurrence of neurological deficits in the context of relapses which are completely or incompletely receded and without any increase of disability and with that stable course in

between the attacks. In 2013 they added the terms of active versus not active and worsening versus stable.

- Primary Progressive (PPMS)

Constant worsening of the neurological conditions and increase in disability right from the beginning and without previous relapsing or remission phases. In 2013 they added the terms of active versus not active and progressing versus non progressing referring to an objective and evidenced change in a limited time period. The PPMS affects about 15 % of the patients.

- Secondary Progressive (SPMS)

Developed from RRMS, by a progressive increase in disability, with or without applied thrusts, after the previous relapsing-remitting course. Furthermore, supplemented by the terms active versus not active and progressing versus non-progressing. The SPMS mostly follows the RRMS after several years. There is no fixed definition of a progression period. However, at least six to twelve months of progression are usually required (Plantone, De Angelis, Doshi, & Chataway, 2016).

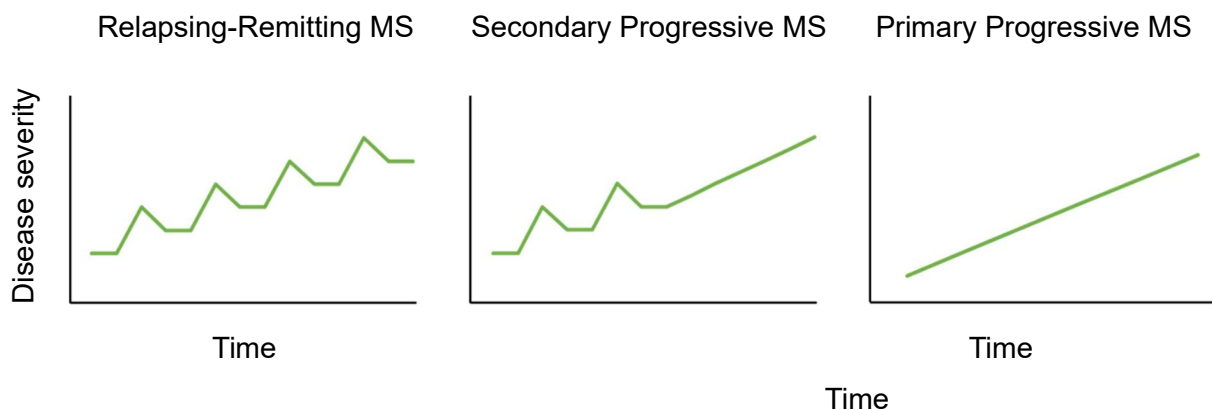


Figure 2. Scheme courses of the four main subtypes of Multiple Sclerosis. Relapsing-Remitting MS showing episodic peaks of symptoms followed by asymptomatic, stable phases without disease progression. Secondary Progressive MS showing initial relapsing remitting disease course turning into constant progression of symptoms. Primary progressive MS showing continuously worsening right from the beginning. (Adapted from (Chedrawe et al., 2018))

In 2014, Lublin et al. (F. D. Lublin et al., 2014) established another disease course, or rather precursor phenomenon which was introduced by the McDonald criteria:

- Clinical Isolated Syndrome (CIS)

Clinical Isolated syndrome (CIS) is presumed to be the first clinical manifestation of MS. It is characterized by an episode with a neurological deficit consistent with MS, but in which the diagnosis of MS cannot yet be made because the temporal dissemination criterion is not met (Hemmer, 2023; F. D. Lublin et al., 2014). 85 % out of patients with a manifest MS showed an acute or subacute episode of neurological symptoms attributed to focal white matter lesions, of which 21 % are presented with optic neuritis (D. Miller, Barkhof, Montalban, Thompson, & Filippi, 2005).

However, spatial dissemination of CNS lesions must be demonstrated for the diagnosis of CIS. Therefore, isolated optic neuritis or isolated myelitis is not CIS unless the criteria for spatial dissemination are met on MRI.

Now, the current 2017 version of the McDonald criteria (Thompson, Baranzini, Geurts, Hemmer, & Ciccarelli, 2018) makes it much easier to demonstrate temporal spread and thus diagnose RRMS earlier, with CIS as a diagnosis declining proportionately (Hemmer, 2023).

1.1.4 Optic Neuritis

As described above, optic neuritis does not only occur in the form of CIS but is also part of the long-term MS symptomatology. In terms of CIS, the conspicuity usually starts in one eye and becomes noticeable by slight pain during eye movement, such as reduced visual acuity and color vision (D. H. Miller, Chard, & Ciccarelli, 2012; D. H. Miller et al., 2008). From this point of view, the symptoms of MS will likely continue to appear during a CIS episode. Patients report a worsening of vision that usually develops in 1-2 days and subsides 3-4 weeks later. They suffer from blurred vision associated with darkened vision and sensitivity to light, as well as low contrast and blurred vision, leading in the worst case to complete amaurosis. Two-thirds report retrobulbar pain in the affected eye, especially during eye movement. The visual changes can sometimes be classified as Uthoff's phenomenon, a temporary deterioration attributed to increased body temperature.

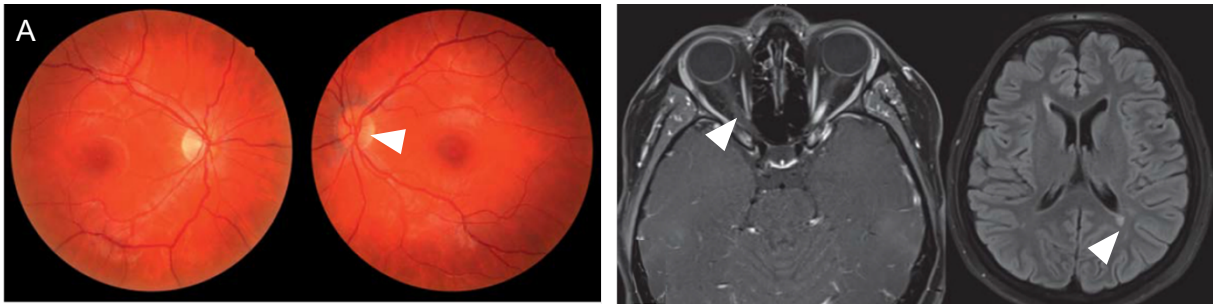


Figure 3. Optic neuritis via fundoscopy and MRI. 23-year-old female patient with optic neuritis and mild papilledema, marked with white arrow (A). Contrast-enhanced MRI of the same patient showing the inflammatory optic nerve and two periventricular areas of demyelination on T2-FLAIR MRI, marked with white arrows. Modified from Wilhelm and Schabet (Wilhelm & Schabet, 2015).

Other patients report nyctalopia, in which vision is better at dusk than in bright daylight, or the focused object is blurred by prolonged fixation, the so-called "fading out" phenomenon. Particularly in the early stages of optic neuritis, patients suffer from flashes triggered by eye movements ("movement phosphenes"). Observable symptoms depend on the area of inflammation in the visual system. An intraocular focus will cause papillitis with orbital and ocular pain accompanied by acute loss of visual acuity. Fundoscopy will show a swollen and hyperemic papilla similar to a congested papilla. In contrast to retrobulbar infestation, where there are no ophthalmologic findings, a typical central scotoma can be demonstrated by perimetry. An associated pupillary dysfunction can be detected by the pupillary escape phenomenon as well as by the swing-flashlight test (Faiss, 2011)

1.1.5 Therapy and prognosis

There is no curative therapy at this point. In questions of prognosis, there are still cohort studies from the 1980s in frequent use. Following those investigations, more than 50 % of the patients will reach a degree of disability (EDSS) of at least 6.0 after 15 years. (Confavreux, Aimard, & Devic, 1980; Weinshenker et al., 1989). However, more recent cohort studies from the last decade provide robust evidence that prognoses are getting much better lately (Tintoré et al. 2015; Bsteh et al. 2016; Cree et al. 2016). According to these studies, less than 10 % of all sufferers achieve an EDSS of 6.0 at 10 and 16 years, respectively (Chung et al. 2020). Similarly, age-adjusted MS-related mortality decreased in Germany between 1990 and 2016 (GBD, 2016). Part of this improved prognosis is due to advances in therapeutic options (Sorensen et al., 2020). In any case, supportive therapy works to delay

the course of the disease and keep the patient psychologically and physiologically mobile for as long as possible (Yamout & Alroughani, 2018). Within the therapeutic approach, the treatment is based on three therapeutic pillars (Faiss, 2011; Hart & Bainbridge, 2016; Hemmer, 2023):

- I. Treatment of exacerbations, primarily with high-dose corticosteroids
- II. Disease-modifying therapy to slow progression via immunomodulation
- III. Symptomatic therapy is designed to alleviate, not prevent, consequential damage

1.2 Myelin and Oligodendrocytes

Within the CNS myelin is formed by oligodendrocytes simultaneously wrapping several internodes of different axons. They are assigned to the central glial cells, which are ten times more common than neurons and indeed make up about 5-8 % of the total cell population in the CNS. Therefore, oligodendrocytes are largely presented in the white matter (Dawson, Polito, Levine, & Reynolds, 2003; Hartline & Colman, 2007; Horner et al., 2000; Lüllmann-Rauch & Asan).

While neurons were already well recorded, the appearance of oligodendrocytes seemed quite suspect and was first described in 1846 by the German pathologist Rudolf Virchow (Virchow, 1856) followed by Deiters (Deiters, 1865) and Golgi (Golgi, 1885) with further significant findings. Virchow first outlined his observations with the term “Nerven Kitt” (Engl.: Nerve glue) (Virchow, 1858), where oligodendrocytes were thought to only stick between the neurons and function as a sort of connection tissue. Decades later Pio del Rio-Hortega was able to differentiate neuroglia into microglia and four types of oligodendrocytes (Del Rio-Hortega, 1920, 1933; Kuhn, Gritti, Crooks, & Dombrowski, 2019; Somjen, 1988).

It is now known that they develop from progenitor cells called oligodendrocyte progenitor cells (OPCs), which are controlled and supported by the proteoglycan NG2 (CSPG4) as well as the platelet-derived growth factor receptor alpha (PDGFR α) (Bercury & Macklin, 2015). To fulfill their final task of myelination, OPCs enlarge as they migrate long distances to their final destination, where they differentiate into mature oligodendrocytes (Luyt et al., 2007). Finally, they form the myelin sheath with their expanded and modified plasma membrane. They form nodes of Ranvier by myelinating several internodes in a discontinuous manner. This discontinuous sheathing allows saltatory transmission of action potentials with conduction velocities up to 200 m/s (Hartline & Colman, 2007; Snaidero et al., 2014).

Myelination, and thus oligodendrocyte development, is regulated by extracellular and axon-dependent factors such as ATP, glutamate, adenosine, or γ -aminobutyric acid (GABA). This transmitter, in turn, often initiates multiple Ca²⁺-dependent intracellular signaling pathways. (Gautier et al., 2015; Ishibashi et al., 2006; Serrano-Regal et al., 2020; Soliven, 2001; Stevens, Porta, Haak, Gallo, & Fields, 2002). Equally important is the activity and communication between oligodendrocytes, which is greatly influenced by intercellular gap junctions. Gap junctions are therefore one of the prerequisites for the survival and development of myelin. (Menichella, Goodenough, Sirkowski, Scherer, & Paul, 2003; Odermatt et al., 2003; Orthmann-Murphy, Abrams, & Scherer, 2008; Rash, 2010). Another

way to improve myelin structure is through mental activity and learning processes (Baumann & Pham-Dinh, 2001; Fields, 2008) those as reading (Kraft, Mitchell, Languis, & Wheatley, 1980) or studying new vocabulary (Pujol et al., 2006). Opposite to developing myelin and myelination is, especially in the pathology of MS, the process of demyelination. Contrary to expectations demyelination is not per se attributed to a leak or exhaustion of OPCs, indeed repeated focal demyelination won't lead to destructed OPCs or reduced remyelination (Penderis, Shields, & Franklin, 2003; Wolswijk, 1998). In chronic diseases like MS, the impairment leads from the OPCs recruitment phase involving, proliferation, migration, and repopulation (Armstrong, Le, Frost, Borke, & Vana, 2002; Woodruff, Fruttiger, Richardson, & Franklin, 2004).

1.3 Cuprizone as a toxin-based Model of Demyelination

Cuprizone (bis(cyclohexanon)oxaldihydrazon) is a neurotoxic, selective and potent copper chelator. Its deleterious effects on the CNS of rodents were first discovered by William Carlton in 1966. Through scientific elaboration in the following decades, the cuprizone model became a straightforward and simple tool for studying various aspects of demyelination and remyelination (Skrupuletz, Gudi, Hackstette, & Stangel, 2011). When cuprizone is administered orally, the effect on cell metabolism is demonstrated by the death of oligodendrocytes, shortly followed by the activation of astrocytes and the initiation of an immune response from the CNS. However, microglia eventually lead to a reversible detectable demyelination process (Torkildsen, Brunborg, Myhr, & Bø, 2008).

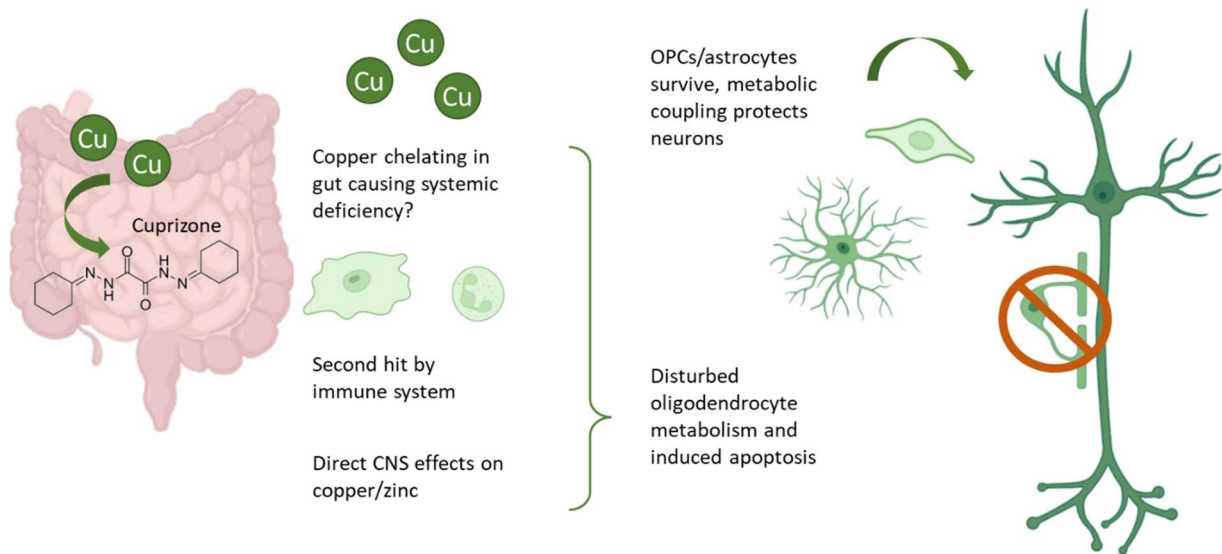


Figure 4. Schematic of the mechanisms by which cuprizone causes demyelination. Resorbed in the intestine, cuprizone is distributed in the plasma and thus in the CNS. In its chelating function, cuprizone disrupts the homeostasis of copper and other metals. Dietary cuprizone treatment leads to disturbances in cellular metabolism and selective apoptosis of oligodendroglial cells, which are particularly vulnerable due to their high metabolic turnover and low antioxidant levels. OPCs and astrocytes are largely spared. Modified by McMurrin (McMurrin, Zhao, & Franklin, 2019).

Looking at the cuprizone metabolism, copper acts as a major tool for several specific enzymes and other electron transport proteins. It is therefore involved in energetic and antioxidant metabolism, such as ceruloplasmin, cytochrome oxidase, or superoxide dismutase (Linder & Hazegh-Azam, 1996). As a result, cuprizone reduces cytochrome and monoamine oxidase (MAO) activity, leading to mitochondrial oxidative stress and the induction of a local immune response. Cuprizone treatment has specific effects on mature oligodendrocytes, where the metabolic machinery that supports myelin synthesis is impaired, resulting in oligodendroglial apoptosis. It is not known why cuprizone treatment only affects specific cell lines, where astrocytes remain largely unaffected compared to oligodendrocytes. Therefore, plausible hypotheses are based on the role of mitochondrial dysfunction and the metabolic need of oligodendrocytes, since higher doses of cuprizone lead to the formation of megamitochondria in the liver (Carlton, 1967; Matsushima & Morell, 2001).

The reduction in myelin-related mRNA expression is evident within the initial week of treatment. Spontaneous remyelination is observed as early as four days after discontinuation of treatment (Lindner et al., 2008; Praet, Guglielmetti, Berneman, Van der Linden, & Ponsaerts, 2014). Demyelination is most commonly seen in the corpus callosum, but also in various other areas such as the hippocampus, external capsule, cerebellar peduncles, and cerebral cortex (McMurran et al., 2019).

In the optic nerve, recent work has described a reduction in myelin sheath thickness (g-ratio) in mouse optic nerve tissue after three weeks of a cuprizone diet (Hainz et al., 2017). A similar observation was made after eight weeks of cuprizone treatment, showing a myelin loss of 20 % and further abnormalities in the myelin such as loosening and paranodal happenings (Bagchi et al., 2014).

1.4 GABA_B Receptors

GABA (γ -aminobutyric) is the major inhibitory neurotransmitter in the mammalian brain besides glycine in the CNS. Fulfilling regulation of neuronal transmission and therefore affecting numerous physiological and psychological processes GABA plays a key role throughout the CNS (Cherubini, Gaiarsa, & Ben-Ari, 1991; Lee, Lee, & Lee, 2019). When first described in 1950 GABA was shown as a major amino construct in the brain (Roberts & Frankel, 1950). Later, its physiological function became the focus of the investigation, initially GABAergic signaling on neurons and more recently its role in glial cells (Farrant & Nusser, 2005; Serrano-Regal et al., 2020).

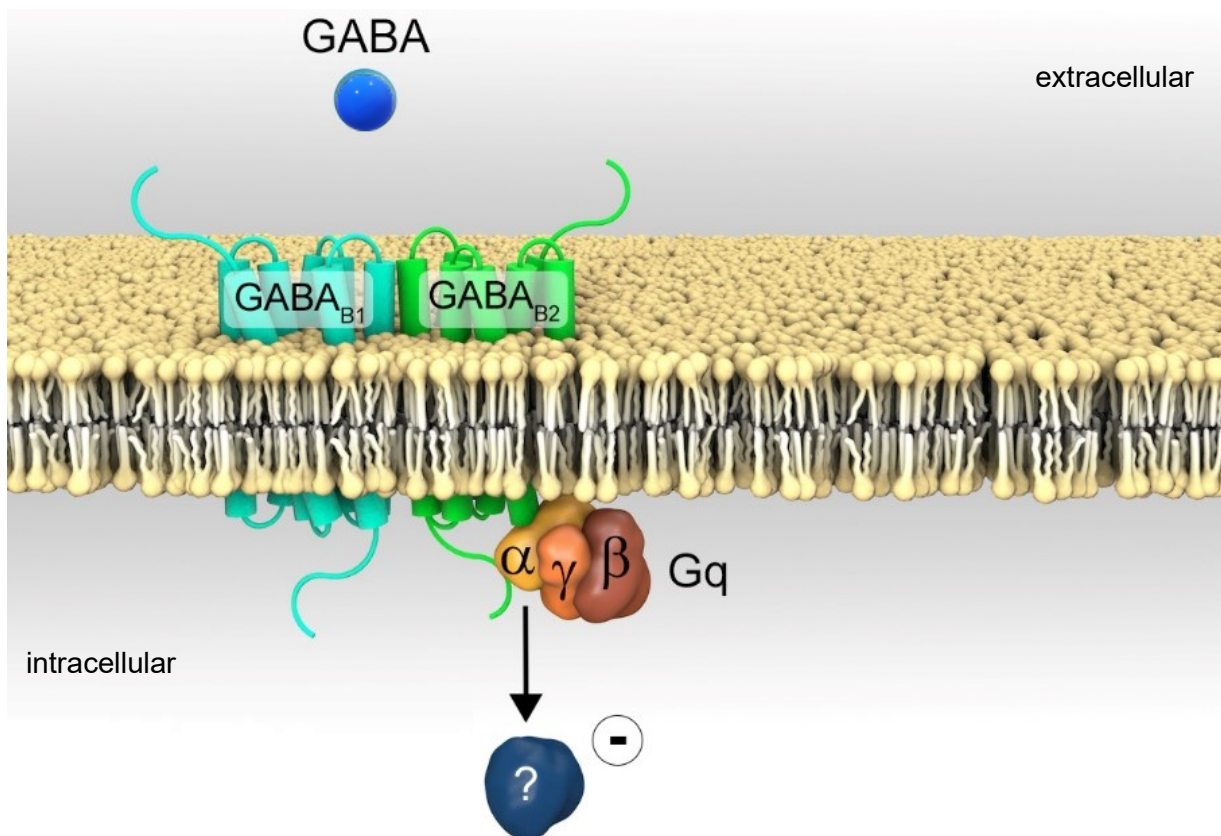


Figure 5. Schematic drawing of the GABA_B receptor in OPCs. Gamma-aminobutyric acid (GABA, green) is the agonist of the GABA_B receptor binding from Extracellular to the N-termini of the B1 subunit (torques) which is coupled to the B2 subunit (green) over C-termini (not shown). Both subunits consist of seven transmembrane domains. The G-protein is bound to the B2 subunit and dissociated and released through agonist binding into an α - (yellow) and $\beta\gamma$ -subunit (orange, brown). The downstream pathways (Gq or Gi/o) in OPCs are not yet clear. Modified from Bai, Kirchhoff and Scheller via BioRender.com (Bai, Kirchhoff, & Scheller, 2021).

Two pathways have been described for the synthesis of GABA. The classical pathway, in which GABA is synthesized from glutamate using glutamic acid decarboxylase (GAD) (Angulo, Le Meur, Kozlov, Charpak, & Audinat, 2008), faces a second pathway in which it can be synthesized under the action of MAO_B enzymes (Sequera, Gardino, Hedin-Pereira, & de Mello, 2007). Recent *in vitro* studies, showed the presence of GABA as well as GAD and MAO_B enzymes in OPCs and mature oligodendrocytes, suggesting a potential role in oligodendroglial development (Serrano-Regal et al., 2019).

Physiological GABA interacts with two types of receptors, GABA_A and GABA_B receptors. GABA_A receptor initiates an ionotropic response including a fast synaptic inhibition by Cl⁻ conductance. On the contrary, the GABA_B receptor is a metabotropic, G-protein-coupled receptor that utilizes several effector proteins: voltage-gated Ca²⁺ channels, G-protein-activated inwardly-rectifying K⁺ channels, and the adenylate cyclase system to generate slow inhibitory neurotransmission (Frangaj & Fan, 2018; Kaupmann et al., 1998). Each GABA_B receptor consists of two major isoforms, GABA_{B1} and GABA_{B2}, whereby each isoform consists of three subunits with a seven-helix transmembrane domain located between an extracellular located N-terminus and an intracellular located C-terminus (Pin & Bettler, 2016). Ultimately receptor agonists interact with the B1 subunit at the N-terminus whereby the B2 subunit ensures the correct B1 subunit cell surface targeting and throughout the G-protein coupling (Bettler, Kaupmann, Mosbacher, & Gassmann, 2004; Galvez et al., 2001).

The GABA_B receptor has not only been well documented in neuronal synapses but has also been found in oligodendrocytes (Bai et al., 2021; Hoppe & Kettenmann, 1989; Kirchhoff & Kettenmann, 1992; Williamson, Mellor, Grant, & Randall, 1998).

2. Materials and Methods

2.1 Materials

2.1.1 Chemicals

Table 1. List of chemicals

Acetic acid (100 %)	VWR International, Darmstadt, Germany
Agarose low melt	Greiner Bio One, Frickenhausen, Germany
Agarose powder	Serva Electrophoresis, Heidelberg, Germany
Dithiothreitol (DTT)	Sigma Aldrich, Taufkirchen, Germany
Ethanol (99 %)	VWR International, Darmstadt, Germany
Ethidium bromide (1 %)	Carl Roth, Karlsruhe, Germany
Ethylenediaminetetraacetate (EDTA)	Grüssing GmbH, Filsum, Germany
Glutaraldehyde (25 %)	Thermo Fisher Scientific, Dreieich, Germany
HCl	Bernd Kraft, Duisburg, Germany
Horse serum	Thermo Fisher Scientific, Dreieich, Germany
Immu-Mount mounting medium	Shandon, Pittsburgh, Pennsylvania
Ketamine (100 mg/ml)	Ketavet, Pfizer, Karlsruhe, Germany
Laemmli running buffer for SDS-PAGE	Serva Electrophoresis, Heidelberg, Germany
Laemmli sample buffer for SDS-PAGE (2x)	Serva Electrophoresis, Heidelberg, Germany
Methanol	VWR International, Darmstadt, Germany
MgCl ₂	Carl Roth, Karlsruhe, Germany
Natrium citrate dihydrate	B. Braun AG, Melsungen, Germany
NaCl	VWR International, Darmstadt, Germany
NaCl solution (0,9 %)	B. Braun AG, Melsungen, Germany
NaHCO ₃	Grüssing GmbH, Filsum, Germany
NaOH	Grüssing GmbH, Filsum, Germany
Paraformaldehyde	Sigma Aldrich, Taufkirchen, Germany

Phosphate buffered saline (PBS 10x)	neuFroxx GmbH, Einhausen, Germany
Protein inhibitor	Roche, Basel, Switzerland
ROTI®Seal	Carl Roth, Karlsruhe, Germany
SDS	Carl Roth, Karlsruhe, Germany
Sucrose	Sigma Aldrich, Taufkirchen, Germany
Transfer buffer	Thermo Fisher Scientific, Dreieich, Germany
Tris-HCl	Carl Roth, Karlsruhe, Germany
Tris(hydroxymethyl)aminomethane	Sigma Aldrich, Taufkirchen, Germany
Triton-X-100	AppliChem GmbH, Darmstadt, Germany
Tween® 20	AppliChem GmbH, Darmstadt, Germany
WesternFroxx washing buffer (10x)	BioFroxx GmbH, Einhausen, Germany
Xylazine (20 mg/ml)	Bayer, Leverkusen, Germany

2.1.2 Consumables

Table 2. List of consumables and their producers.

Coverslips	Menzelgläser, Braunschweig, Germany
Eppendorf® reaction tubes 0.5 ml, 1.5 ml, 2 ml and 5 ml	Sarstedt, Nümbrecht, Germany
Falcon tubes	Greiner Bio-One, Frickenhausen, Germany
Glass pipettes	VWR International, Darmstadt, Germany
Object slides	Karl Hecht, Sondheim, Germany
Optical clear cover foil	Sarstedt, Nümbrecht, Germany
Pipette tips	Sarstedt, Nümbrecht, Germany
Precellys ceramic kit	Peqlab, Erlangen, Germany
Single-use pipette 5 ml and 20 ml	Greiner Bio One, Frickenhausen, Germany
Syringe 0.5 ml	B. Braun AG, Melsungen, Germany
48-well cell culture plates	Sarstedt, Nümbrecht, Germany
96-well PCR plates	Brand, Wertheim, Germany

2.1.3 Kits and Mixes

Table 3. List of kits

2x DreamTaq™ Hot Start Green PCR Master Mix	Thermo Fisher Scientific, Dreieich, Germany
REExtract-N-Amp™ Tissue PCR Kit	Sigma-Aldrich, Taufkirchen, Germany
WesternBright™ Quantum	Advansta, Menlo Park, USA
WesternFroxx Kit pure	BioFroxx GmbH, Einhausen, Germany
Restore™ PLUS Western Blot Stripping- Puffer	Thermo Fisher Scientific, Dreieich, Germany

2.1.4 General Buffers and Solutions

Table 4. List of buffers and solutions with components.

All buffers were prepared with deionized and RNase-free H₂O from an ultrapure water system (GenPure, Thermo Fischer Scientific, Dreieich, Germany).

Anti-freezing solution

Sodium phosphate buffer (PB), 0.2 M	25	%	(v/v)
Sucrose	15	%	(v/v)
Ethylene glycol	35	%	(v/v)
ddH ₂ O	25	%	(v/v)

Phosphate buffered saline (PBS, 10x)

NaCl	1.37		M
KCl	27		mM
Na ₂ HPO ₄	100		mM
KH ₂ HPO ₄	18		mM

Phosphate buffered saline (PBS, 1x)

PBS (10x)	10	%	(v/v)
ddH ₂ O	90	%	(v/v)

Phosphate buffered saline Tween® 20 (PBST, 10x)

PBS (10x)	99.5	%	(v/v)
Tween 20	0,5	%	(v/v)

4 % PFA in PBS

Paraformaldehyde	4	%	(w/v)
NaOH*	10		M
HCl**	6		M

*added dropwise until PFA is dissolved

**added dropwise until pH \approx 7.4

2.5 % Glutaraldehyde in PBS

Glutaraldehyde (25%)	10	%	(v/v)
PBS (1x)	90	%	(v/v)

Ketamine/Xylazine in 0.9 % in NaCl

Ketamine (100 mg/ml)	14	%	(v/v)
Xylazine (20 mg/ml)	5	%	(v/v)
NaCl solution (0.9 %)	8		(v/v)

Tris acetate EDTA buffer (TAE, 50x)

Tris(hydroxymethyl)aminomethane	2		M
Acetic acid (100 %)	1		mM
Ethylenediaminetetraacetate (EDTA), 0.5 M, pH 8	1		mM

Agarose gel

Agarose powder in TAE buffer	1.5 or 2	%	(w/v)
Ethidium bromide (1 %)	0.00025	%	(v/v)

Blocking, primary and secondary antibody solution

Horse serum 5 % (v/v)	5	%	(v/v)
Triton X-100 0.3 % (v/v)	0.3	%	(v/v)
1x PBS	94.7	%	(v/v)

Secondary antibody solution

Horse serum	2	%	(v/v)
1x PBS	98	%	(v/v)

Western blot homogenization buffer

Sucrose (80 %)	13.7	%	(v/v)
Protein inhibitor	4	%	(v/v)
Tris-HCl, 1 M	1	%	(v/v)
NaHCO ₃ , 1 M	0.05	%	(v/v)
MgCl ₂ , 1 M	0.05	%	(v/v)
ddH ₂ O	81.2	%	(v/v)

Western blot sample buffer

Laemmli sample buffer (2x)	99	%	(v/v)
DTT	1	%	(v/v)

Western blot transfer buffer

Methanol	20	%	(v/v)
ddH ₂ O	70	%	(v/v)
Transfer buffer	10	%	(v/v)

Western blot stripping buffer

Acetic acid	6	%	(v/v)
ddH ₂ O	91.18	%	(v/v)
NaCl	2.82	%	(v/v)

2.1.5 Dyes and additional chemical substances**Table 5. List of dyes and additional chemical substances.****Dyes**

4',6-Diamidino-2'-phenylindole dihydrochloride (DAPI)	Sigma-Aldrich, Taufkirchen, Germany
Sudan Black B (SBB) Merck	Merck, Darmstadt, Germany
Ethidium bromide	Sigma-Aldrich, Taufkirchen, Germany

Enzymes

Hot Start Taq DNA Polymerase	Axon, Kaiserslautern, Germany
------------------------------	-------------------------------

Respiration gas mixture

Oxygen	0.6 L/min
Nitrous oxide	0.4 L/min
Isoflurane	1.5 % - 5 %

Tamoxifen

Tamoxifen was diluted in Miglyol®812 to 10 mg/ml	Carbolution, Neunkirchen, Germany
--	-----------------------------------

2.1.6 Primers for Genotyping

Table 6. List of PCR primers used for genotyping.

All following primers were synthesized by Sigma Aldrich.

Mouse line	Primer number	Annealing temperature	Sequence	bp
GABA_B	24392 fwd	65 °C	5'-GCTCTTCACCTTTCAACCCAG-CCTCAGGCAGGC-3'	742 KI
	24393 rev	65 °C	5'-CCTCTGCCTTCCTCCACATGT-TTCTCCT-3'	526 WT
GCaMP3	27632 KI fwd	58 °C	5'-CACGTGATGACAAACCTTGG-3'	245 KI
	27490 KI rev	58 °C	5'-ACATTAAAGCAGCGTATCC-3'	
	14025 wt fwd	58 °C	5'-CTCTGCTGCCTCCTGGCTTCT-3'	327 WT
	14026 wt rev	58 °C	5'-CGAGGCGGATCACAAGCAATA-3'	
NGCE	19398 fwd	60 °C	5'-GGCAAACCCAGAGCCCTGCC-3'	829 KI
	19399 wt rev	60 °C	5'-GGCAAACCCAGAGCCCTGCC-3'	
	19400 Cre ^{ERT2} rev	60 °C	5'-GCCCCGACCGACGATGAAGC-3'	557 WT

2.1.7 Antibodies

2.1.7.1 Primary Antibodies for Immunohistochemistry and Western blot

Table 7. List of primary antibodies used for immunohistochemistry and Western blot.

Antibody	Host	Clonality	Dilution	Use	Company
Anti-adenomatous polyposis coli clone 1 (CC1)	Mouse	monoclonal	1:200	IHC	Calbiochem
Glial fibrillary acidic protein (GFAP)	Rabbit	polyclonal	1:1000	IHC, WB	Dako
Ionized calcium-binding adapter molecule 1 (Iba1)	Goat	polyclonal	1:1000	IHC	Abcam
Degraded myelin basic protein (dMBP)	Rabbit	polyclonal	1:2000	IHC	Millipore
Myelin basic protein (MBP)	Mouse	polyclonal	1:20.000	ICH, WB	Biologends
Oligodendrocyte transcription factor 2 (Olig2)	Rabbit	polyclonal	1:500	IHC	Millipore
Platelet-derived growth factor receptor alpha (PDGFR α)	Goat	polyclonal	1:500	IHC	R & D Systems
α -Tubulin	Mouse	monoclonal	1:100	WB	Sigma-Aldrich

2.1.7.2 Secondary Antibodies for Immunohistochemistry

Table 8. List of secondary antibodies used for immunohistochemistry.

Antibody	Host	Dilution	Company
Alexa 488 conjugated anti-mouse IgG	donkey	1:1000	Invitrogen
Alexa 488 conjugated anti-rabbit IgG	donkey	1:1000	Invitrogen
Alexa 546 conjugated anti-goat IgG	donkey	1:1000	Invitrogen
Alexa 546 conjugated anti-mouse IgG	donkey	1:1000	Invitrogen
Alexa 647 conjugated anti-goat IgG	donkey	1:1000	Invitrogen
Alexa 647 conjugated anti-rabbit IgG	donkey	1:1000	Invitrogen

2.1.8 Mouse lines

Experiments were conducted with crossbreeding of different mouse lines. The transgene mouse line $GABA_B^{fl/fl} \times NG2-Cre \times GCaMP3$ was used for immunohistochemistry and Western blot analysis.

Table 9. Utilized mouse lines and corresponding abbreviations.

Mouse line	Abbreviation	Reference
TgH(Rosa26-CAG-lox/Stop/lox-GCaMP3)	GCaMP3	(Paukert et al., 2014)
TgH($GABA_B^{fl/fl}$)	$GABA_B^{fl/fl}$	(Haller et al., 2004)
TgH($NG2-Cre^{ERT2}$)	$NG2-Cre^{ERT2}$	(Huang et al., 2014)

2.1.8.1 TgH ($NG2-Cre^{ERT2}$) $NG2-Cre^{ERT2} \times$ TgH (Rosa26-CAG-lox/Stop/lox-GCaMP3) GCaMP3

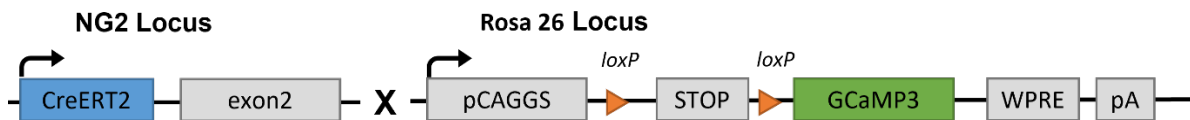


Figure 6. Construct of the $NG2-Cre^{ERT2}xGCaMP3$ mouse line. Cre^{ERT2} : open reading frame of the tamoxifen dependent Cre recombinase Cre^{ERT2} . pCAGGS: CAG promotor. STOP: transcriptional stop sequence. GCaMP3: cDNA of genetically encoded Ca^{2+} indicator GCaMP3.

The $GABA_B$ receptor knockout mouse line allows studying the effects of a functional loss of the $GABA_B$ receptor. Exon 7 and 8 of the $GABA_{B1}$ gene were flanked with lox511 sites by homologous recombination (Haller et al., 2004). After the recombination of lox511 sites in homozygously floxed mice, a knockout of the $GABA_B$ receptor is achieved. To investigate the consequences of a $GABA_B$ receptor knockout in NG2 positive cells, mice of the $GABA_B^{fl/fl}$ mouse line were bred to $NG2-Cre^{ERT2} \times GCaMP3$ mice, to induce a cell type-specific conditional knockout (Figure 1). In addition, GCaMP3 is expressed to visualize calcium transients in this cell type.

2.1.8.2 TgH (GABA_B-floxed) GABA_B^{fl/fl} x TgH (NG2-Cre^{ERT2}) NG2-Cre^{ERT2} x TgH (Rosa26-CAG-lox/Stop/lox-GCaMP3) GCaMP3

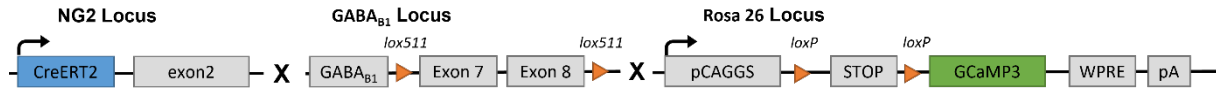


Figure 7. Construct of the GABA_B x NG2-Cre^{ERT2} x GCaMP3 mouse line. Cre^{ERT2}: open reading frame of the tamoxifen dependent Cre recombinase Cre^{ERT2}. GABA_{B1}: start of the GABA_{B1} locus. pCAGGS: CAG pro-motor. STOP: transcriptional stop sequence. GCaMP3: cDNA of genetics.

The GABA_B receptor knockout mouse line allows studying the effects of a functional loss of the GABA_B receptor. Exon 7 and 8 of the GABA_{B1} gene were flanked with lox511 sites by homologous recombination (Haller et al., 2004). After the recombination of lox511 sites in homozygously floxed mice, a knockout of the GABA_B receptor is achieved. To investigate the consequences of a GABA_B receptor knockout in NG2 positive cells, mice of the GABA_B^{fl/fl} mouse line were bred to NG2-Cre^{ERT2} x GCaMP3 mice, to induce a cell type-specific conditional knockout (Figure 1). In addition, GCaMP3 is expressed to visualize calcium transients in this cell type.

2.1.9 Animal maintenance

2.1.9.1 Ethics statement

Mice are housed at the animal facility of the CIPMM. Housing conditions followed the European and German guidelines for the welfare of experimental animals (Landesamt für Verbraucherschutz, Saarland, license number: 36/2016). Mice are held at a 12-hour day/night cycle with food and tap water available *ad libitum*.

2.1.9.2 Cuprizone food

High nutrient (breeding) powder feed was purchased from sniff Spezialdiäten GmbH (Soest, Germany). The cuprizone added to this feed was purchased from Carbolution Chemicals GmbH (St. Ingbert, Germany). "Powder" cuprizone food was freshly made by thoroughly mixing finely powdered cuprizone with powder feed at a concentration (w/w) of 0.2 % (77 g

powder food, 3.2 g sugar powder, 0.16 g cuprizone) or 0.3 % % (77 g powder food, 3.2 g sugar powder, 0.24 g cuprizone).

2.1.9.3 Mice administration

Python-based Relational Animal Tracking (PyRAT, from Scionics Computer Innovation GmbH, Dresden, Germany) database was used to administer relevant information in regard to the animal: mouse number, date of birth, gender, pedigree, genotype, and breeding behavior. Experimental techniques (e.g. drug administration) conducted were added to the database as they were performed.

2.1.9.4 Tamoxifen treatment

To activate the recombination in PCET mice, animals were injected intraperitoneal with tamoxifen diluted in miglyol (10 mg/mL) at a dose of 100 mg/kg bodyweight. Mice were injected once for five consecutive days at age four or eight weeks depending on the experimental design. The treatment was performed by the animal caretakers of the CIPMM.

2.1.10 Software and Devices

Adobe InDesign CC 2020, Adobe Illustrator CC 2020, BioRender professional science figure design website <https://biorender.com>, Image J and Microsoft Power Point 365 were used to design given figures. Graphs and statistics were generated with GraphPad Prism 8. For basic calculations, Microsoft Excel 365 was used. Word processing was done in Microsoft Word 365. Western blot data were analyzed using ImageJ software and exported to Microsoft Excel 365. Scanned optic nerve sections were visualized and exported as TIF files using Zen blue 2.6. (Zeiss, Oberkoch, Germany). To quantify scanned slices, Image J and Zen blue 2.6 were used. Fluorescence intensity measurements and counting of cells were likewise performed in ZEN 2.6 Blue Edition. For statistical analysis, GraphPad Prism was used. Database research was done using the internet service PubMed of the “National Center for Biotechnology Information”. The used devices are listed in Table 10.

Table 10. List of devices and their producers with the corresponding application.

Device	Manufacture	Application
AxioScan.Z1	Zeiss, Oberkochen, Germany	Automatic slide scanner
Centrifuge 5428, 5430R, 5804	Eppendorf, Hamburg, Germany	Centrifuge
Cryostat CM3050	S Leica, Wetzlar, Germany	optic nerve slicing
Gel Doc™XR+ system	Thermo Fisher Scientific, Dreieich, Germany	Gel documentation system for Western blot
Electrophoresis power supply	Consort, Turnhout, Belgium	Power supply
Gel electrophoresis chambers and agarose gel supplies	Workshop of the CIPMM, Homburg, Germany	Gel electrophoresis
peqSTAR Thermo Cycler	Peqlab Biotechnology GmbH, Erlangen, Germany	DNA amplification
Precellys24	Peqlab Biotechnology GmbH, Erlangen, Germany	Homogenization of tissue
Preparation and perfusion instruments	F.S.T. Pharmacia, Heidelberg, Germany	Whole-body perfusion and spinal cord extraction
Quantum gel documentation system	Peqlab Biotechnology GmbH, Erlangen, Germany	PCR gel pictures
Serva gel electrophoresis chamber	Serva Electrophoresis, Heidelberg, Germany	Gel electrophoresis for Western blot analysis
Shaker DRS-12	NeoLab, Heidelberg, Germany	Shaker
Vibratome VT1000S	Leica, Wetzlar, Germany	Tissue slicing

2.2 Methods

2.2.1 Genotyping

2.2.1.1 Tail samples

Mousetail samples were collected after weaning at the age of three to four weeks by animal caretakers of the CIPMM. The discarded ear tissue was removed and stored at - 20 °C until DNA extraction.

2.2.1.2 DNA extraction

DNA was extracted with the Extract-N-Amp™ Tissue PCR Kit. Extraction solution was mixed 1:4 with tissue preparation solution and 65 µL of the mixture were added to the vials, ear tissue was shaken at room temperature for 10 minutes at 700 rpm and subsequently incubated in a water bath at 100 °C for 20 min. 50 µL neutralization buffer was added and the solution was transferred into new vials for genotyping PCR and further experiments. The extracted DNA was stored at 4 °C and used for genotyping of transgenic mice using PCR.

2.2.1.3 Polymerase chain reaction (PCR)

The polymerase chain reaction (PCR) allows the amplification of a specific DNA sequence (Mullis and Faloona 1987). 2 µL of the DNA sample was mixed with the proper amount of DreamTaq™ Hot Start Green PCR Master Mix and oligonucleotide primers (Table 6), and water was added to reach a total volume of 20 µL. The 96-well PCR plate was covered by adhesive foil, centrifuged and placed in a PCR cycler. The appropriate program was selected depending on the annealing temperature of the primer and the number of cycles. The general process of PCR is subdivided in DNA denaturation (95 °C), followed by the annealing step (around 58-60 °C), in which primers anneal to complementary DNA regions, and the third step (72 °C), where the Taq-Polymerase duplicates DNA fragments, increasing the DNA amount exponentially. The three steps above are repeated several times in order to amplify the DNA fragment for subsequent genotype identification. Those three steps are preceded by three minutes at 95 °C, for an initial denaturation of the DNA secondary structure, and they are followed by 15 minutes at 72 °C, for the final extension of the amplified sequences.

2.2.1.4 Agarose gel electrophoresis

Gel electrophoresis is used to separate DNA fragments according to their molecular weight. Based on its negative charge, the DNA runs from the cathode (-) to the anode (+) in the electric field. The size (bp) of the DNA fragment determines the speed while the agarose gel acts like a filter. Smaller fragments run faster through the gel and thus will be detected in the lower part of the gel. For genotyping 1.5% or 2 % agarose gels with ethidium bromide were used. The ethidium bromide intercalates into DNA molecules and can be detected by UV-light. The gel chamber and the comb were produced at the institute's workshop. Gels were run at 150 V, 300 mA for 20-40 min. For documentation the Quantum gel documentation system was used.

2.2.2 Experimental design of tamoxifen and cuprizone treatment

Transgenic mice of the *GABA_{knockout}* cohort were injected with tamoxifen to induce the DNA recombination caused by the Cre^{ERT2} DNA recombinase. Cre^{ERT2} is a chimeric protein consisting of the Cre DNA recombinase fused to a mutated oestrogen receptor domain that recognizes 4-hydroxytamoxifen (Feil et al., 2009). Tamoxifen is metabolized to 4-hydroxytamoxifen in the liver of mice (Crewe, Ellis, Lennard, & Tucker, 1997). Cre^{ERT2} is expressed in the cytosol and retained by heat shock proteins. Upon ligand binding, the Cre^{ERT2} recombinase can translocate into the nucleus and recombine floxed sequences. This system allows a conditional induction of the Cre/lox system (Feil et al., 1996).

The intraperitoneal injection with tamoxifen diluted in miglyol®812 (10 mg/ml) was performed by the animal caretakers of the CIPMM according to the weight of the animals (100 mg/kg body weight) (Jahn et al., 2018). Mice of the *GABA_{knockout}* cohort (*GABA_B^{fl/fl}* x NG2-Cre^{ERT2} x GCaMP3 mouse line) were treated once a day for five consecutive days in the fourth postnatal week.

Due to the SARS-CoV-2 pandemic outbreak, organizational issues at that time impeded the proper and correct maintenance of the experimental plan. For this reason, the second cohort called *Non-induced_{ctrl}*, of transgene mice (*GABA_B^{fl/fl}* x NG2-Cre^{ERT2} x GCaMP3 mouse line) did not receive tamoxifen injections and therefore DNA recombination induced by the Cre^{ERT2} DNA recombinase could not be accomplished. However, I took advantage of this inconvenience to investigate if the new cuprizone food protocol formulation will show the same effects than hard chow cuprizone treatment and whether the new treatment shows its effects at an even earlier stage.

At eight weeks of age, mice were given a 0.3 % cuprizone diet for one week, followed by a 0.2 % cuprizone diet for two weeks. At eleven weeks of age, mice were fed normal chow. The *GABA^{knockout}* cohort was analyzed two weeks after the end of (post) the cuprizone diet (2 WPC remyelination), while the *Non-induced^{ctl}* cohort was immediately after the end of the cuprizone treatment (0 WPC demyelination). Control mice of the same mouse strain received mouse chow without cuprizone and were perfused at the age of 13 weeks (*GABA^{knockout}* cohort) and 11 weeks (*Non-induced^{ctl}* cohort), respectively.

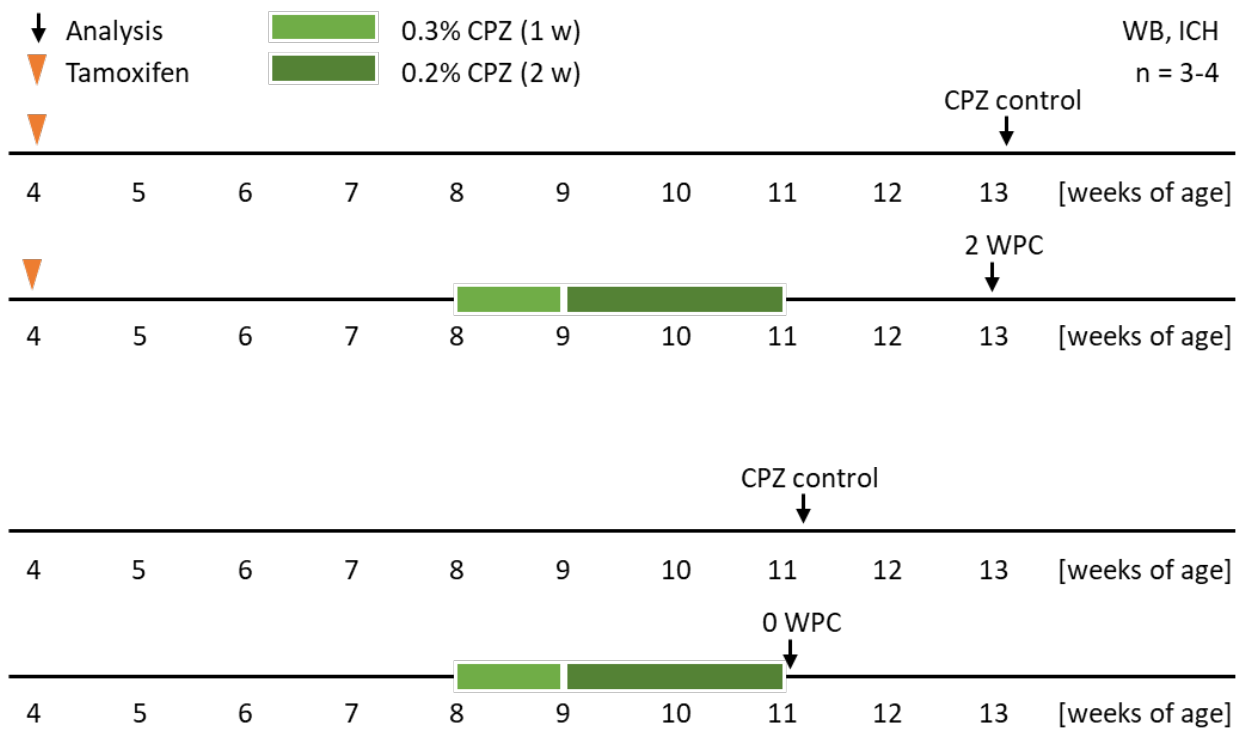


Figure 8. Tamoxifen injection and cuprizone treatment protocol of *GABAB^{fl/fl} x NG2-CreERT2 x GCaMP3* mice. Two different cohorts have been observed. (A) *GABA* cohort was analyzed two weeks after end of cuprizone treatment (2 WPC) and (B) *Non-induced^{ctl}* cohort immediately after ending cuprizone treatment (0 WPC), *Non-induced^{ctl}* cohort therefore did not underline tamoxifen injections. Black arrows indicate the time point of analysis with the corresponding group name. An asterisk marks groups of cuprizone treated mice. Red triangles show time of tamoxifen injections.

2.2.3 Tissue sampling

Mice were anesthetized with ketamine/xylazine (f.c. 10.4%/f.c. 5%) in 0.9 % NaCl (100 μ L/10 g body weight), and the depth of anaesthesia was confirmed by checking the hind limb pinch reflex. The abdominal skin was incised to expose the peritoneum. The peritoneum was cut from medial to lateral and the diaphragm was cut longitudinally. The pericardium was separated from the peritoneum by cutting laterally along the thoracic cavity to the clavicle. A butterfly needle was then carefully inserted into the left ventricle and perfusion with PBS was started using a peristaltic pump. Simultaneously, an incision was made in the right atrium to drain the blood. The mice were perfused by PhD student Phillip Rieder, CIPMM, Homburg. The color change in the liver from red to pale yellow was used to indicate the transition between blood and perfusion buffer. After perfusion with 5 ml PBS, the solution was changed to 4 % formaldehyde (FA) in PBS for tissue fixation. Fixation was considered complete after perfusion with 5-10 ml FA. The head was sectioned and the brain and optic nerve were dissected. The brain and one half of the optic nerve construct (Fig. 9) were postfixed in a tube with 4 % PFA at 4 °C overnight. The next day, the 4 % PFA was replaced with PBS.

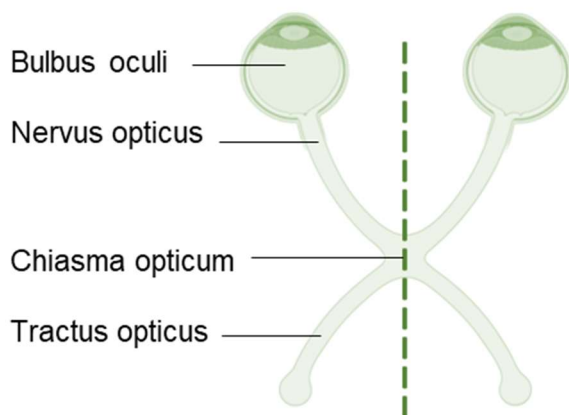


Figure 9. Schematic representation of optic nerve tissue. For the mice from the $GABA_{knockout}$ cohort, the optic nerves were dissected at the chiasma opticum. One nerve from each mouse was used for immunohistochemistry and the other for Western blot. For the $Non-induced_{ctf}$ cohort, whole tissue was used for either Western blot or immunohistochemistry by dividing the cohort into two subgroups.

The optic nerves were dissected at the chiasma opticum to maximize tissue yield. Subsequently, a portion of the fixed tissue was stored in PBS at 4 °C, and the optic nerve used for Western blotting were snap frozen on dry ice and stored in 1.5 ml tubes at - 80 °C. The tissue was further processed for protein extraction.

2.2.4 Immunohistochemistry

2.2.4.1 Vibratome slices

The brain tissue was cut in two, rostral to the cerebellum. It was then sectioned at 40 µm using a Leica VT1000S vibratome. The sections were collected in 48-well plates containing PBS and then processed for immunostaining.

2.2.4.2 Cryostat slices

Before optic nerve slicing, the tissue was incubated for two hours with 30 % sucrose, to remove water from the cells. This enables the freezing without damage. The optic nerve was then embedded in Tissue-Tek® and stored in the Cryostat until they are frozen. Following the embedded tissue was cut at - 20 °C on a Leica CM3050 S Cryostat into 10 µm thick sections. The slices were picked up on SuperFrost Plus™ object slides and were then further processed for immunostaining.

2.2.4.3 Immunostainings

optic nerve immunohistochemical analyses were performed on slide-mounted sections for cryostat slices, and free floating vibratome slices. Cryostat slices were mounted on SuperFrost Plus™ object slides. After drying, the optic nerve tissue was already adhered to those object slides and a circle with the ImmEdge™ pen was drawn around the tissue slices. This pen provides a heat-stable, water-repellent barrier that is compatible with buffers with or without detergent and thereby keeps the reagents localized on the mounted tissue. Cryostat slices were incubated with 50 mM Glycine for 15 minutes at room temperature and washed afterwards once with Triton buffer (0.2 % Triton X in PBS) and once with blocking buffer (10 % HS in PBS), each for 15 min. After incubation for one hour at RT in blocking buffer, the slices were incubated with primary antibodies (Table 7.) diluted in blocking solution over night at 4 °C. Horse serum was used to reduce unspecific binding of the primary antibody. The antibodies naturally occurring in the serum occupy all available binding sites, which then only become available to the primary antibodies, having a sufficiently high affinity to displace the horse serum antibodies. Triton X-100 is a detergent added to permeabilize the cell membranes. The next day, optic nerve slices were washed once with blocking buffer, once with Triton buffer and afterwards again 2x with blocking buffer at RT to remove excessive and unbound antibodies. Secondary antibodies (Table 8.) diluted in blocking buffer were added and slices were incubated for two hours at RT. For nucleic acid staining, DAPI (1:1000

dilution) was added to the secondary antibody solution. Incubation and the subsequent steps were conducted in the dark to prevent bleaching of the fluorophores. After two washing steps for 10 minutes with Triton buffer, the optic nerve slices were incubated with Sudan Black B (SBB) (20 % in 70 % EtOH) for 15 minutes at RT in the dark, following another short washing step with PBS. SBB helps to reduce tissue autofluorescence and background, while preserving the specific fluorescence hybridization signals (Oliveira et al., 2010). Finally, the optic nerve slices were mounted in Immu-Mount on microscope slides. Immunostaining of brain slices was performed as described above, except the brain slices were stained in 48-well plates. Additionally, the tissue was incubated with 99 % Ethanol for 10 minutes at RT in the beginning, the washing steps were performed with PBS and the slices were not incubated with glycine and Sudan Black B.

Brain tissue got immunostained differently since I did not use Cryostat slices and instead worked with the vibratome. Vibratome slices were incubated with 99 % EtOH for 10 minutes at room temperature (RT) and washed afterward 3x with PBS. Then, the slices were incubated with 1 % SDS in PBS for 10 minutes at RT and washed 3x with PBS. After incubation for one hour at RT in blocking buffer, the slices were incubated with primary antibodies (Table 7) and diluted in blocking solution at 4 °C on a shaker overnight. Horse serum was used to reduce unspecific binding of the primary antibody. The antibodies naturally occurring in the serum occupy all available binding sites which then only become available to the primary antibodies having a sufficiently high affinity and specificity to displace the horse serum antibodies. Triton X-100 is a detergent added to permeabilize the cell membranes. The next day, brain slices were washed 3x for 10 minutes with PBS at RT to remove excessive and unbound antibodies. Secondary antibodies (Table 8) diluted in secondary antibody solution, were added and the slices were incubated on a shaker for two hours at RT. For nucleic acid staining, DAPI (f.c. 0.025 %) was added to the secondary antibody solution. Incubation and the subsequent steps were conducted in the dark to prevent bleaching of the fluorophores. After three washing steps for 10 minutes with PBS, the spinal cord slices were mounted in Immu-Mount on microscope slides with coverslips.

2.2.4.4 Zeiss Axioscan.Z1

All slides were scanned with the fully automated slide scanner AxioScan.Z1. The slide scanner is an epifluorescence microscope equipped with an LED light source (Colibri 7; Zeiss Jena, Germany). A Plan-Apochromat 10x/0.45 objective and a Plan-Apochromat 20x/0.8 objective are used for image acquisition. Appropriate excitation and emission filter sets were used to excite the fluorophores with the correct wavelengths and to capture only

the light emitted by the fluorophores. Images were recorded in 5 µm thick stacks, and a variance intensity projection was prepared for analysis (Huang et al., 2018). Using Zen blue 2.6 software, the files were visualized and exported as "TIF" files.

The stained mouse sections were quantified by fluorescence intensity measurements. In the figures, the brightness of the stained sections has been adjusted to make them stand out from the background. Fluorescence intensities were measured from the original data and were automatically measured with ZEN blue. Labelled neurons and interneurons were counted with ZEN blue.

2.2.4.5 Immunofluorescence measurements

The final immunofluorescence measurement was performed using ZEN blue 3.1 edition. For MBP and GFAP, the software directly measured multiple areas and therefore normalized to the square micrometre (µm²). For Iba1 staining, antibody positive cells were counted if they were also DAPI positive and then normalized to area. For optic nerve staining, the results of immunofluorescence measurement and counting were normalized to DAPI, whereas the brain got normalized to the immunofluorescence of the hippocampal fimbria as a comparable core value.

2.2.5 Western blot analysis

Snap frozen optic nerve tissue samples stored at - 80 °C were homogenized with 10 - 15 ceramic beads in 300 µl homogenization buffer using the Precellys®24. A total of 5 µg protein were applied on a 4-20 % gradient gel (SERVA Electrophoresis GmbH, Heidelberg) and electrophoretically separated for 30 minutes at 80 V followed by 90 minutes at 120 V. To transfer separated proteins on to a nitrocellulose membrane, a Wet blot for 24h at 40 V was performed. Ponceau S staining was used for the detection of protein bands to show a succeeded Western blot. Therefore, the nitrocellulose membrane was washed 3x for 5 minutes with water and then stained with Ponceau S for five minutes, the now visible protein bands were also used cut the membrane precisely around the 35 kDa mark. Ponceaus S was removed after cutting by washing the membrane 3x five minutes with PBS.

The transferred proteins were detected using the WesternFroxx System (BioFroxx GmbH, Einhausen). The primary and secondary antibodies for blotting were added to the WesternFroxx solution. The advantage of this system is the combination of blocking, primary and secondary antibody incubation at the same time. After incubating for 60 minutes with the

Western-Froxx solution. Subsequently, the membrane was incubated for five minutes in WesternBright™ and detected by the Gel Doc™XR+ gel documentation system.

After analyzing MBP and tubulin in the initial round, the section that had been previously incubated with tubulin underwent a stripping step before being blocked once again on the same membrane. Subsequently, in the second round GFAP was detected. During the stripping process, the primary and secondary antibodies were eliminated, thus producing an antibody-free membrane for the second blocking trial. To successfully strip the blot, the chemiluminescent substance was removed by neutralizing it in the washing buffer. Next, it was incubated with the Western Blot Stripping Buffer for 10 minutes, and then subjected to another washing step before undergoing blocking antibody incubation.

The membrane pictures were analyzed with Image Lab (version 6.1, Bio-Rad). Therefore, the light intensity of the different proteins was measured and normalized by a housekeeping gene (Tubulin). Manually drawn rectangular ROIs were placed above the different bands, while the size of the ROIs always remained the same. One band represents one mouse. The percentage values were calculated with Microsoft Excel 2016.

2.2.6 Statistics

All data sets were analyzed in GraphPad Prism 8. Before the statistical analysis, the data sets were tested for normality, using the Shapiro-Wilk normality test. By passing the Shapiro-Wilk normality test the statistical analysis was done with an unpaired two-tailed t-test. The following p-values were assumed: * $p < 0.05$, ** $p < 0.01$, *** $p < 0.001$, **** $p < 0.0001$. Data sets not passing the normality test were analyzed by the Mann-Whitney test, the following p-values were assumed: * $p < 0.05$, ** $p < 0.01$, *** $p < 0.001$, **** $p < 0.0001$.

3. Results

3.5 Optic nerve investigations of cuprizone induced myelin protein changes and astroglial activation during demyelination phase

The pathophysiology of demyelination in Multiple Sclerosis (MS) has undergone significant advances in recent years. A key role has been played by the knowledge gained from experiments with animal models of demyelination, such as the cuprizone model (Torkildsen et al., 2008). Most studies are based on the effect that feeding cuprizone to mice will lead to synchronous demyelination in large areas of the brain. Perfectly represented by the corpus callosum, showing relevant changes in cellular, molecular, biochemical and morphological parameters (Matsushima & Morell, 2001). Since most studies have focused on the mouse brain, the following experiments were performed on optic nerve tissue to provide a comprehensive overview of cuprizone induced changes in other parts of the central nervous system (CNS). From a medical perspective, this tissue is of special interest since visual disruptions are among the first symptoms to present in affected patients. This is particularly evident in the constellation of the clinically isolated syndrome (CIS), which is strongly associated with MS (D. H. Miller et al., 2012). The objective of this study was to assess the compatibility of the cuprizone powder dietary formulation model with optic nerve tissue and to correlate the results with spinal cord and brain findings. The latter were based on comparable laboratory studies indicating a significant reduction in myelin level in the cuprizone-treated group when compared to the control group of mice (Braun, 2020, Bachelor Thesis; Damo, 2019, Master Thesis; Rieder, 2023, PhD Thesis; Schablowski, 2019, Bachelor Thesis).

The following experiments were performed with the mouse lines $GABA_B^{fl/fl} \times NG2-CRE^{ERT} \times GCaMP3$. I called this group *Non-induced_{ctl}*, since only cuprizone effects without knockout situation were studied to capture the changes in the optic nerve caused by the treatment. Therefore, this line did not receive the tamoxifen injections and did not feature cell-type-specific conditional knock-out in NG2 positive cells. The cohort was treated with cuprizone for three weeks at eight weeks of age (one week 0.3 % cuprizone followed by two weeks 0.2 % cuprizone) and evaluated immediately thereafter at eleven weeks of age. Therefore, the cohort was considered to be in the demyelination phase (Gudi, Gingele, Skripuletz, & Stangel, 2014). They were compared to a control group of the same age who did not receive

cuprizone treatment. The *Non-induced_{ctrl}* group was split up, one half was used for Western blot analyses and the other half for immunohistochemistry. Fluorescence intensity measurements were normalized to the fluorescence intensity of DAPI. Since several unsuccessful attempts to induce reliable demyelination had been reported by members of the department, the previous standard cuprizone treatment regimen was modified. Instead of feeding the animals with cuprizone containing pellets, a freshly prepared cuprizone powder formulation was used for the first time. Parallel studies with spinal cord tissue were performed by members of the laboratory. Here, the new cuprizone diet showed a strong effect and presented the expected strong decrease in myelin content by immunohistochemical measurements. Thus, the cuprizone powder formulation protocol was proven to be working in spinal cord tissue (Dallorto, 2021, Master Thesis)

3.5.1 Immunohistochemistry analyses revealed no changes in myelin proteins

Myelin basic protein (MBP) is one of the key proteins of the myelin sheath, along with proteolipid protein (PLP). In the CNS, it is well described as the executive molecule of myelin (Moscarello, 1997). The function of MBP has been extensively studied in MS models, showing its responsibilities in the formation, maintenance and adhesion of cytosolic surfaces as these maintain the regular function of the myelin sheath (Boggs, 2006). In previous work of the laboratory, the mRNA expression of MBP and PLP (preliminary qRT-PCR data) was decreased in the cuprizone treated cohort (cuprizone treatment via pellet chow) compared to control mice (Braun, 2020, Bachelor Thesis; Damo, 2019, Master Thesis; Schablowski, 2019, Bachelor Thesis). And the new cuprizone treatment (freshly prepared cuprizone powder formulation) also strongly supported a decrease in myelin content of spinal cord tissue (Dallorto, 2021, Master Thesis). Therefore, reduced MBP level in mature optic nerve tissue following the cuprizone diet might be expected. To demonstrate an efficient effect of the new cuprizone protocol formulation on optic nerve glial cells, cuprizone fed mice were compared with age-matched mice on regular chow. Both optic nerves, connected at the remnants of the chiasma opticum (Fig. 10 D1), were immunohistochemically stained for MBP and degraded MBP (dMBP) to investigate a sustained effect of cuprizone treatment. To quantify changes in myelin, fluorescence intensity was measured for both markers. No difference was made in the measurement location, and the entire optic nerve was quantified.

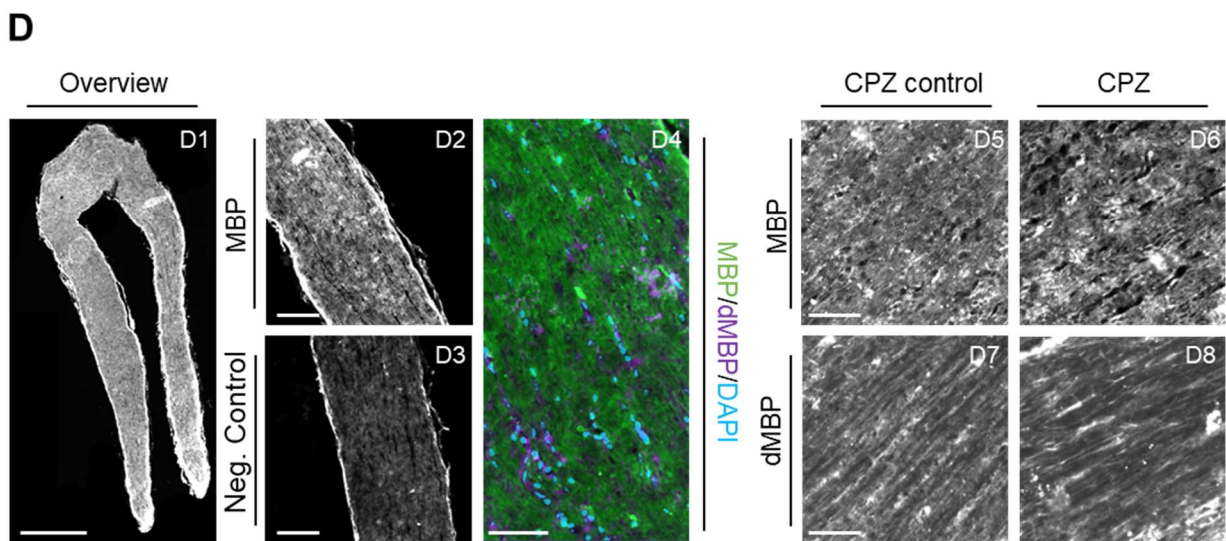
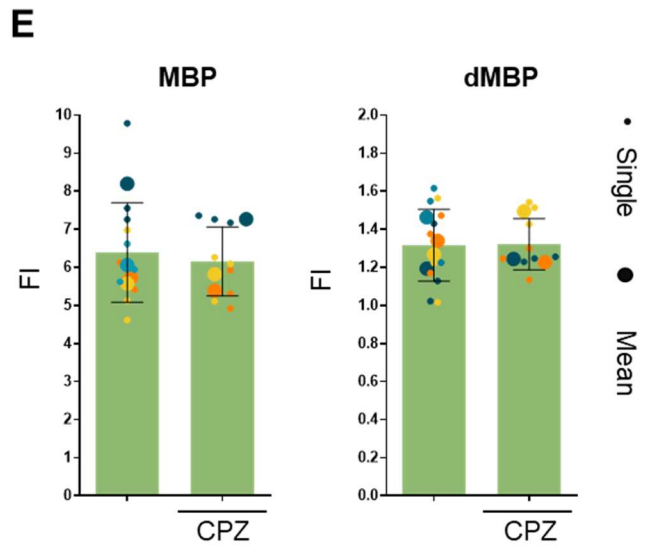
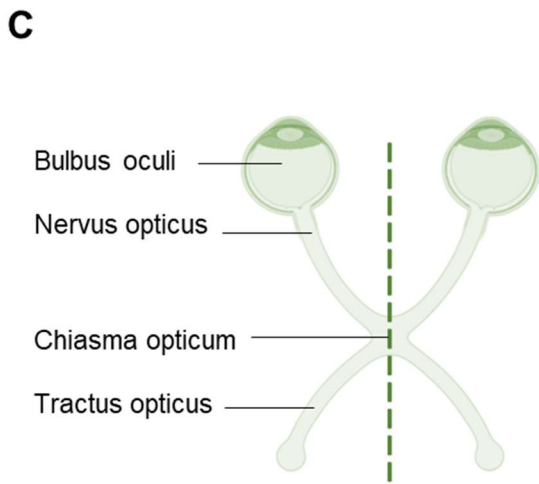
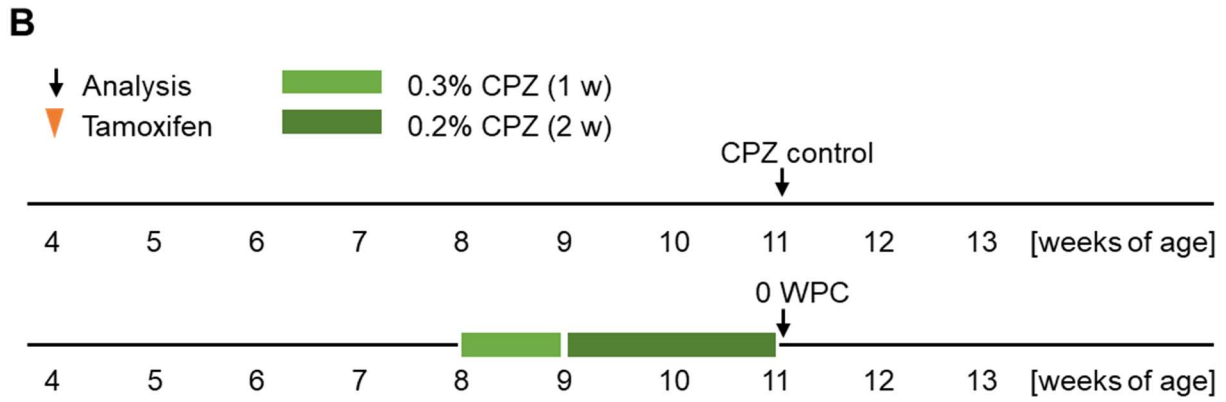
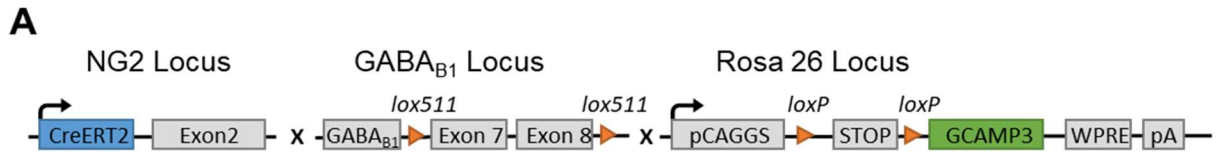


Figure 10. No change of protein level in CPZ treated cohorts. (A) Construct of *GABAB1/fl x NG2-CreERT2 x GCaMP3* mice. (B) Experimental design for CPZ treatment. (C) Scheme of optic nerve tissue preparation showing the tissue with both optic nerve and chiasma were used for immunohistochemistry. (D) Immunohistochemical staining of MBP and dMBP. (D1) Exemplary overview presentation of cryostat section of optic nerve stained with MBP. (D2-3) Comparison of MBP with negative control (secondary antibody only) showing successful MBP staining in optic nerve tissue. Immunostained optic nerve sections for MBP (D51-6) and dMBP (D7-8) for each cohort. (E) Optic nerve fluorescence intensity measurements of MBP and dMBP in all groups, normalized to DAPI. Error bars indicate mean with SD of the cohort. One color represents one animal, with large dots representing the mean for each mouse and each small dot representing a single slice of the sectioned optic nerve as shown in the overview (D1). Two-tailed *t*-test was used for statistical analysis. Scale bar = 500 μ m (D1), 20 μ m (D2-3), 50 μ m (D4), 50 μ m (D5-8). *n* = 3-4

Immediately after discontinuing cuprizone treatment (0 WPC), no change in myelin level was detected by fluorescence intensity measurements (Fig. 10 E). Mean variation did not show much variability. A successful staining was shown in comparison to the negative control (Fig. 10 D2-3). Subsequently, neither MBP nor dMBP showed the expected changes representative of myelin loss. The MBP and dMBP expression level showed no reduction and appeared almost the same (MBP cuprizone control: 6.393 ± 1.386 ; cuprizone: 6.158 ± 0.9439 , $p=0.6661$; dMBP cuprizone control: 1.316 ± 0.2123 ; cuprizone: 1.322 ± 0.1398 , $p=9.437$).

Overall, the immunohistochemical data did not support the expected decrease in myelin content after cuprizone diet and therefore did not validate the new cuprizone powder diet protocol formulation for optic nerve tissue at the chosen observation period in the demyelination phase after finishing three weeks of cuprizone diet (Gudi et al., 2014).

3.5.2 Western blot analyses revealed high variability in myelin levels and astroglial activation

Previous studies showed that already one week post cuprizone treatment oligodendroglial loss as well as activated astrocytes and microglia can be observed in the corpus callosum (Buschmann et al., 2012). The loss of myelin (MBP) is followed by reactive astrocytes who will be represented by an upregulated level of glial fibrillary acidic protein (GFAP) (van der Valk & Amor, 2009). First reported in 1969, the intermediate filament GFAP was quickly adapted as an astroglial marker in the CNS. Especially elevated expression level are associated as an indicator of gliosis shown in scar formations and other pathologies (Eng,

Ghirnikar, & Lee, 2000; Eng, Vanderhaeghen, Bignami, & Gerstl, 1971; Eriksson et al., 2009; Geisler & Weber, 1983).

Unpublished spinal cord data from the department showed a downregulation of myelin level, especially in older mice (13 weeks of age), associated with prolonged cuprizone treatment. At the same time, an upregulation of astroglial markers after cuprizone treatment was shown by Western blot analysis and fluorescence intensity analysis (Braun, 2020, Bachelor Thesis; Dallorto, 2021, Master Thesis)

I would expect similar demyelination effects in the optic nerve as in the spinal cord. Since the optic nerve is one of the first tissues to show symptoms in MS, an even more severe demyelination process could be expected. Combined with the subsequent induction of the immune system, I would expect an activation of astrocytes.

In order to investigate whether the new cuprizone powder chow protocol formulation treatment ultimately leads to myelin loss and astroglial activation in optic nerve tissue, Western blot analysis were performed. I used MBP and GFAP as quantifiable targets as two of the basic markers for investigating oligodendroglial induced neuronal degeneration activity.

Mice from the *Non-induced_{ctrl}* group were used and both optic nerve compartments connected by the remnants of the chiasm were analyzed. Tubulin was used as a housekeeping gene for normalization and an additional normalization was performed with their age-related untreated cuprizone control group.

Immediately after ending cuprizone treatment (0 WPC) I could not detect any changes in neither myelin level nor astroglial activation (Fig. 11 E, F). The protein measurements showed a normal distribution. However, the results presented a wide scattering of values in the cuprizone treated mice. For illustrative purposes, the range of each cohort was calculated, measured as the difference between the smallest and largest values (Hedderich & Sachs, 2021). In the cuprizone treated animals, the range was more than doubled compared to the cuprizone control animals (GFAP range cuprizone control: 0.6394, cuprizone: 1.743; MBP range cuprizone control: 0.4070, cuprizone: 1.508).

The final values could only suggested a tendency of elevated myelin level (MBP cuprizone control: genetic control: 1.0 ± 0.1315 ; cuprizone 1.389 ± 0.5007 , $p = 0,0519$). Statements on the tendencies of the astroglia could not be made due to the high degree of scatter (cuprizone control: 1.0 ± 0.6394 ; cuprizone 1.135 ± 1.135 , $p = 0,5462$).

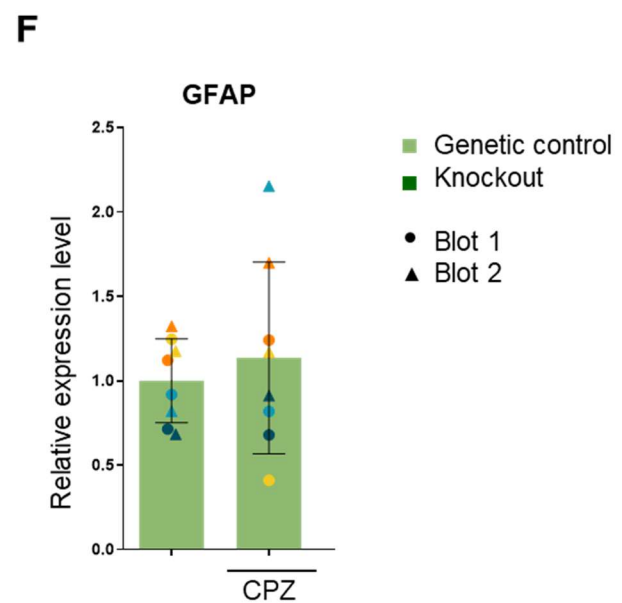
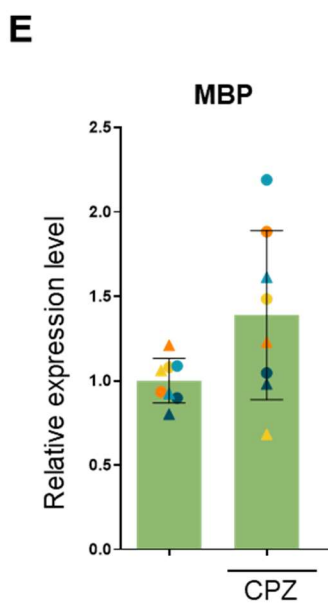
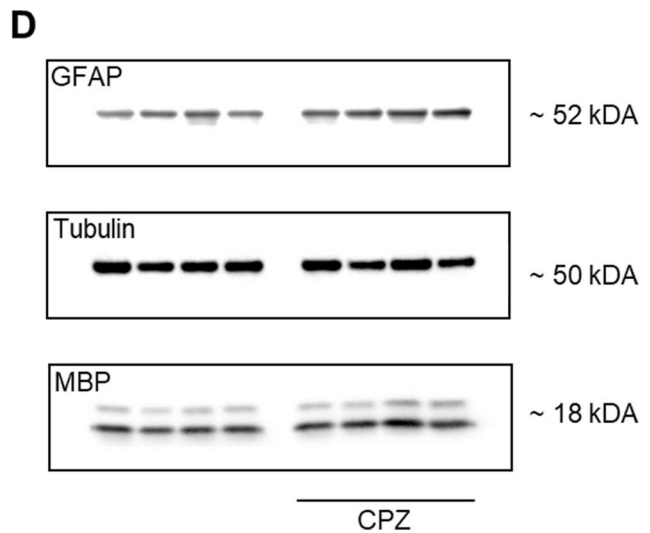
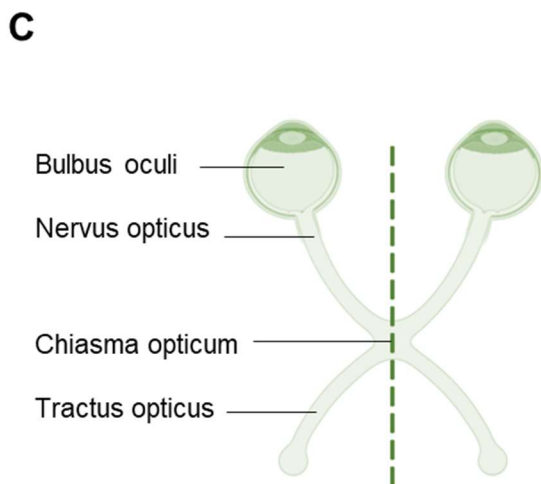
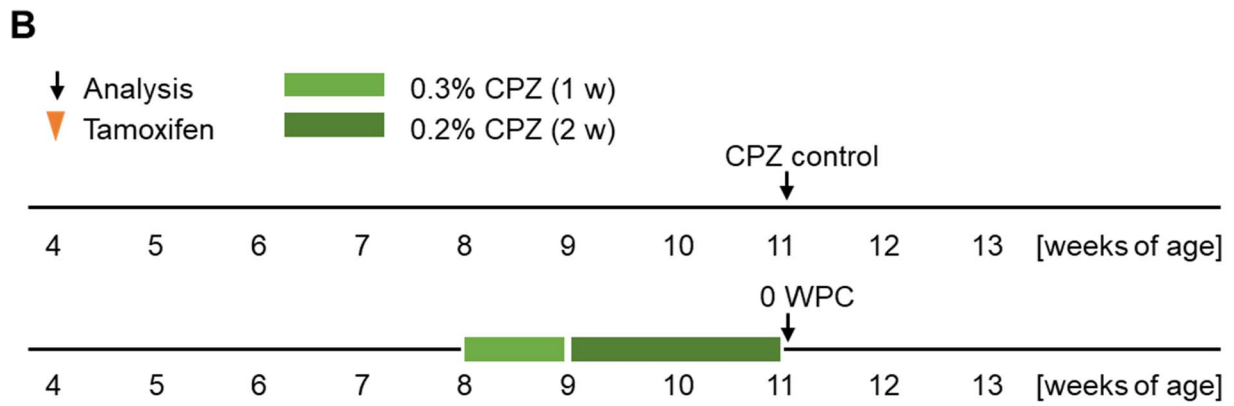
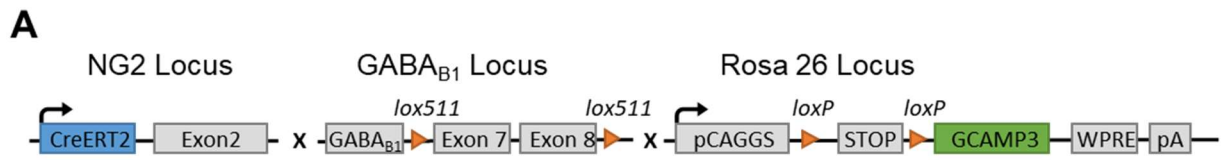


Figure 11. No change of protein level in CPZ-treated cohorts. CPZ-treated mice show high variability. (A) Construct of GABAB f/f x NG2-CreERT2 x GCaMP3 mice. (B) Experimental design for CPZ treatment. (C) Scheme of optic nerve tissue preparation showing the whole tissue with both optic nerve and chiasma used for Western blot. (D) blot 1 of treated mice immediately after ending cuprizone diet (0 WPC) and their untreated age-related control group. GFAP and MBP were used as target proteins to investigate astroglial activation and myelin level changes. Tubulin was used as a housekeeping gene. (E-F) Quantification of MBP (E) and GFAP (F). Bars show mean values with SD. Each color represents one mouse, with dots representing blot 1 and triangles representing the repeat, blot 2. Values were normalized to tubulin and additionally to the mean of their age-matched untreated control group. A two-tailed t-test was used for statistical analysis. $n = 4$.

Generally, a distinctive astroglial activation would align with fluorescence measurements from spinal cord areas (Dallorto, 2021, Master Thesis). The indicated tendency of increasing myelin instead of expected reduction, especially in this age and treatment group representing the early demyelination phase (Gudi et al., 2014), was seen before in fluorescence measurements of the department (Braun, 2020, Bachelor Thesis) Further investigations should be made to calculate the response in different age groups and treatment periods. In cuprizone treated mice.

Subsequently, Western blot data did not show the expected changes after cuprizone powder chow protocol. A decrease in myelin proteins as well as increased astroglial activation did not materialize. However, strong variability was observed in cuprizone treated mice for both, MBP and GFAP measurements. This might reflect post treatment changes on the cellular level.

3.6 Immunohistochemical analyses investigating the effects of cuprizone treatment and GABA_B receptor loss on protein expression changes during the remyelination phase in the optic nerve.

This group of mice will be referred to as *GABA_Bknockout*, since only this group was analyzed for the GABA_B receptor as a target. The protocol included injection of tamoxifen once a day for five consecutive days at four weeks of age to induce Cre^{ERT}-dependent recombination. Genetic control mice did not receive tamoxifen injections and therefore expressed GABA_B receptors regularly. Starting at eight weeks of age, mice were fed with cuprizone powder chow formulation for three weeks (one week 0.3 % cuprizone followed by two weeks 0.2 % cuprizone). At eleven weeks of age, the mice were returned to normal chow without cuprizone. They were perfused two weeks after the end of treatment (2 WPC) at 13 weeks of age. Studies showed that the mice in this phase are already in the remyelination period (Gudi et al., 2014). cuprizone control mice were fed regular mouse chow (without cuprizone) and likewise perfused at 13 weeks of age (Fig. 12 B, 14 B). Subsequently, this led to four groups: knockout with genetic control and cuprizone treated knockout with cuprizone treated genetic control. The optic nerve tissue used for the *GABA_Bknockout* group was separated so that one optic nerve was used for Western blot analysis and the other one for fluorescence intensity measurement. After automated scanning of the slides, fluorescence measurements were normalized to the fluorescence intensity of DAPI. A negative control was used to verify successful staining.

3.6.1 Knockout mice revealed increased myelination

As described before the myelin basic protein (MBP) is one of the most common proteins used in MS studies (Boggs, 2006). To initially analyze the *GABA_Bknockout* cohort in terms of oligodendroglial behavior, MBP and degraded myelin basic protein (dMBP) were used as target. Previous unpublished spinal cord data from the department suggest that GABA_B receptor knockout is a protective factor with respect to demyelination and a supportive factor with respect to remyelination (Rieder and Scheller unpublished). Thus, mice from knockout cohorts showed milder demyelination and faster remyelination compared to genetic control mice. Therefore, I wanted to investigate whether these effects were also present in optic nerve tissue.

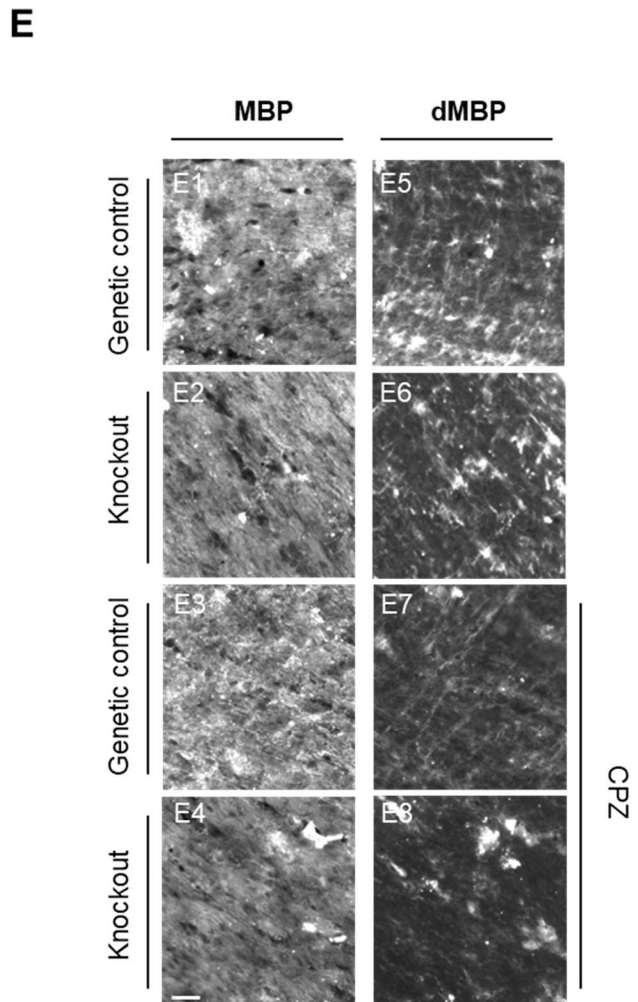
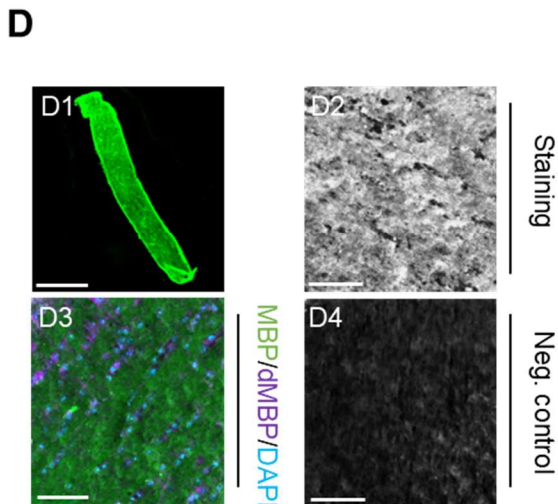
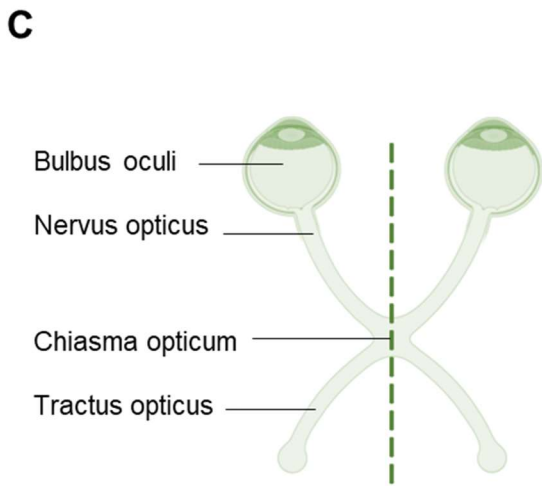
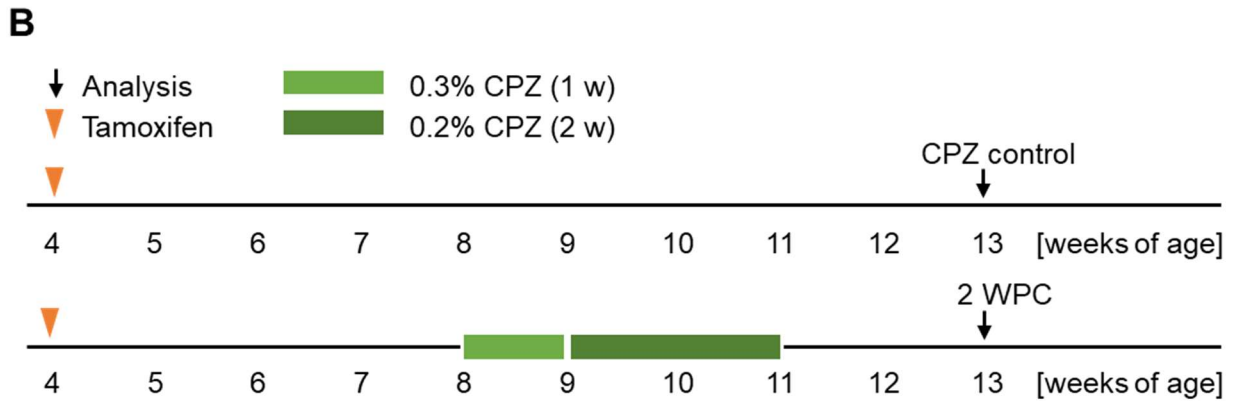
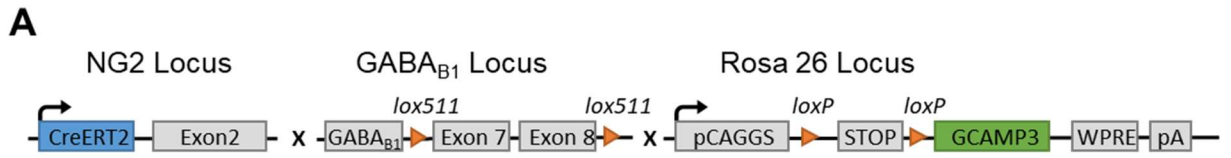


Figure 12. Comparison of MBP and dMBP expression level. (A) Construction of *GABAB1/fl x NG2-CreERT2 x GCaMP3* mice. (B) Experimental design of CPZ treatment. (C) Scheme of optic nerve tissue preparation showing the tissue with both optic nerve and chiasm were used for immunohistochemistry. (D1) Overview of optic nerve cryostat sections stained with MBP and (D2) merge showing both MBP and dMBP staining in color. (D3-4) Comparison of MBP with negative control (secondary antibody only) showing successful MBP staining in optic nerve tissue. (E) Immunostained optic nerve sections of dMBP (E1-4) and MBP (E5-8) for each cohort. Scale bar: D1 = 500 μ m, D2-4 = 50 μ m, E1-8 = 20 μ m. n = 3-4

Ultimately, a difference in MBP measurements was shown in the untreated cuprizone control cohorts. Here, the knockout mice showed a higher amount of myelin compared to the genetic control mice (Fig. 13 A). This supported the hypothesis that deleting GABA_B receptors improves myelin structure. Whereas cuprizone treated mice did not show any changes in myelin level, in MBP or dMBP fluorescence intensity measurements. But as seen before in the Western blot analyses of the *Non-induced_{ctrl}* cohort, cuprizone treatment led to a wide range of individual MBP measurement results among the mice (MBP range: cuprizone control: 4.061 genetic control, 5.726 knockout; cuprizone: 7.034 genetic control, 7.161 knockout). The MBP measurements therefore showed aligning results as seen in *Non-induced_{ctrl}* cohorts. No change was observed between the cuprizone treated genetic control mice and the cuprizone treated knockout mice. Within cuprizone treatment the GABA_B receptor knockout did not confirm the expected protection of myelin. (Cuprizone control: 5.694 ± 1.160 genetic control, 7.864 ± 1.914 knockout; cuprizone: 7.003 ± 2.190 genetic control, 6.572 ± 2.305 knockout).

In contrast to MPB, the dMBP cuprizone controls showed no change in cohort values. All means showed little or no shift. The untreated knockout cohort showed one outlier (light blue mice, Grubbs outlier test, Alpha = 0.2) which, however, does not substantial shift the final mean value. dMBP also showed a large range in between individual mouse values. Considering the outlier in the untreated knockout cohort, the range is particularly striking in the cuprizone treated mice and is therefore an indication of a change, of whatever nature, after cuprizone treatment. (Cuprizone control: 1.437 ± 0.4047 genetic control, 1.664 ± 0.5131 knockout; cuprizone: 1.316 ± 0.4331 genetic control, 1.428 ± 0.4171 knockout). While the immunohistochemistry results of MBP showed a difference in the cuprizone control mice, the cuprizone treatment actually resulted in a wide range of values in all cohorts. This raises the question of whether the new formulation of the cuprizone dietary protocol leads to myelin changes in the optic nerve tissue, and if so, how and when they are expressed. Further studies are needed in different age groups, adjusted cuprizone treatment protocols.

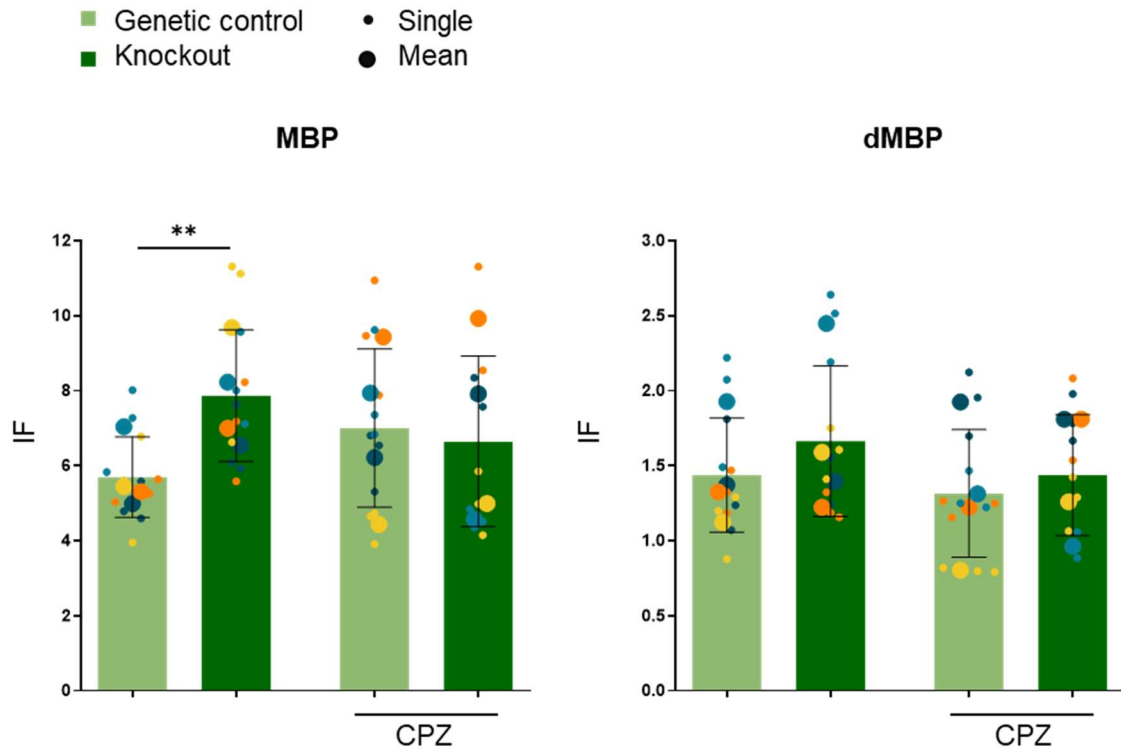
A

Figure 13. Increase of MBP expression level in knockout mice of cuprizone control cohorts. (A) Measured fluorescence intensity of MBP and dMBP in the optic nerve in all groups, normalized to DAPI. Error bars indicate mean with SD of the cohort. One color represents one animal, with large dots representing the mean for each mouse and small dots representing single slices of the sectioned optic nerve. A two-tailed t-test was used for statistical analysis: * ($p < 0.05$), ** ($p < 0.01$), *** ($p < 0.001$), **** ($p < 0.0001$). $n = 3-4$

3.6.2 Immunohistochemistry revealed cuprizone treated mice with astroglial activation

To further observe processes like gliosis around demyelinating events, I focused on the activity of astrocytes and microglia. I used glial fibrillary acidic protein (GFAP) as the most common marker for reactive astrocytes (van der Valk & Amor, 2009; Zhang et al., 2019). Astroglial activation was expected after myelin loss and could already been shown in spinal cord observations with the same cuprizone food protocol formulation (Dallorto, 2021, Master Thesis).

On the other hand, to study pathological behavior in the CNS, microglial activation must also be considered. Hardly any disease process in the CNS occurs without the involvement of microglial dys-/functions (Liddelow et al., 2017; Ransohoff, 2016). Therefore, I worked with the widely used anti-ionized calcium-binding adapter molecule 1 (Iba1) antibody to detect microglia and monocyte appearance (Ahmed et al., 2007; Zhan et al., 2020). Anti-Iba1 antibodies do not selectively label microglial cells, but they serve as a highly effective tool for labeling monocytes and their derivatives (Ginhoux et al., 2010; Q. Li & Barres, 2018). After cuprizone induced demyelination, the expectation would be an inflammatory response and a consequent activation of the immune system. At the cellular level, I would anticipate a proliferation of microglia cells and astrocytes.

GFAP and Iba1 fluorescence intensity were measured in all four cohorts. The immunohistochemistry was performed with one optic nerve of each mouse (Fig. 14 D1). Simultaneously a successful staining was controlled via negative control (Fig. 14 D3-4). While Iba1 primarily marks the cell body with in particular its fine peripheral processes, GFAP mainly marks the stem extensions (Zhan et al., 2020). The light green staining shows the thicker GFAP astrocyte bodies, while the purple Iba1 staining presents narrow microglial cell spurs (Fig. 14 D2, white arrows).

Especially in GFAP measurements, the cuprizone treated mice showed a wider range of individual mouse value (GFAP range: cuprizone control: 1.058 genetic control; 1.323 knockout, cuprizone: 1.880 genetic control; 2.536 knockout) (Fig. 15 A), same as seen before in the *Non-induced_{ctl}* cohort as well as in the MBP and dMBP measurements of *GABA_{knockout}* cohort.

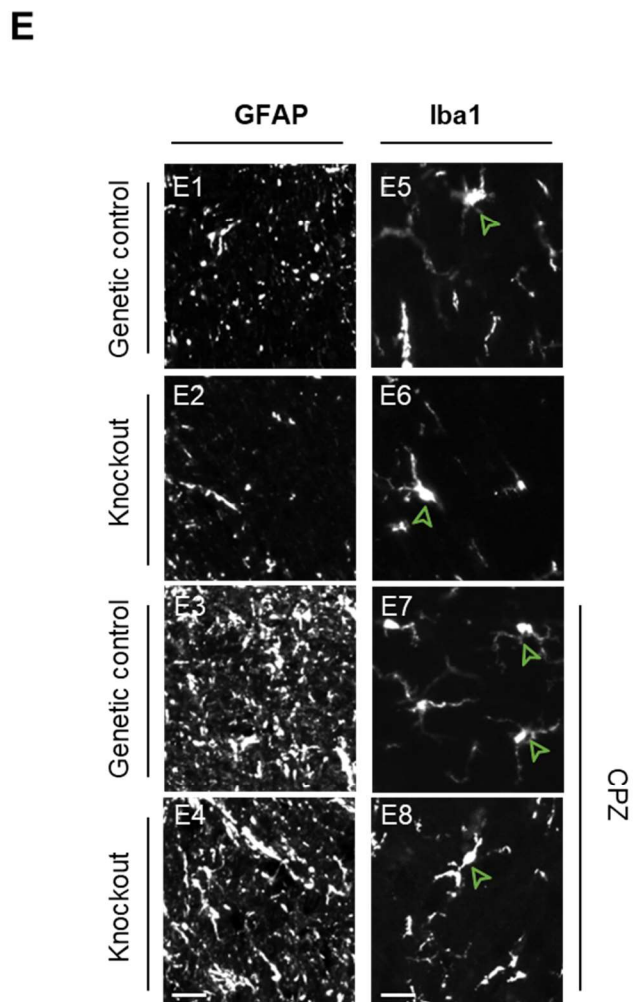
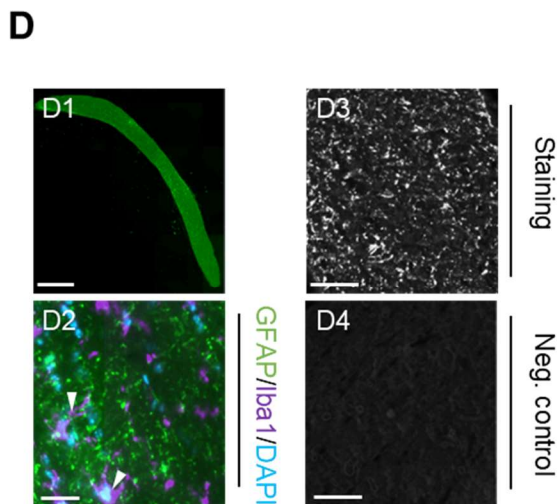
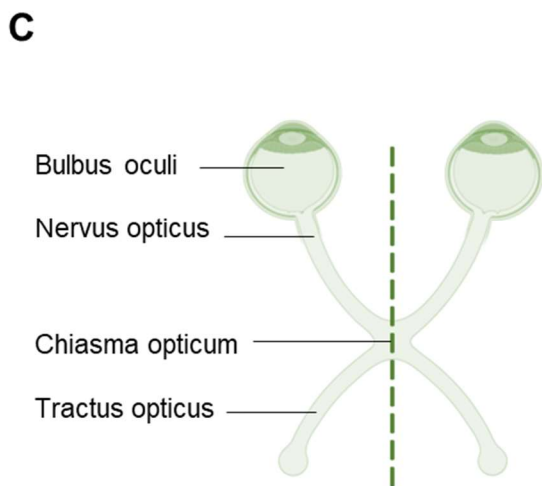
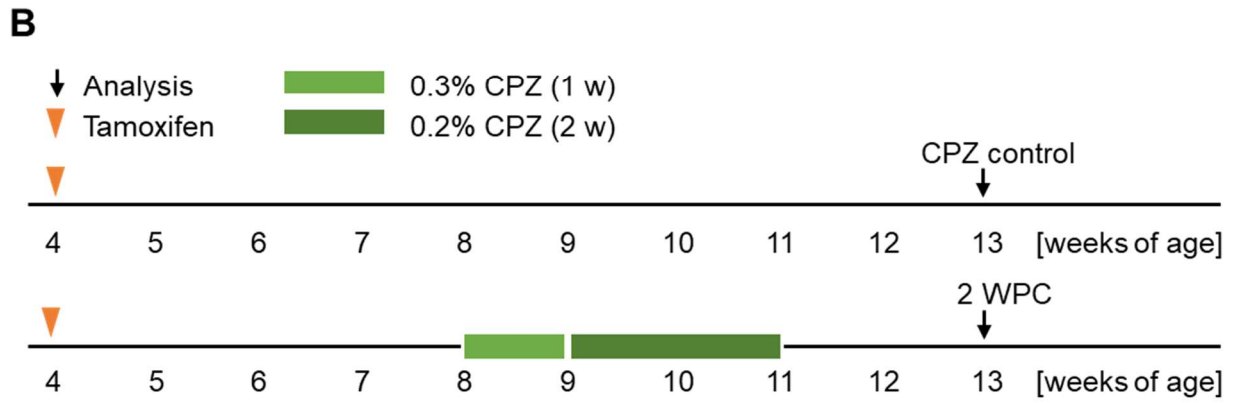
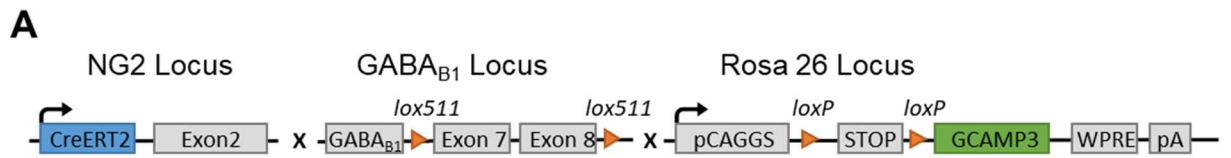


Figure 14. Comparison of GFAP and Iba1 expression level. (A) Construct of GABAB^{fl/fl} x NG2-CreERT2 x GCaMP3 mice. (B) Experimental plan for CPZ treatment. (C) Scheme of optic nerve tissue preparation showing the division made for Western Blot and IHC analysis. (D1) Exemplary overview presentation of cryostat cut optic nerve stained with GFAP and (D2) merge showing both, the GFAP and Iba1 staining in color. Iba1 cells counted for quantification are exemplary marked with white arrowheads. (D3-4) Comparison of GFAP with negative control (only secondary antibody) showing a successful GFAP staining in optic nerve tissue. (E) Immunostained optic nerve slices of GFAP (E1-4) and Iba1(E5-8) for each cohort. Scale bar: D1 = 500 μ m, D2 = 25 μ m, D3-4 = 50 μ m, E1-8 = 20 μ m. n = 3-4

The entire optic nerve showed strong GFAP expression with a sometimes difficult delineation of the astrocytes from the background tissue (Fig 14 D2). An increase of astroglial activity was seen between the genetic control cohorts (cuprizone control: 1.856 ± 0.3125 genetic control; cuprizone: 2.261 ± 0.5026 genetic control). Here, the cuprizone treated mice showed higher level of astroglial activity compared to the untreated control group. This indicates an inflammatory reactions two weeks after the ending of cuprizone treatment in the optic nerve. Those results are aligning with spinal cord investigation from the department performed at the same time period (Dallorto, 2021, Master Thesis)

The knockout cohorts did not show any change in astrocyte activity. Neither compared to their genetic control nor to the cuprizone treated knockout mice. There was merely a tendency towards heightened GFAP expression post cuprizone treatment, which becomes apparent when looking at the histological images, where both cuprizone treated groups showed a denser appearance of astrocytes (Fig. 14 E). The intracohort values of cuprizone treated knockout mice diverge strongly. This may suggest a divergent response to cuprizone treatment. (Cuprizone control: 1.856 ± 0.3125 genetic control, 2.034 ± 0.3528 knockout; Cuprizone: 2.261 ± 0.5026 genetic control; 2.454 ± 0.9893 knockout).

In addition to astrocyte reactivity, microglial activation was examined and determined by Iba1 positive cell counting. Mice with deletion of the GABA_B receptor showed no change in Iba1 level. However, there was a slight tendency of increased microglial level for the cuprizone treated genetic control mice to towards the cuprizone control mice. Similar to astroglial activation, the microglial activity tended to be increased after cuprizone treatment. Larger cohorts should be studied in this regard. The knockout cohorts did not show any change and similar was seen comparing cuprizone treated cohorts, the microglial activity appeared unaltered. (cuprizone control: 148.6 ± 26.49 genetic control; 171.1 ± 31.36 knockout, cuprizone: 189.6 ± 26.39 genetic control; 189.3 ± 58.90 knockout).

Overall, the main difference was seen when comparing astrocyte activity in cuprizone control mice versus treated mice. The astrocyte and microglial results are vaguely aligning in terms of increased activity after cuprizone treatment. Thus, astrocyte activity in the optic nerve tissue was consistent with measurements in the spinal cord and brain (Dallorto, 2021, Master Thesis; Zhan et al., 2020). In order to draw conclusions about the cuprizone treatment, astroglial and microglial measurements would have to be aligning. A clear change was the scatter of the individual values after cuprizone treatment. The increase in staining was indicative of an ongoing change in the cells under cuprizone.

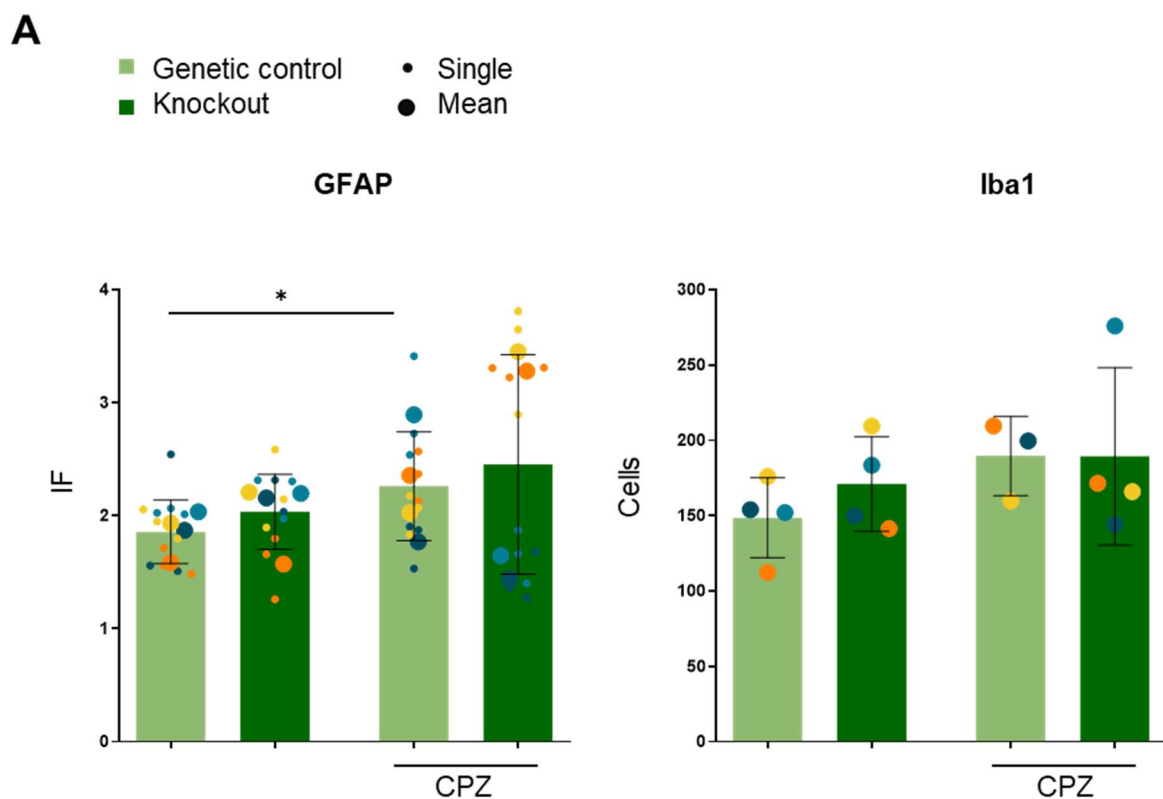


Figure 15. Increase of GFAP expression in genetic control mice after cuprizone treatment. (A) Measured fluorescence intensity of GFAP and counted cells per mm² Iba1 in the optic nerve of all groups, normalized to DAPI. Error bars indicate the mean with SD of the cohort. One color represents one animal, with large dots representing the mean for each mouse and small dots in GFAP representing the individual slice of the sectioned optic nerve. A two-tailed t-test was used for statistical analysis: * ($p < 0.05$), ** ($p < 0.01$), *** ($p < 0.001$), **** ($p < 0.0001$). $n = 3-4$

3.7 Western blot analyses investigating the effects of cuprizone treatment and GABA_B receptor loss on protein expression changes during the remyelination phase in the optic nerve

To further quantify glial activity in the *GABA_Bknockout* group, Western blot analysis were performed. I again used the two proteins myelin basic protein (MBP) and glial fibrillary acidic protein (GFAP). Both were investigated for optic nerve tissue via immunohistochemistry, where already one nerve of each mouse was used for fluorescence measurements (Fig. 16 C). Both markers were now used for Western blot performance to investigate optic nerve myelin level changes and astroglial activation after cuprizone treatment and the concurrent influence of the deleted GABA_B receptor. In terms of myelin processes, I would expect to see a reduction in myelin levels after cuprizone treatment, with less severe effects in the knockout animals. This would suggest a protective factor of the GABA_B knockout leading to less profound demyelination. The Western blot analyses were performed the same way as for the *Non-induced_{ctl}* group.

The Western blot results from optic nerve tissue did not show any change in myelin proteins (Fig. 16 E). The findings therefore corresponded with the results of the immunofluorescence measurements. The cuprizone treated cohorts appeared to have almost identical MBP level. The same applied to the knockout cohorts with and without cuprizone treatment. In contrast to the immunohistochemical staining and the results of the *Non-induced_{ctl}* group, myelin level in genetic control cohorts tended to show more of a decrease after cuprizone treatment. But the effect did was weak and the cohort additionally showed the highest range of individual mouse values. It is also particularly noticeable that the respective values of the first (circle) and second (triangle) Western blot are relatively deviating from each other.

Subsequently no difference in the MBP Western blot results based on their mean value were found (cuprizone control: 1.000 ± 0.2392 genetic control; 0.8633 ± 0.1611 knockout). Overall, the MBP Western blot results remain questionable especially considering that tissues from the same mice were used for both immunohistochemistry and Western blot analyses. (cuprizone control: 1.000 ± 0.2392 genetic control; 0.8633 ± 0.1611 knockout, cuprizone: 0.8628 ± 0.1925 genetic control; 0.8275 ± 0.1681 knockout).

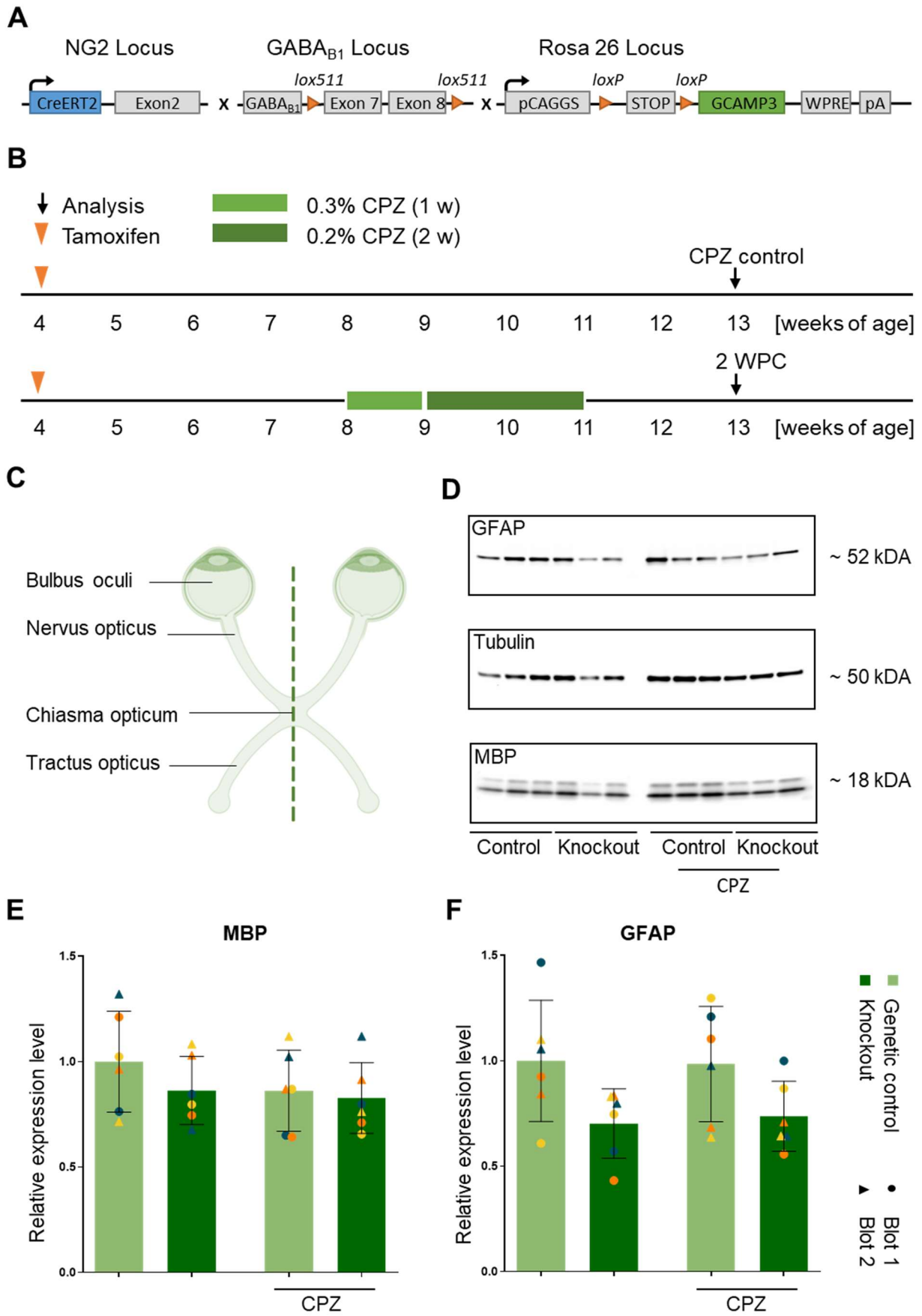


Figure 16. No change of protein level measurable in CPZ treated or knock-out cohorts. (A) Construct of *GABAB1/fl x NG2-CreERT2 x GCaMP3* mice. (B) Experimental plan for CPZ treatment. (C) Scheme of optic nerve tissue preparation showing the division made for Western Blot and IHC analysis. (D) blot 1 of treated mice two weeks after ending CPZ treatment (2 WPC) and their untreated age-related control group. As target proteins MBP and GFAP were used to investigate myelin level and astroglial activation changes. As a housekeeping gene, tubulin was used. (E-F) Quantification of MBP (E) and GFAP (F) level. Bars illustrate the means with SD. Each color represents one mouse, whereby dots show blot 1 and triangles the repetition, Blot 2, which was executed at different time points variety. Values were normalized to tubulin and additionally to the mean of their age-related untreated control group. $n = 3$

Astrocyte activation was tracked by GFAP measurements and showed no significant results. All four cohorts displayed a wide range and variability of mouse values. While fluorescence intensity measurements in particular showed a significant difference between the genetic control mice, Western blot analysis showed only trends that were in contrast to the immunohistochemistry results. The values from genetic control to knockout mice, both within the cuprizone treatment and cuprizone control groups, showed a tendency toward decreased astroglial activity after deletion of the $GABA_B$ receptor (cuprizone control: 1.000 ± 0.2878 genetic control; 0.7023 ± 0.1646 knockout, cuprizone: 0.9850 ± 0.2732 ; 0.7370 ± 0.1658). In the immunohistochemistry, no similar trends were observed and both control cohorts tended to higher astroglial values than mice without the $GABA_B$ receptor.

Regardless of the cuprizone diet, the knockout animals had similar mean values. The same applied to the genetic control cohorts, also showing no difference towards cuprizone treatment. The ratio of knockout to genetic controls from the cuprizone treated versus cuprizone control cohorts appeared to be close to one, implicating that there is no difference in the proportions (ratio of decreasing GFAP tendency cuprizone cohorts/cuprizone control cohorts= 1.0654). Therefore, the results were to demonstrate a detectable effect of the new cuprizone powder food protocol formulation by Western blot analysis based on optic nerve tissue. The $GABA_B$ knockout subsequently showed a tendency to decreased GFAP expression in knockout mice. The Western blot data tended to display an astrocyte downregulation as seen in previous data from the department. All of the Western blot analysis showed a strong scattering of the values and, as already seen in MBP measurements. Additionally, there appeared to be variations in the individual western blot runs' respective values. Larger cohorts should be investigated to further point out the difference between immunohistochemistry and Western blot results. Especially in combination with both analysis methods, it should be possible to set directing statements about the changes in optic nerve tissue.

3.8 Corpus callosum and other brain areas reveal astroglial and microglial activation two weeks after cuprizone treatment

To compare the results of my optic nerve research not only with previous data from the department, but also with concurrent data from other regions of the CNS, I extended the investigation to include the brain tissue of the *GABA_B knockout* mice. This would allow to directly correlate the events in the optic nerve with the findings in the mouse brain. Since these are the same animals on which the optic nerve studies were conducted, the same modified cuprizone treatment protocol was applied.

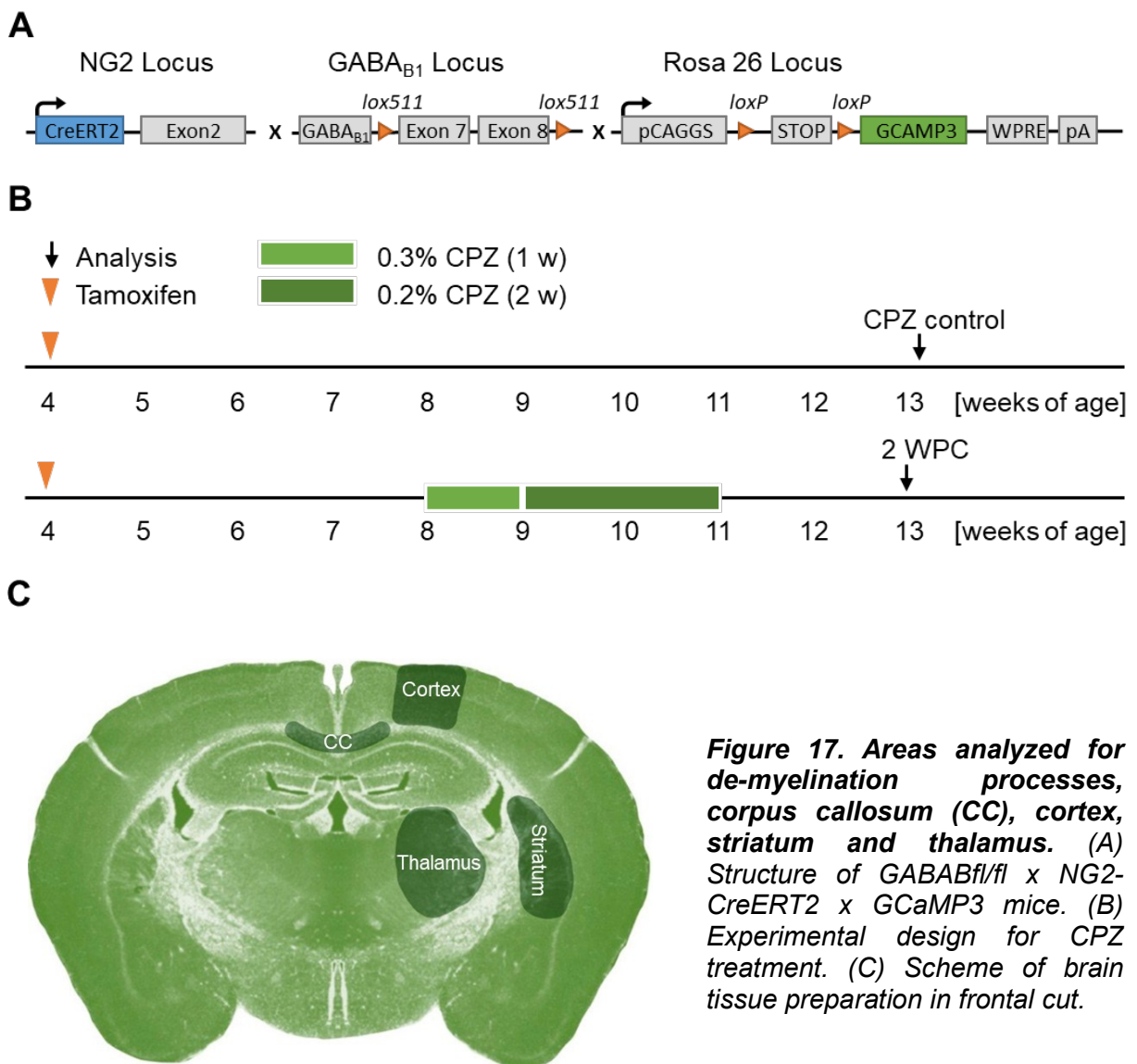


Figure 17. Areas analyzed for de-myelination processes, corpus callosum (CC), cortex, striatum and thalamus. (A) Structure of *GABAB^{fl/fl} x NG2-CreERT2 x GCaMP3* mice. (B) Experimental design for CPZ treatment. (C) Scheme of brain tissue preparation in frontal cut.

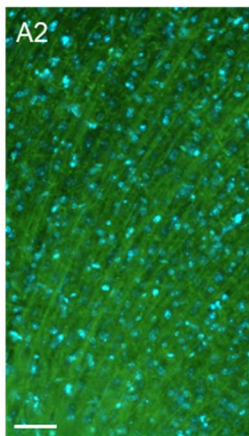
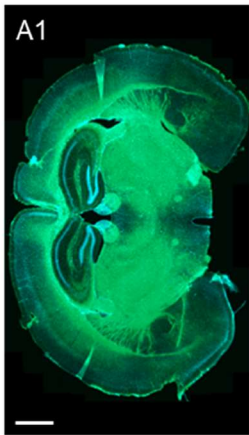
Ultimately, four groups were formed, two knockout cohorts and two genetic control cohorts with one group each treated with cuprizone and one cuprizone control group. Since I neither wanted to dissect the brain tissue into halves nor to split the cohort, to avoid smaller samples I only performed immunohistochemistry analyses. Fluorescence intensity measurements from the brain were normalized to the fluorescence intensity of the fimbria area as basic value of the cell distribution. Microglial cells, meanwhile, were tallied and standardized with concurrent cell counting of the fimbria. The ZEN blue software was utilized for measurements, cell counting, and analyses.

To classify upon the optic nerve findings, I analyzed further regions of the CNS. In addition to the pioneer region of the corpus callosum, I investigated different areas for demyelination processes induced by cuprizone. Beyond the latter the cortex, the striatum and the thalamus area were examined (Fig. 18 B).

For fundamental investigations of neuronal activity, I used the same markers as already presented for optic nerve tissue. In order to identify differences in myelination via immunohistochemistry, myelin basic protein (MBP) was examined. So far optic nerve tissue seemed to be resilient in terms of oligodendroglial change towards the cuprizone powder food protocol. In general, with the modified cuprizone diet I would expect a downregulation of myelin level, as has been seen before in spinal cord measurements (Dallorto, 2021, Master Thesis)

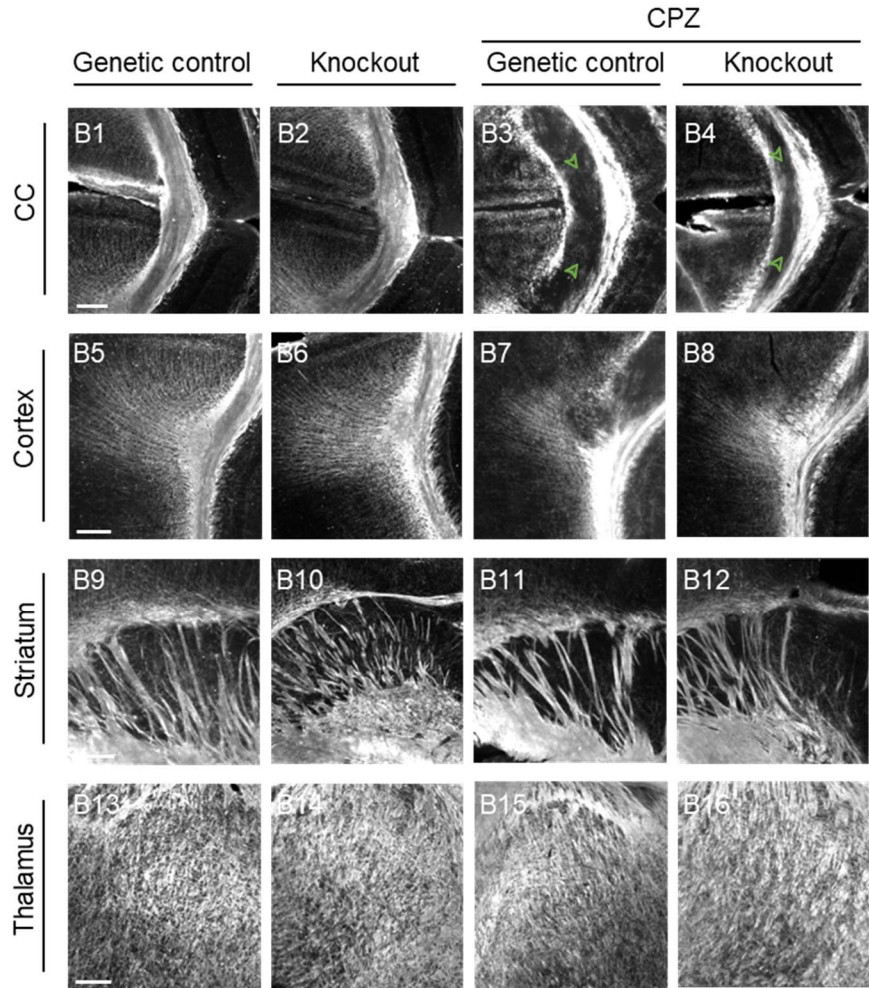
However, as already seen in the optic nerve studies, it was particularly noticeable in the brain tissue that MBP measurements showed a wide range of values (Fig. 18 C). Due to the wide scatter of values, the MBP staining did not show any change among the groups. Nevertheless, all regions surveyed showed tendencies of decreased myelin level after cuprizone treatment. This would underline a successful demyelination after cuprizone powder food protocol formulation. On the other hand, statements about the knockout effect could only be made cautiously, since there were no clear trends, and the strong scatter of the values was a further complicating factor. Larger cohorts with additional myelin markers should be studied for this purpose. (CC cuprizone control: 8661 ± 4527 genetic control, 8086 ± 3892 knockout; Cuprizone: 4940 ± 4234 genetic control, 3328 ± 3607 knockout; Cortex cuprizone control: 2979 ± 2483 genetic control, 3682 ± 2650 knockout; Cuprizone: 1658 ± 1243 genetic control; 2093 ± 3158 knockout; Striatum cuprizone control: 5077 ± 3533 genetic control, 7033 ± 4794 knockout; Cuprizone: 3432 ± 1730 genetic control, 4026 ± 5304 knockout; Thalamus cuprizone control: 7618 ± 4273 genetic control, 8555 ± 4733 knockout; Cuprizone: 5849 ± 2902 genetic control, 2618 ± 923.4 knockout).

A Overview



DAPI / MBP

B



C

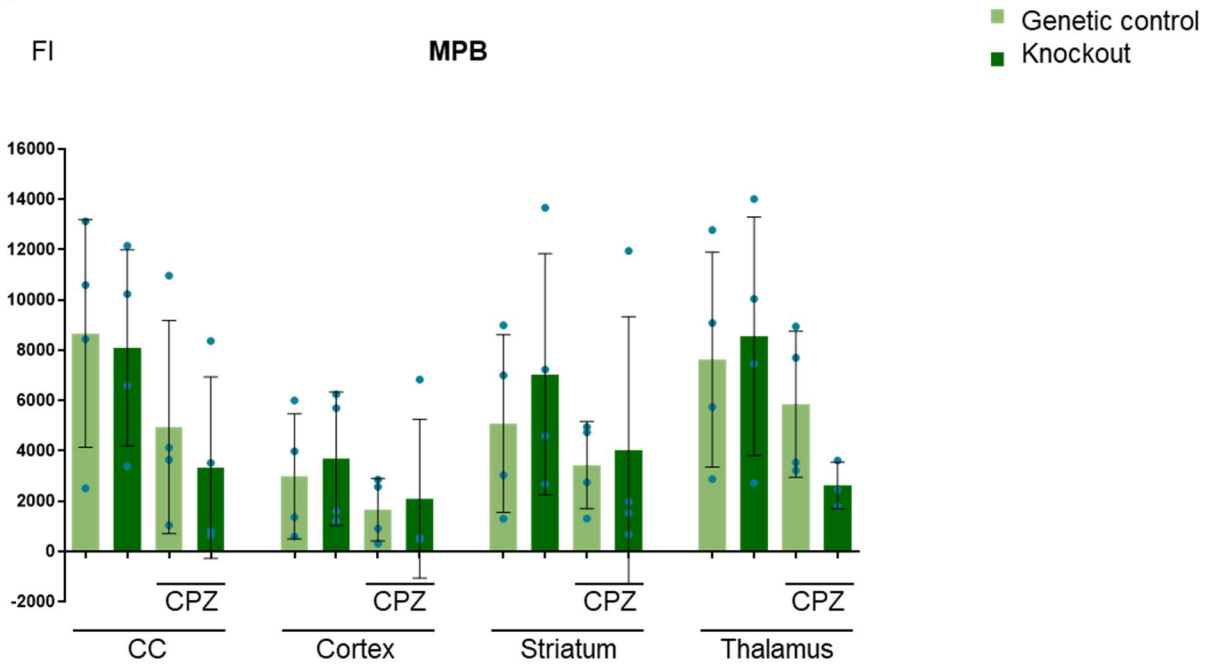


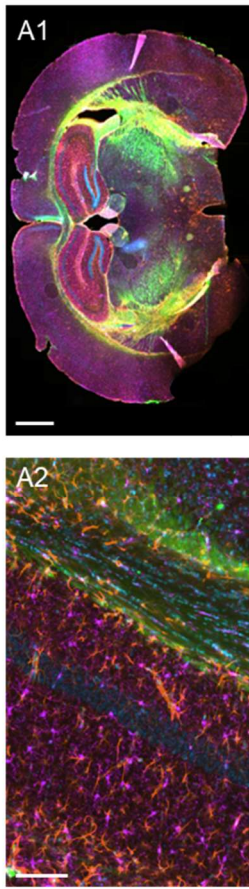
Figure 18. No change in MBP levels. Tendencies of decreased myelin levels after CPZ treatment. (A1) Overview of vibratome sectioned and stained brain tissue (A2) with corresponding MBP merge in color. (B) Immunostained brain sections of MBP for each cohort showing the areas of corpus callosum (CC), cortex, striatum, and thalamus. (C) Measured fluorescence intensity of MBP in all groups, normalized to the area of the fimbria. Error bars indicate mean with SD of the cohort. Each point represents one mouse. Two-tailed t-test was used for statistical analysis. Scale bar: A1 = 1000 μ m, A2 = 50 μ m, B1-12 = 200 μ m. CPZ = cuprizone. n = 4

The individual brain regions all behaved similarly in terms of the missing strong response towards cuprizone. However, most of the observed areas appeared to exhibit a trend consistent with the anticipated demyelination. Overall, MBP measurements tended to support a demyelinating event two weeks after ending cuprizone treatment in the early remyelination phase (2 WPC). In any case, larger cohorts ought to be evaluated using conceivably additional myelin markers.

Furthermore, astroglial and microglial activity was captured. I used the most common astroglial marker, glial fibrillary acidic protein (GFAP) (Fig. 19), which is found in polymerized activated astrocytes in situations of gliosis (Eng & Ghirnikar, 1994). In addition, I examined the ionized calcium-binding adaptor molecule 1 (Iba1) (Fig. 20), as it is known to be a specific marker for microglia in the CNS (Ahmed et al., 2007). GFAP and Iba1 were therefore examined immunohistochemically to investigate astroglial and microglial activation after cuprizone diet in the remyelination phase (Gudi et al., 2014). Optic nerve tissue already showed a trend toward increased astrocyte and microglial level in cuprizone treated mice. The same was seen in spinal cord tissue with identical cuprizone powder diet protocol formulation (Dallorto, 2021, Master Thesis) and also with previous hard block cuprizone diet (Damo, 2019, Master Thesis).

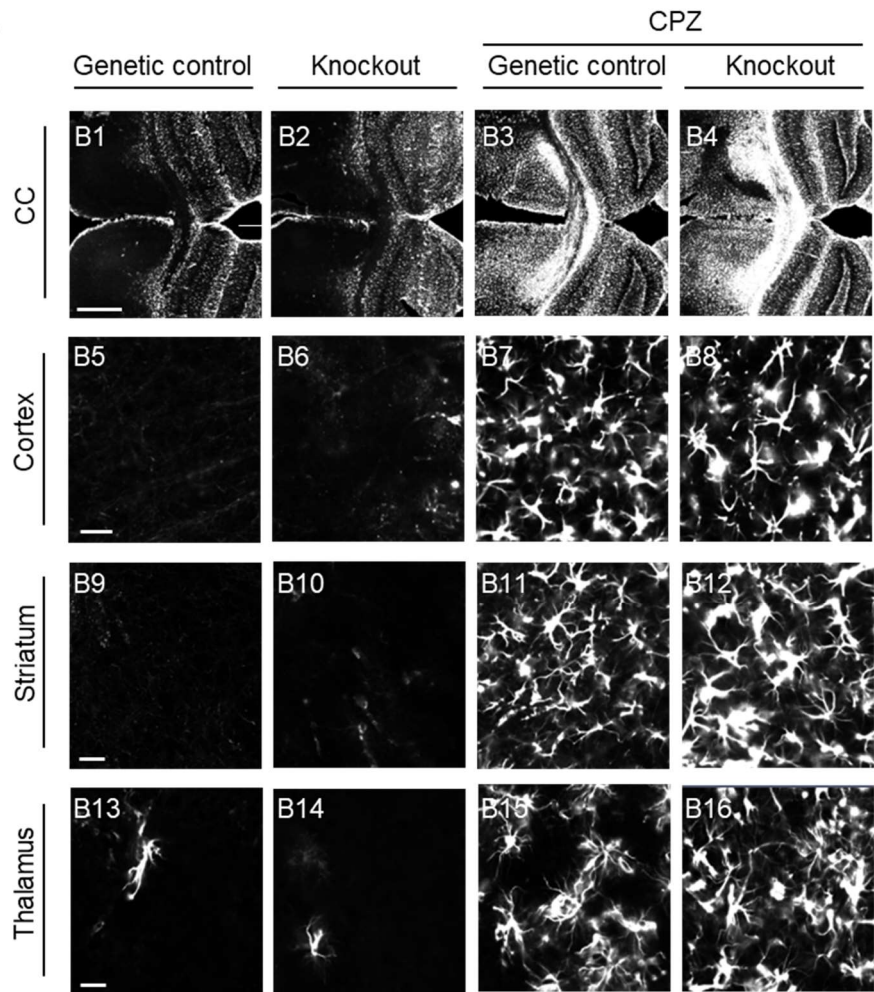
Significant changes were seen in the cuprizone treated cohorts towards their untreated age related control mice. GFAP also showed some scattering, mainly in the cuprizone treated groups, but by far not to the same extent as MBP results. Corpus callosum, cortex and thalamus presented a significant increase of astrocytes after cuprizone treatment in the genetic control cohorts (Fig. 19 C). These results aligned with optic nerve findings. The same areas also showed significant increase in astroglial activity within the knockout cohorts after cuprizone diet.

A Overview



DAPI/Iba1/
GFAP/MBP

B



C

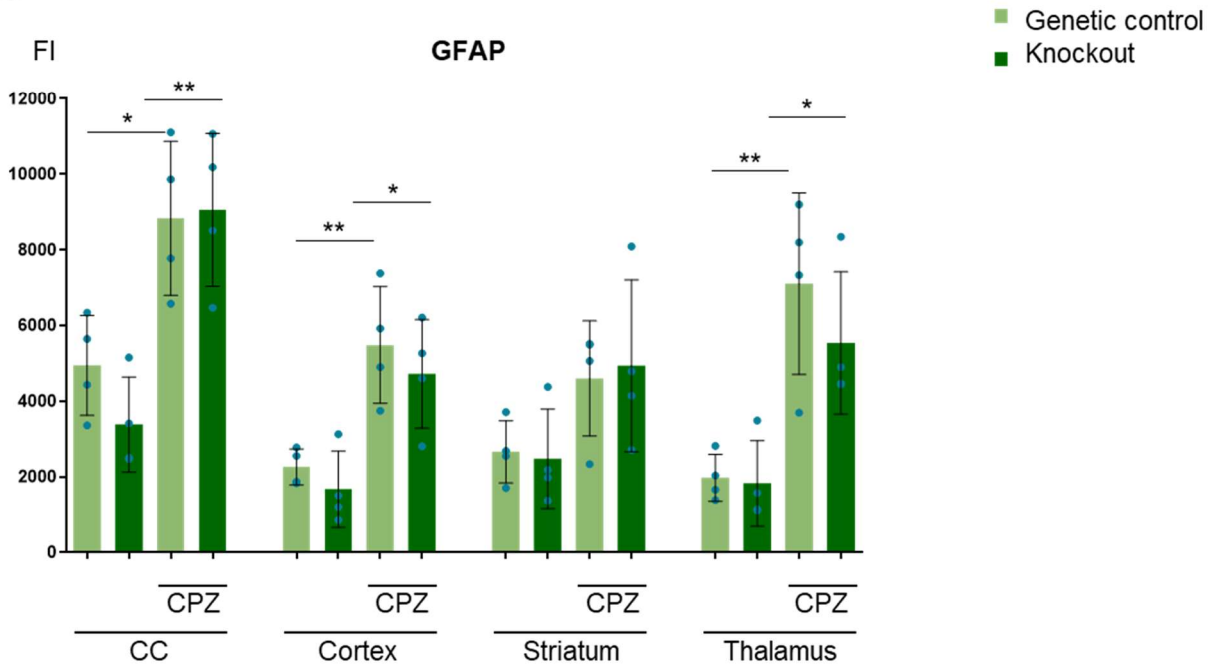


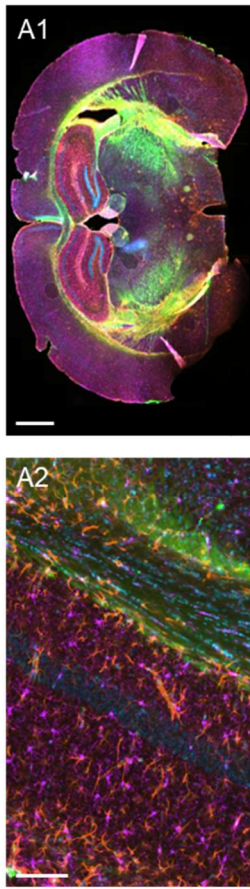
Figure 19. Significant increase of astroglial activity (GFAP) in knockout and genetic control mice after CPZ diet in areas of corpus callosum (CC), cortex and thalamus. (A1) Overview of vibratome sectioned and stained brain tissue (A2) with corresponding GFAP merge in color. (B) Immunostained brain sections for GFAP for each cohort showing the areas of corpus callosum (CC), cortex, striatum, and thalamus. (C) Measured fluorescence intensity of GFAP in all groups, normalized to the area of the fimbria. Error bars indicate mean with SD of the cohort. Each point represents one mouse. A two-tailed t-test was used for statistical analysis: * ($p < 0.05$), ** ($p < 0.01$), *** ($p < 0.001$), **** ($p < 0.0001$) Scale bar: A1 = 1000 μm , A2 = 50 μm , B1-4 = 200 μm , B5-16 = 25 μm . $n = 4$

(CC cuprizone control: 4944 ± 1317 genetic control; 3384 ± 1257 knockout, cuprizone: 8832 ± 2036 genetic control; 9059 ± 2025 knockout; Cortex cuprizone control: 2258 ± 477.8 genetic control; 1673 ± 1002 knockout, cuprizone: 5486 ± 1542 genetic control; 4721 ± 1436 knockout; Thalamus cuprizone control: 1974 ± 622.1 genetic control; 1828 ± 1127 knockout, cuprizone: 7106 ± 2398 genetic control; 5539 ± 1881 knockout). The striatum displayed tendencies in the same direction as the other regions, although it was the only area that did not exhibit significant changes in astrocyte activation. This trend was also reflected in the histological images, where the striatum showed a clear astroglial activation in all cuprizone treated cohorts, marked by a concise increase in GFAP stained cells (Fig. 19 B). (Striatum cuprizone control: 2662 ± 823 genetic control; 2476 ± 1313 knockout, cuprizone: 4601 ± 1525 genetic control; 4933 ± 2276 knockout).

Overall, the main difference was always shown from cuprizone control to cuprizone treated mice with a reactive increase of astrocyte activity after myelin destruction. Here too, the knockout effect did not cause much of a difference. Although in all areas, the cuprizone control mice present slight tendencies of decreased astrocyte activity in knockout groups. Nonetheless a successful astrocyte activation two weeks post cuprizone treatment in the early remyelination phase (Gudi et al., 2014) (2 WPC) was shown in all areas and therefore support a situation of glial change after cuprizone powder food formulation treatment.

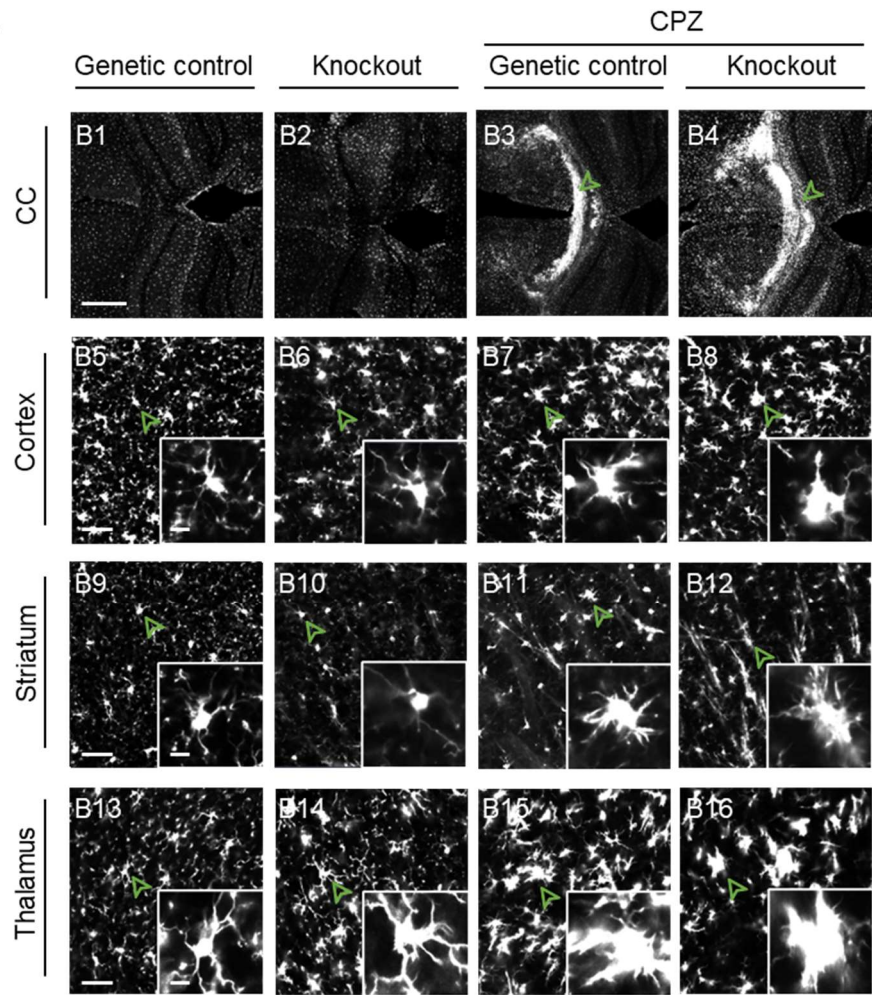
Measurements of microglial activity in the corpus callosum were consistent with the GFAP results (Fig. 20 C). Again, the cuprizone treated cohorts showed an increase in microglial activity towards the cuprizone control mice (CC cuprizone control: 7230 ± 1490 genetic control; 6038 ± 1301 knockout, cuprizone: 21291 ± 8054 genetic control; 24454 ± 11032 knockout). Cuprizone treatment indeed resulted in a higher scatter of values compared to the cuprizone control mice. Nevertheless, the genetic control mice showed a huge increase in microglial activity after cuprizone diet. The same applied to the knockout cohort, which also showed an increase in Iba1 level after the cuprizone powder chow protocol. Similar to the GFAP studies, the knockout effect could not be demonstrated to the expected extent.

A Overview



DAPI/Iba1/
GFAP/MBP

B



C

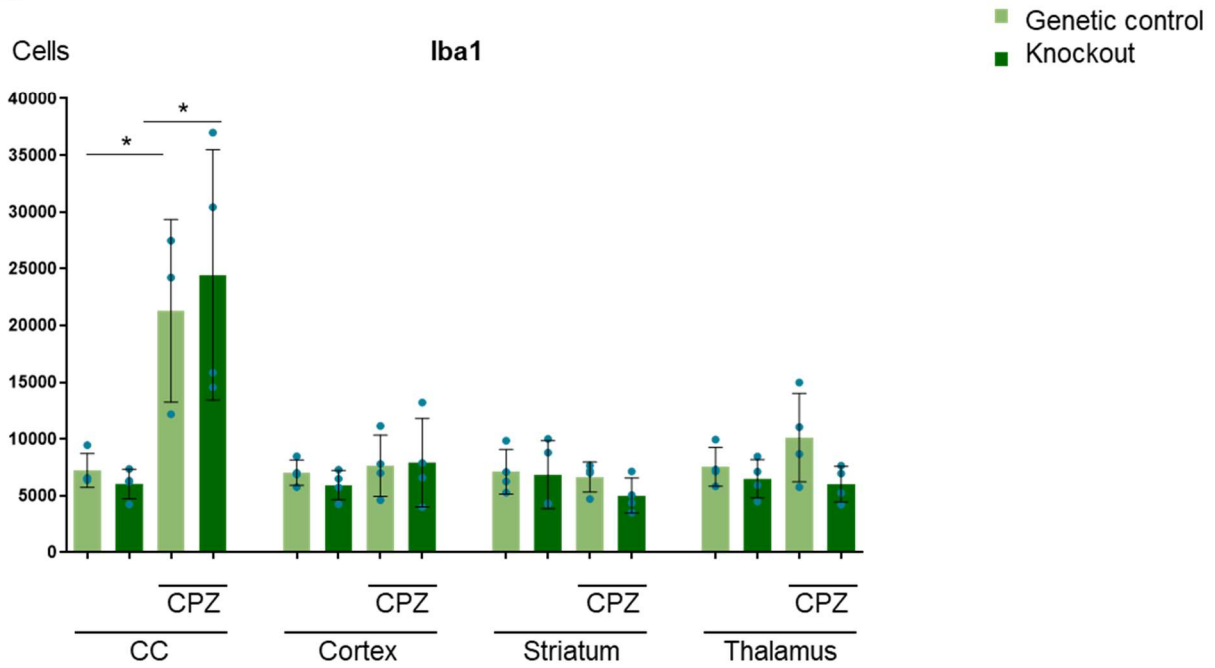


Figure 20. Increase of microglia (Iba1) activation in knockout and genetic control after CPZ diet in the corpus callosum (CC). (A1) Overview presentation of vibratome cut and stained brain tissue (A2) with corresponding Iba1 merge in color. (B) Immunostained brain sections of Iba1 for each cohort showing the areas of corpus callosum (CC), cortex, striatum and thalamus. (C) Number of Iba1-positive cells in all groups, normalized to the area of the fimbria. Error bars indicate mean with SD of the cohort. Each point represents one mouse. Two-tailed t-test was used for statistical analysis: * ($p < 0.05$), ** ($p < 0.01$), *** ($p < 0.001$), **** ($p < 0.0001$). Scale bar: A1 = 1000 μm , A2 = 50 μm , B1-4 = 500 μm , B5-16 = 50 μm , B5-16 Cell-Zoom = 10 μm . $n = 4$

However, these findings could not be transferred to the other brain regions studied. Neither the cortex, striatum nor thalamus showed any tendency for altered microglial activity in the form of increased cell numbers. Here, both cuprizone treatment and GABA_B knockout did not display changed Iba1 activity. Nevertheless, the microscopic examination of the histological sections did reveal a modification. Not in the quantity of microglial cells but in their morphology. In all cohorts treated with cuprizone, the microglial cells showed notably greater size and stronger extensions compared to the cuprizone control cohorts. This trend was consistent across all brain regions assessed (Fig. 20 B). (Cortex cuprizone control: 7033 \pm 1114 genetic control; 5944 \pm 1293 knockout, cuprizone: 7639 \pm 2704 genetic control; 7917 \pm 3889 knockout, Striatum cuprizone control: 7116 \pm 1965 genetic control; 6857 \pm 2988 knockout, cuprizone: 6642 \pm 1317 genetic control; 5021 \pm 1542 knockout, Thalamus cuprizone control: 7556 \pm 1722 genetic control; 6499 \pm 1697 knockout, cuprizone: 10119 \pm 3893 genetic control; 6018 \pm 1572 knockout).

Anyhow, a successful microglial activity increase could be proven in corpus callosum areas two weeks post cuprizone treatment (2 WPC) and can therefore support the efficiency of the new cuprizone powder food protocol formulation.

4. Discussion

Multiple Sclerosis (MS) is a progressive autoimmune disease of the central nervous system (CNS). It is characterized by chronic inflammation and eventually demyelination, gliosis and neuronal loss among other things (Compston & Coles, 2002; Gold, Wolinsky, Amato, & Comi, 2010; Noyes & Weinstock-Guttman, 2013). Focal events typically occur in the form of plaques within the white matter (Matute & Pérez-Cerdá, 2005). Although it is known that inflammatory processes occur simultaneously with neuronal degeneration (Trapp et al., 1998), it has yet not been possible to identify a molecular trigger for these demyelinating events. So far, landmarks of treatment appear in the form of oligodendroglial demise, astrogliosis and activation of immune cells such as microglia, and finally axonal loss (Lassmann, 2014). Subsequently, this axonal damage is responsible for the neurological symptoms and clinical manifestations of MS, which, among other, include visual impairment, weakness, numbness, cognitive dysfunction, vertigo, spasticity, and balance or coordination problems (Calabresi, 2004; Chiaravalloti & DeLuca, 2008). However, in order to establish the best possible treatment regimens, it is important to fully understand the pathogenesis of MS and to find the mechanisms that specifically affects myelin and oligodendrocytes in conditions of demyelination. Many current studies focus on the influence of glial-myelin interactions within de- and remyelination. To gain these insights, animal models that mimic myelination are widely used. In this project, I chose to use cuprizone as a toxin-induced murine model of demyelination, which primarily affects oligodendrocytes (Barnett & Prineas, 2004). The latter are also abundant in the optic nerve. Here, the key component of optic nerve tissue is compact white matter which therefore mainly consist of glial cells and axons. Besides, a unique acting astrocyte population was suggested in specific parts of the optic nerve (Mazumder et al., 2022; Sun, Lye-Barthel, Masland, & Jakobs, 2009). In general, the visual system has a significant and distinct role in the course of MS. This is particularly evident since the introduction of the term clinically isolated syndrome (CIS) into the process of classification and diagnosis. CIS describes the first clinical episode within MS, reflecting an inflammatory demyelinating process and is often seen in the optic nerve (D. H. Miller et al., 2012; D. H. Miller et al., 2008; Polman et al., 2011). Therefore, I chose to concentrate the research on this part of the visual system. As numerous studies concentrate on CNS outcomes, I aimed to explore the optic nerve in addition to the ongoing research projects from the CIPMM laboratory. However, modeling de- and remyelination with optic nerve tissue has remained a challenge due to its limited accessibility, relatively small size, and dense nature (Pajoohehsh-Ganji & Miller, 2020).

4.5 Myelin gain after oligodendroglial GABA_B receptor loss and strong variability of myelin values after cuprizone powder food diet

Cuprizone, a copper-chelating agent, is one of the most commonly used models to study mechanisms around myelin changes (Praet et al., 2014) and to run drug testing trials in preclinical research. Many of its features are consistent with current histopathologic data in MS (Torkildsen et al., 2008). T and B cells are not thought to have a central role in cuprizone-induced demyelination (Hiremath, Chen, Suzuki, Ting, & Matsushima, 2008; Wolf et al., 2018), therefore, the toxin's effect does not represent the chronic inflammation observed in progressive MS (Kipp, Nyamoya, Hochstrasser, & Amor, 2017). Similar to relapsing-remitting MS (RRMS), white matter lesions regress after cuprizone withdrawal, leading some authors to suggest that the cuprizone model particularly mimics the RRMS disease course (Ransohoff, 2012; Vega-Riquer, Mendez-Victoriano, Morales-Luckie, & Gonzalez-Perez, 2019). Subsequently, compared to other animal models, the cuprizone model is particularly suitable for studying the mechanisms of the immune response that lead to myelin and axonal degeneration and monitoring remyelination processes (Kuypers, Bankston, Howard, Beare, & Whittemore, 2016; Lindner, Fokuhl, Linsmeier, Trebst, & Stangel, 2009; Skripuletz et al., 2013; Slowik et al., 2015; Voskuhl et al., 2019).

The exact mechanisms of oligodendroglial damage caused by cuprizone treatment have not been fully elucidated. By a toxic oxidative effect on mitochondria, cuprizone reduces energy metabolism and finally causes demyelination (Gudi et al., 2009; Kalman, Laitinen, & Komoly, 2007). Such involvement of mitochondria is also suggested for both, oligodendroglial death and tissue degeneration in MS (Kalman et al., 2007). Therefore, oligodendroglial cells are particularly amenable to cuprizone treatment due to their high metabolic demands (Hochstrasser, Exner, Nyamoya, Schmitz, & Kipp, 2017). However, the myelin destructing effect is indeed reversible leading to remyelination after cuprizone treatment is discontinued (Mohamed et al., 2019).

For my studies, I have defined two groups of mice. Both received the cuprizone treatment at eight weeks of age, starting with one week of 0.3 % cuprizone, followed by two weeks of 0.2 % cuprizone. After these three weeks of toxin, the first mice, the *Non-induced_{ctl}* cohort, were sacrificed at 11 weeks of age (0 WPC). They are thought to be in the early stages of demyelination since the cuprizone was just removed. While the second cohort was fed regular food for a subsequent two weeks (2 WPC). These mice, the *GABA_{knockout}* cohort, were

examined at 13 weeks of age and they were already supposed in a remyelination phase. Gudi et al. suggested that the peak of demyelination in the corpus callosum occurred after five weeks of cuprizone feeding, with the onset of a detectable remyelination phase between week five and six. Here, at the age of eight to 10 weeks, the mice received a 5-week treatment consisting of a modified dietary with a 0.2 % dose of cuprizone. During the first three weeks, an early phase of demyelination was observed, which turned into severe demyelination from week four onwards. The cuprizone treatment was stopped after the peak of demyelination in week five (Gudi et al., 2014). Based on this scheme, the mice in this study were classified and examined.

Looking at the optic nerve, recent studies have shown that cuprizone treatment also has an effect on the optic nerve tissue. Similarly, structural changes in myelin were observed after cuprizone feeding (Bagchi et al., 2014; Hainz et al., 2017; Namekata et al., 2014). It was also possible to detect functional changes in the retina (Namekata et al., 2014).

However, current data showed a significant reduction in the efficacy of the previously used cuprizone containing pellet formulation (Hochstrasser et al., 2017). In fact, the CIPMM department also had several problems inducing consistent demyelination after three weeks of cuprizone diet, as reported by several members of the laboratory. It has previously been demonstrated that utilizing freshly prepared daily cuprizone powder mixed with finely ground rodent chow resulted in strong and reproducible demyelination in the corpus callosum. Nevertheless, it should be reminded that the preparation is time consuming and carries the risk of inhalation of toxins (Hochstrasser et al., 2017). Subsequently, pellet fed was replaced with ground rodent chow which was provided for the mice at the age of eight weeks. The treatment protocol included one week of 0.3 % cuprizone diet followed by weeks of 0.2 % cuprizone diet.

Furthermore, the loss of the GABA_B receptor was monitored as a potential target for the treatment of MS. The receptor knockout was particularly observed in its role as a possible mediator for regulatory input on myelin interfering cells, which has already been demonstrated *in vitro*. Here, oligodendrocyte progenitor cells (OPCs) showed increased proliferation and migration rates when treated with a GABA_B receptor-specific agonist (baclofen) (Luyt et al., 2007; Serrano-Regal et al., 2019). In addition to astrocytes and neurons, the receptor is also expressed in cells of the oligodendroglial lineage, but indeed very little is known about GABA_B receptor in oligodendrocytes and OPCs. To investigate the effects of oligodendroglial GABA_B receptors influencing demyelination in the optic nerve, I used the conditional knockout mouse line on the GABA_B^{fl/fl} x NG2-Cre^{ERT2} x GCaMP3 (*GABA_Bknockout* cohort) and examined them two weeks after ending of cuprizone treatment.

To point out differences in myelination, immunohistochemical staining with fluorescence intensity measurements were executed for myelin basic protein (MBP) and degraded myelin basic protein (dMBP). The role of MBP has been extensively studied in MS models showing its responsibilities in the formation, maintenance and adhesion of cytosolic surfaces as these maintain the regular function of the myelin sheath (Boggs, 2006). By neutralizing membrane phospholipids, MBP pulls two bilayers together like a zipper, forming the main dense line and allowing myelin to grow (Min et al., 2009). As a result to the cuprizone diet, a decrease in MBP and an increase in dMBP fluorescence intensity was expected. The GABA_B receptor knockout was considered to have a protective effect on myelin. Also, previous data from the department suggested that knockout mice showed a less severe myelin loss and recovered myelin faster after demyelination than control mice. Therefore, a greater amount of myelin was expected in the knockout groups.

All fluorescence intensity measurements were normalized to DAPI to correct several variables and factors such as variations in antibody dilution, blocking efficiency, or differences in antigen retrieval that affect staining. Unlike spinal cord data, treated with the identical freshly prepared cuprizone powder food formulation, the optic nerve immunohistochemistry data revealed no changes in myelin expression after cuprizone treatment. However, the GABA_B receptor loss revealed a change in the *GABA_Bknockout* group. The cuprizone control animals showed significantly higher myelin levels in the knockout cohort. This supported the hypothesis of a myelin protective role through the GABA_B receptor knockout.

To supplement the findings from immunohistochemistry and compare changes in the protein levels of myelin, we conducted Western blot analysis. Tissue for Western blot analysis was snap frozen and stored at - 80 °C immediately after perfusion and was not fixed like tissue for immunohistochemistry. This prevented fixation induced tissue and protein changes such as shrinkage (Siu, Cheung, & Wong, 1986). In addition, all samples used for Western blot analysis were homogenized and processed simultaneously, at least within each cohort. Subsequently, Western blot data did not reveal any changes. No reduction in myelin expression was observed after cuprizone diet in either the *Non-induced_{ctl}* or *GABA_Bknockout* group. The same applied for the GABA_B receptor loss, which did not result in any alterations towards myelin. Notably, the *Non-induced_{ctl}* group exhibited a strong increase in the variability of individual values in the cuprizone treated animals.

Western blot analyses are commonly used since they avoid typical sources of error by processing all samples at the same time and under the same conditions. To prevent potential inaccuracies in protein loading, housekeeping genes were used as an internal loading

control. Typically, housekeeping proteins are characterized by relatively constant expression in the tissue of interest. β -actin and glyceraldehyde-3-phosphate dehydrogenase (GAPDH) are thereby the two most commonly used loading controls (Dittmer & Dittmer, 2006). After unsuccessful attempts with GAPDH as the housekeeping gene, it was replaced by tubulin, a protein of about 50 kDa, which is also commonly used. Tubulin is involved in cell division, intracellular traffic and cell shape (Borisy et al., 2016; Ledbetter & Porter, 1963; Lin et al., 2020). β -actin (~ 50 kDa), a structural protein (Bork, Sander, & Valencia, 1992), was also tested but like GAPDH did not show the desired Western blot results as seen with tubulin. Because the protein sizes of MBP (~18 kDa) and tubulin (~50 kDa) are fairly apart, there was no interference with the target genes. Regarding MBP possible effects of membrane stripping on the results were avoided by using tubulin as the housekeeping gene and the possibility of simultaneous execution.

Generally, it should be pointed out that technically all possible housekeeping genes used for loading control could also be altered in their protein expression by cuprizone treatment. This problem is not unknown, as it has often been shown that the expression of housekeeping genes also changes, especially when considering developmental and disease conditions. (Eaton et al., 2013; Gilda et al., 2015; Goasdoue, Awabdy, Bjorkman, & Miller, 2016; Moskowitz & Oblinger, 1995; Yperman, De Visscher, Holvoet, & Flameng, 2004). Since β -actin and GAPDH are also frequently used in the department, they should be further investigated to extend the results based on tubulin. In general, several recent papers have suggested that the use of housekeeping genes for Western blot loading controls should be carefully reviewed (Dittmer & Dittmer, 2006). Thereby, three main questions arise. 1. Due to the generally high expression level of the housekeeping genes, they tend to exaggerate the linear spectrum of values. This effect also appeared comparing the expression level of my MBP and tubulin analyses (Fig. 11 D, 16 D). 2. Housekeeping protein expression level cannot be assumed to be constant under different experimental conditions. And 3. Using a housekeeping gene as a loading control can often require stripping or reprobing. I also used stripping for the GFAP staining since GFAP and tubulin are about the same protein size and cannot be stained at the same time. Stripping can indeed affect the quantity of blotting due to the potential loss of protein during the stripping process (Gilda et al., 2015; Gilda & Gomes, 2013; Moritz, 2017; Sander, Wallace, Plouse, Tiwari, & Gomes, 2019).

To avoid such issues in future research, contemporary studies are deliberating further methods of Western blot quantification. The fundamental concept would be to incorporate housekeeping genes and introduce an alternative loading control such as the total protein staining method. Here, Ponceau S is the most commonly used method for total protein normalization. This method of loading control has the advantage of not relying on a single

protein. It also benefits from a fast staining time and easy removal of the dye after the staining process (Gilda & Gomes, 2013). Additionally, the Ponceau S method works well with antibody-antigen binding, unlike other conventional methods such as Coomassie Blue and silver staining, which are not suitable for immunoblots (Litovchick, 2020a). Sander et al. showed that Western blot sensitivity is not affected by Ponceau S staining. They suggested a 2-minute staining with a standard concentration of 0.01 % Ponceau S in 1 % acetic acid for Western blot normalization. After Ponceau S staining, images were quantified using Image Lab software (Sander et al., 2019). In my optic nerve trials I also used Ponceau S staining to get a previous insight of blotting quality and protein loading prior to antibody staining (see attachment). However, it was not utilised for general Western blot quantification. When carrying out Western blot analysis of optic nerve tissue, it is worth considering this method of normalizing loading controls.

Due to experimental limitations in the electrophoresis gel, only three animals per cohort were used. In order to validate the initial Western blot analyses, a second run was performed with a time delay. Each run on its own concluded that the level of myelin were not changing, and also showed approximately the same mean values for each cohort. However, there was an inconsistent variation between the first and second blot. This could be explained by the given moderate sensitivity and high error rate of the Western blot analysis. Some Western blot protocols working with mouse or rat optic nerve suggest a blocking with 5 % skim milk in TBS-T (pH 7.4, 0.1% Tween® 20). This may provide an option for quality improvement of Western blot analyses (Kwon, Nakaya, Abu-Asab, Kim, & Tomarev, 2014; Suzuki et al., 2014).

Subsequentially, cuprizone powder food formulation did not show the expected demyelination via MBP or dMBP in optic nerve tissue. This raises the question of whether 1. The cuprizone treatment was generally unsuccessful, 2. The prevented cuprizone protocol is particularly unsuitable for examination of the optic nerve, or 3. The demyelination was not properly detectable with the tools used.

There are several reasons to exclude a general inability to induce demyelination with the new cuprizone formulation protocol. The administration of cuprizone resulted in a marked scattering of values in the optic nerve. The range of values for *GABA_{knockout}* mice in the genetic control was about two initially, whereas cuprizone treated animals had a range almost three times as high. Moreover, the rise in especially astrocyte activity demonstrated by immunohistochemistry indicates the presence of an inflammatory process in response to cuprizone feeding. Finally, my data from several brain regions also showed a trend towards

myelin loss after the cuprizone diet. Myelin destruction was also confirmed by spinal cord data collected at the same time in the CIPMM department (Dallorto, 2021, Master Thesis)

On the second point of whether the cuprizone treatment protocol provided is appropriate for the purpose of examining optic nerve tissue, I found that recent studies using the optic nerve proposed different cuprizone treatment protocols. Marena et al. suggested a treatment period of seven weeks. The experimental plan provided a 0.2 % cuprizone diet in eight-week-old male mice for seven consecutive weeks. After this seven-week treatment they were returned to the regular diet. For histological analyses the animals were examined immediately after ending the treatment (day 0 post treatment, 15 weeks of age) and 15 days after returning to normal diet (day 15 post treatment, 17 weeks of age). These two groups were compared with independent healthy control mice aged approximately 10 weeks. A significant loss of myelin was observed in both cuprizone treated cohorts (0 and 15 days post-treatment) compared to the untreated control group. Similarly, the activity of microglia/macrophage cells (Iba1-positive cell counts) was also significantly increased in cuprizone treated mice (Marena et al., 2022). This experimental design differed markedly from the CIPMM laboratory cuprizone treatment protocol, both in terms of treatment duration and examination time. Both the *Non-induced_{ctl}* and *GABA_{knockout}* groups received only three weeks of cuprizone treatment. Which, compared to Marena et al. would only be less than half the duration. However, my treatment therefore involved higher doses of cuprizone (0.3 %) in the diet. While the *Non-induced_{ctl}* group was examined immediately after the three weeks of treatment (11 weeks of age), the *GABA_{knockout}* group was examined two weeks after the end of cuprizone diet (13 weeks of age). This time point is most comparable to the cohort studied by Marena et al. 15 days after returning to regular feeding. Therefore, it may be a possibility to adjust the cuprizone protocol for optic nerve tissue investigations.

The third possible source of error that should be investigated is whether fluorescence intensity analysis of MBP and dMBP is the best possible quantification of myelin level in optic nerve tissue. In this regard, it has been demonstrated that the two proteins are very useful for quantifying myelin changes in the corpus callosum (Kashani et al., 2015; Zhao et al., 2021). However, in addition to MBP, other myelin-specific proteins are associated with physiological myelination, axonal signaling, as well as communication and interaction between myelin and axons. The myelin oligodendrocyte glycoprotein (MOG), an antigen found specifically on the outer surface of the myelin sheath of the CNS and myelin-associated glycoprotein (MAG), a type I transmembrane glycoprotein that is also located in the myelin sheath, specifically in the oligodendroglial membrane, and which appears to be involved in the maintenance of myelinated axons in the CNS (Kroepfl, Viise, Charron, Linington, & Gardinier, 1996; Quarles, 2007). Both proteins are also frequently used in the CIPMM laboratory for

immunohistochemical studies of the brain or spinal cord. Very recently a lot has been published about the MOG antibody since it became a target of the immune system in MOG antibody disease and the differentiation towards AQP4-Neuromyelitis Optica Spectrum Disorder and Relapsing-remitting MS (Adamus et al., 2012; Cortese et al., 2023; Petrikowski et al., 2021).

Another alternative for specific myelin staining is the use of histochemical methods. One of the most important is the Luxol Fast Blue (LFB) stain, first introduced by Kluver and Barrera in 1953 (Kluver & Barrera, 1953). The LFB staining can be extended to the MCOLL method, named for the simultaneous staining of myelin and collagens. This combination of histochemical characterization of myelin and fibrillar collagens in healthy, degenerative and regenerative states has been particularly successful in peripheral nerve tissue (Carriel et al., 2013; Carriel, Garzón, Alaminos, & Campos, 2011; Carriel, Garzón, Alaminos, & Cornelissen, 2014). LFB staining indeed has been successfully used for optic nerve analysis. Marena et al. performed longitudinal myelin staining with LFB in two sections, quantifying the percentage of demyelinated area on the entire optic nerve section. Optic nerve thickness was then measured in four inner axial segments (Hildebrand & Mohseni, 2005; Marena et al., 2020; Marena et al., 2022). Since we have seen the best results for optic nerve tissue with cryostat sectioning, the LFB method would be a great complementary method since the staining is well compatible with cryostat slicing (Carriel, Campos, Alaminos, Raimondo, & Geuna, 2017; Kluver & Barrera, 1953).

Conclusively, the combination of histochemical and immunohistochemical quantification of myelin processes should definitely be considered in future studies of myelin changes under cuprizone treatment in optic nerve tissue. Especially since MBP and dMBP staining did not show conclusive results at the chosen observation times, the longitudinal LFB study could provide more sensitive data.

And yet another method of visualizing myelin structures cannot be ignored. Most of the knowledge about the organization of myelin structures is based on the use of the electron microscope (EM) (Aggarwal, Yurlova, & Simons, 2011). In this setting, many studies focus on individual structures of the central or peripheral nervous system via EM. There are also a variety of approaches and protocols for the examination of the optic nerve by using EM (Calkins, Pocius, Marracci, & Chaudhary, 2020; Melling, Karimian-Teherani, Mostler, & Hochmeister, 2005; Ono et al., 2022; Ronchi et al., 2014). In general, these are studies performed on fixed, dehydrated tissue. This alternation reveals a periodic structure of electron-dense and electron-light layers. They are known as the major dense line, representing the tightly compact cytoplasmic myelin membranes, and the interperiodic line,

formed by the densely packed outer membrane (Aggarwal et al., 2011). Ono et al. investigated the ultrastructure of putative oligodendrocyte precursor cells (pOPC) in the postnatal mouse optic nerve using serial block-face scanning electron microscopy (SBF-SEM). They reconstructed 3D profiles that revealed the shapes and distributions of glial cells and their cytoplasmic organelles. With this new approach using SBF-SEM, they were able to take serial electron micrographs of individual cells and capture the ultrastructure of the entire cell at the subcellular level (Ono et al., 2022). Giacci et al. also worked with 3D reconstruction of axons and myelin. They analyzed CNS injury and the resulting changes in myelin and axons. Rats with partially transected optic nerves were compared to uninjured control rats (Giacci et al., 2018). This emphasizes that many aspects of myelin can be very well characterized by electron microscopic methods. In any case, this provides an extension to further studies of the mouse optic nerve examining changes in myelin and axons under cuprizone treatment.

Even though the effectiveness of cuprizone can be assumed, there are numerous of animal models to extend the study of de- and remyelination processes and simulating MS (Torre-Fuentes et al., 2020). One of these is the lysophosphatidylcholine (LPC) model, which is also based on toxin-induced demyelination. It is widely used to study myelin loss or repair as well as potential treatment trials (Plemel et al., 2018). Like the cuprizone model, the LPC-induced treatment does not aim to simulate inflammatory happenings in MS, but rather to model the process of de- and remyelination (Denic et al., 2011). In general, there is no single model that reflects all the many factors that characterize the pathogenesis of MS. Over time, a wide range of models have been developed to reproduce different features of the disease (Torre-Fuentes et al., 2020). Due to the systemic effect of Cuprizone, it would be intriguing to consider integrating the LPC model in future studies of the optic nerve, especially in order to make more specific statements about myelin changes.

The LPC model implements a focal reversible demise of myelin caused by the intoxication of oligodendrocytes (El Waly, Buttigieg, Karakus, Brustlein, & Debarbieux, 2020). Early on, those observations of demyelination via LPC were also described in the optic nerve (Shikishima, Mizuno, Kawai, & Matsuzaki, 1985). However, the focal treatment of murine optic nerve via injections is obviously an extensive and challenging procedure. A common protocol for LPC treatment is to inject the optic chiasm. This indeed carries the risk of injuring the surrounding tissue, and in the process of repairing the injected chiasm, progenitor cells are recruited from the surrounding tissue and thus the 3rd ventricle (Dehghan et al., 2016; Mozafari et al., 2011). Another possibility for LPC treatment was proposed by Dehghan et al. by injecting the optic nerve just behind the globe. This method provided easy access to the tissue through a small and short surgical procedure. This approach would guarantee the

exposure of the optic nerve to a potent and consistent dose of toxin across all the mice. Ideally, this methodology would reduce the variability seen in my results.

In extend, this protocol investigated the application of an LPC-loaded agarose gel (AL-LPC) to the mouse optic nerve to achieve long-term demyelination. In the long term, this extended LPC model, would aim to induce a prolonged demyelination time with latent axonal damage to resemble the progressive MS course. They used mice at the age of eight to 12 weeks and studied the progress of demyelination at seven, 14, and 28 days after LPC or AL-LPC application. To quantify the myelin status, they performed visual evoked potential (VEP) and histological staining. Subsequently, this model successfully provided an extended window of demyelination that ultimately led to latent axonal damage (Dehghan, Aref, Raoufy, & Javan, 2021). Since my immunohistochemistry results did not fully demonstrate successful demyelination, this method would provide the opportunity to monitor myelin over time and not run the risk of missing the peak period of myelin loss.

In this study, too, LFB and MBP staining were among others evaluated. Both showed significant myelin changes and therefore reinforce the notion of combining immunohistochemistry and histological staining for optimal outcomes (Dehghan et al., 2021). In the CIPMM laboratory, the LPC model has also been frequently used to demonstrate demyelination in the spinal cord (El Waly et al., 2020) and in addition different protocols have been established to then study tamoxifen induced GABA_B receptor knockout (Dallorto, 2021, Master Thesis). Furthermore, I aimed to investigate how the loss of the GABA_B receptor influences de- and remyelination. In the immunohistochemistry staining the *GABA_B knockout group* revealed an increase of myelin in the cuprizone control cohorts. Here, the immunofluorescence measurements of MBP were about one third increased after deleting the oligodendroglial GABA_B receptor. Two hypotheses could explain the general protective effect of the GABA_B receptor. 1. The loss of oligodendroglial GABA_B receptors leads to a stronger differentiation of OPCs into mature oligodendrocytes, which are therefore able to provide more myelin for the axons. 2. Reduced oligodendrocyte death after cuprizone diet in GABA_B receptor knockout cohorts. The latter statement could not be reflected in the optic nerve results as cuprizone did not show the desired myelin reduction. However, both hypotheses can be investigated by following different markers of the oligodendrocyte lineage. These include oligodendrocyte transcription factor 2 (Olig2), OPC markers such as platelet-derived growth factor alpha (PDGFR α), or mature oligodendrocyte markers such as anti-adenosine polyposis coli clone 1 (CC1) (Baron, Metz, Bansal, Hoekstra, & de Vries, 2000; Bhat et al., 1996; Calver et al., 1998; Yu et al., 2013). All of the above were immunohistochemically stained for optic nerve tissue to complement the MBP results but subsequently no conclusive results were obtained due to low tissue availability. Therefore,

larger cohorts should be immunohistochemically examined to classify the total amount of OPCs and mature oligodendrocytes in $GABA_B$ receptor knockout mice with and without cuprizone diet.

However, since loss of the $GABA_B$ receptor appears to have a protective effect on myelin, as seen in previous data from the department and also in the cuprizone control cohorts of the $GABA_{knockout}$ cohort, future experiments should focus on the influence of $GABA_B$ receptor knockout in oligodendrocyte lineage cells. The focus will be to compare mice immediately after cuprizone treatment with mice in the remyelination phase, two to four weeks after treatment.

4.6 Astrocyte and microglia activity after cuprizone treatment and loss of oligodendroglial GABA_B receptors

Next to neurons, astrocytes are the most abundant cell type in the central nervous system. They partake in various vital functions within the CNS (Sofroniew & Vinters, 2010). Over time the activity of astrocytes has been associated with demyelinating diseases such as MS (Nair, Frederick, & Miller, 2008). They play a vital role in promoting a neurodegenerative cascade, which specifically occurs in the later stage of the disease and can be identified in the context of astrocytic scars in MS lesions (Gudi et al., 2014; Hibbits, Yoshino, Le, & Armstrong, 2012). They have been shown to have a crucial role in the demyelination process via the release of chemokines that attract both peripheral immune cells, such as T cells, monocytes, or dendritic cells, and resident CNS cells, such as microglia and NG2 glial cells, to the site of inflammation (Mayo, Quintana, & Weiner, 2012). Early on, astrocytal heterogeneity has been described. They have been classified into two primary groups, gray matter showing protoplasmic astrocytes and white matter presenting fibrous astrocytes. The former have been widely studied and show significant variation in morphology and activity, both across and within different areas of the brain. Subsequently, most of the knowledge about astrocytes is based on investigating gray matter astrocytes (Khakh & Deneen, 2019; Pestana, Edwards-Faret, Belgard, Martirosyan, & Holt, 2020; Westergard & Rothstein, 2020). Furthermore, there is evidence that regional heterogeneity of astrocytes may be a contributor to differences in disease susceptibility. In various pathologies, astrocytes have demonstrated varying transcriptional programs in based on the situation at hand (Itoh et al., 2018; Kaiser et al., 2006; Zamanian et al., 2012).

As the optic nerve is mainly composed of compact white matter, its astrocyte activity is of particular interest. Indeed, a uniquely active astrocyte population has been suggested in optic nerve tissue. Anatomically, the optic nerve is segmented into the proximal unmyelinated optic nerve head (ONH) and the myelinated distal part, the optic nerve proper (ONP) (Fig. 21) (Mazumder et al., 2022; Sun et al., 2009). The former have been suggested to present a unique astrocyte population. Therefore, the ONH astrocytes may differ in four main points: First, the astrocyte population found in the ONH has a unique transversally oriented morphology, not observed in the corpus callosum or spinal cord. This population appears to be the only one of its kind in the ONH (Sun et al., 2009). Second, these astrocytes exhibit an immunocytochemical profile distinct from those found in the ONP, showing an elevated expression of Aquaporin 4 (APQ4) and glial fibrillary acidic protein (GFAP) among others (Bernstein et al., 2020; Nguyen et al., 2011; Qu & Jakobs, 2013). Third, the ONH is a non-

myelinated region with limited microglia and NG2 glial cells (Sun et al., 2009). Fourth, the vascularization plexus of the ONH is more intricate than the one of the ONP.

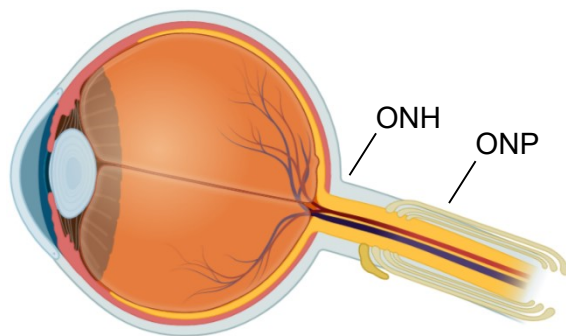


Figure 21. Unmyelinated optic nerve head (ONH) and myelinated optic nerve proper (ONP). Different astrocyte populations were found in the unmyelinated head (ONH) part of the optic nerve compared to the myelinated proper (ONP) part. Modified from (Mazumder, Julé, Cullen, & Sun, 2022). Retrieved from <https://app.biorender.com/illustrations>.

In my optic nerve studies, I used GFAP, the glial fibrillary acidic protein, to analyze the astrocyte status. It is the most frequently utilized marker for astroglia, and it polymerizes in activated astrocytes during astrogliosis (Eng & Ghirnikar, 1994). Similar to MBP observations, immunohistochemistry staining and Western blot analysis were performed for GFAP to investigate astroglial reactivity. For the *Non-induced_{ctf}* cohort the latter were the only GFAP analysis conducted. The cohort was studied in the early demyelination phase (Gudi et al., 2014) to examine astrocyte activation immediately after finishing cuprizone treatment (0 WPC). Whereas, in the 13-week-old *GABA_{knockout}* cohort both, immunohistochemistry and Western blot analyses were performed two weeks after ending cuprizone diet (2 WPC). Again, in the *GABA_{knockout}* group, protein level were examined within two conditions. First, the general phase of remyelination (Gudi et al., 2014) after withdrawing cuprizone diet, and secondly, the alterations brought about by the loss of oligodendroglial GABA_B receptors.

The association between astrocyte activation and demyelinating events in the cuprizone model has been previously demonstrated (Sen, Almuslehi, Coorsen, Mahns, & Shortland, 2020; Skripuletz et al., 2010). Nevertheless, the role of astrocytes in this process is not conclusively understood. An increasing number of studies suggest that astrocytes are a key cell type involved in a number of regenerative processes (Gudi et al., 2014). In the *GABA_{knockout}* cohort I was able to demonstrate an increase of GFAP immunofluorescence measurements in genetic control mice after cuprizone diet. The optic nerve therefore showed significantly increased astrocyte activity in the early remyelination phase. This would support the idea that astrocytes promote remyelination processes, such as OPC migration and oligodendrocyte proliferation, as well as lesion repair in the context of anti-inflammatory pathways (Moore, Abdullah, Brown, Arulpragasam, & Crocker, 2011; Williams, Piaton, & Lubetzki, 2007). In fact, if astrocytes are activated beforehand, they can reduce myelin loss

in the brain under cuprizone treatment (Laflamme et al., 2018), while their dysfunction can cause altered morphology of oligodendrocytes and an inability to myelinate properly (Leppert et al., 2023). On the other hand neuronal damage in trauma or ischemia will likewise induce astrogliosis (Anan'ina et al., 2020; Jeffery & Blakemore, 1995). So the increased astrocyte activity seen in the optic nerve could represent not only pre-remyelination activation but also a response to destruction and myelin loss.

In this study, it was not differentiated between ONH and ONP (Fig. 21) the immunofluorescence measurements and Western blot of the whole nerve were reviewed. Since the mouse optic nerve already provides relatively little tissue, and only one optic nerve from each *GABA_Bknockout* mice could be used for histology, I aimed to minimize the loss of extra tissue as far as possible. Nevertheless, it would be beneficial for further studies to investigate how the astrocyte populations of ONH and ONP (Mazumder et al., 2022) respond separately to cuprizone treatment and the conditional loss of GABA_B receptors.

It would be beneficial to further investigate the increase in GFAP in the optic nerve after cuprizone treatment. As previously stated, GFAP polymerizes in activated astrocytes (Eng & Ghirnikar, 1994), as would be the case in this study. In this regards, numerous studies have already addressed the various GFAP subtypes or isoforms (Messing & Brenner, 2020; van Bodegraven, Sluijs, Tan, Robe, & Hol, 2021). Higher resolution techniques, such as RNA sequencing, have revealed differential RNA processing in various tissues between healthy and diseased conditions or during different developmental stages (Ameur et al., 2011; Bentley, 2014; Elkon, Ugalde, & Agami, 2013; Herzel, Ottoz, Alpert, & Neugebauer, 2017). This analysis could provide additional insight into questions such as whether there is increased expression of GFAP in cells or increased GFAP levels per cell. Additionally, we can investigate how GFAP behaves in GABA_B knockout animals versus genetic control animals and compare different GFAP isoforms in the optic nerve to those present in brain or spinal cord tissue. Once these questions are answered, we can consider the therapeutic potential of GFAP isoforms as new targets, as evidenced by their relevance in glioblastoma development (Radu, Petrescu, Gorgan, & Brehar, 2022).

The Western blot analysis, however, did not confirm any changes in either of my cohorts. One issue I encountered was the selection of the housekeeping gene tubulin. Both GFAP and tubulin are about 50 kDa, making it impossible to perform immunodetection of both proteins at the same time. I therefore decided to reprobe by use Western blot stripping. MBP and tubulin were incubated in the first immunodetection run and GFAP in a subsequent run. It is essential to perform the stripping process with utmost precision to enhance its effectiveness and ensure the removal of the first antibody while retaining both the target

protein and membrane integrity. Nevertheless, stripping can lead to a reduction in quality. 1. Stripping can cause a decreased signal since some of the protein antigens may be washed from the membrane. 2. If the stripping process was incomplete, and not all of the antibodies were fully removed, this may result in cross reactivity or non-specific binding upon reincubation (Litovchick, 2020b).

Therefore, potential sources of error could be avoided by refraining from stripping and instead utilizing another housekeeping gene such as GAPDH. Nevertheless, my trial blots demonstrated that tubulin yielded better results than GAPDH. The quantification of western blot using e.g. Ponceau S instead of housekeeping genes has been previously described and can be applied when blotting with GFAP in the same manner.

Looking at the Western blot results of the *GABA_Bknockout* cohort once again, the analysis did not reveal any significant findings. However, there was a trend towards lower astrocyte activation in the knockout animals compared to the genetic control animals. Both genetic control cohorts and both knockout cohorts showed almost the same values and therefore their ratio to each other is almost the same with or without cuprizone treatment. These results provide a starting point for further Western blot analysis, but their reliability remains to be confirmed.

Hypothetically, a decrease in astrocyte activity within the optic nerve caused by the loss of oligodendroglial GABA_B receptors would display a cellular downregulation. Activated astrocytes also appear to be involved in the recruitment of immune cells such as macrophages, microglia, and leukocytes. Furthermore, by initiating an inflammatory process through the release of communication proteins such as cytokines and chemokines, they potentially contribute to demyelination (Kiray, Lindsay, Hosseinzadeh, & Barnett, 2016; Ponath, Park, & Pitt, 2018; Williams et al., 2007). However, if the GABA_B receptor plays a role in this downregulation, comparable outcomes should also manifest in the *GABA_Bknockout* animals. Given that immunohistochemistry yielded superior results, future investigations of the optic nerve ought to analyze larger cohorts at varied time intervals post cuprizone treatment.

In addition to immunohistochemistry measurements and Western blot analyses, there are several other methods available for examining astrocyte activity or microglial behavior. One of these increasingly important methods for detecting immune cells has been demonstrated using single-cell resolution techniques. Single-cell sequencing was already briefly introduced when considering different GFAP isoforms and their relevance in MS model. The method of single-cell resolution can also provide further insight into the diversity of astrocytes, highlighting distinct astrocyte distribution, transcription programs, and functions (Batiuk et al.,

2020; Bayraktar et al., 2020). In general, chemical and biological analyses of individual cells offer direct comprehension of the mechanisms underlying cellular heterogeneity, as the single cell operates as the fundamental functioning unit of life. Consequently, single-cell analysis methods are revolutionizing the understanding of cell identity and heterogeneity. They are extensively utilized, particularly for CNS cell subtyping, and have already unveiled several neuronal specificities in different brain areas (Saunders et al., 2018; Zeisel et al., 2018). Here, two methods in particular are commonly used when studying single cells, such as immune cells (Khan & Khan, 2021). 1. Fluorescence-activated cell sorting (FACS) is the most commonly utilized cell separation technique, which is already applicable to a broad range of cell types (Gross et al., 2015). Usually, FACS cell sorting techniques employ a flow cytometric (FCM) analyses beforehand to label specific antibodies and sort cells from a single cell suspension (Hu, Zhang, Xin, & Deng, 2016). FACS can thus be considered a specialized technique of FCM, where the cell sorting is finally based on the specific light scattering and fluorescent characteristics of each cell (Herzenberg & Sweet, 1976; Ibrahim & van den Engh, 2003). 2. Single-cell RNA sequencing (scRNA-SEQ) as a novel technique to investigate the transcriptional activity of individual cells at an early developmental stage. By generating transcription profiles of thousands of cells. This technique can reveal the differential expression of individual cell genomes and provide cell mapping of tissue or organs. It comprises the methodological stages of cell isolation, for instance, through FACS, cell lysis, PCR amplification, library preparation, and finally sequencing, if applicable in the form of high-throughput sequencing, followed by data analysis (Khan & Khan, 2021; Tang et al., 2009).

These methods present an intriguing approach, particularly in relation to optic nerve tissue, which contains a variety of immune cells and has a crucial role in the disease patterns of MS. Further studies could aim to categorize astrocytes and microglia more specifically, enabling the establishment of targeted therapies in the long run.

Along with astrocytes, microglial cells play an essential role in monitoring inflammatory events in the CNS. They are part of the glial cell family, which are crucial to the optic nerve's health. These cells interact to maintain neuronal activity and structural stability. Oligodendrocytes create brief rows of neighboring cells along the optic nerve's length, which are divided by astrocytes. This network of oligodendrocytes, astrocytes, NG2 cells, and microglia is further subdivided by septa of neuroglia along with elastic and collagenous fibers, resulting in well-defined nerve bundles (Butt, Pugh, Hubbard, & James, 2004). I already established that the optic nerve is composed primarily of white matter, consisting mainly of glial cells and therefore also of microglia. Since the ONH is not myelinated, there are fewer microglial cells present in that area (Mazumder et al., 2022; Sun et al., 2009). In

the experimental autoimmune encephalomyelitis (EAE) model, a frequently utilized rodent model of MS, activation of microglia and macroglia has been shown to result in removal of damaged myelin and optic nerve fibers (Voss et al., 2012). In recent studies, microglia have shown to be abundant in the optic nerve and often found around localized tissue lesions, presumably to clear cellular debris, yet microglia have been shown to act both pro- and anti-inflammatory (Horstmann et al., 2016; Horstmann et al., 2013).

I performed immunohistochemistry staining for anti-ionized calcium-binding adapter molecule 1 (Iba1) antibody to detect microglia and monocyte activation (Ahmed et al., 2007; Zhan et al., 2020). Microglial status was observed in the 13-week-old *GABA_{knockout}* cohort. After the completion of cuprizone treatments, the mice were considered to be in the remyelination phase (Gudi et al., 2014). The Iba1⁺ cells were thereby counted and then normalized. My immunofluorescence measurements did not reveal any changes. All cohorts treated with cuprizone displayed increased variability, as already observed in the myelin assays. This also indicates a potential alteration following treatment with cuprizone powder food.

However, there was an indicated trend of increased Iba1⁺ cells observed in the genetic control groups after cuprizone treatment. These observations would be consistent with the latest spinal cord findings from the department. Here, a significant increase in Iba1⁺ cells was observed in the spinal cord of mice exposed to the same cuprizone protocol and studied at a comparable time period (Dallorto, 2021, Master Thesis). These studies are therefore in line with current scientific knowledge. Marena et al. demonstrated an increase of Iba1⁺ cells in murine optic nerve in their modified cuprizone treatment plan. Both microglia and macrophage cells had gained in comparison to control animals at both time points, immediately after treatment and 15 days after ending the cuprizone diet. At the same time, they were able to record the onset of remyelination and recovery of nerve conduction through VEPs (Marena et al., 2022).

This underlines the approach taken from Gudi et al. to the occurrence of remyelination in the *GABA_{knockout}* group (Gudi et al., 2014). As the various tasks and capabilities of microglial cells indicate, there exists diverse perspectives on these findings. As a result of toxic cuprizone treatment or neuronal trauma resulting from injury, a transition from the regular, resting position of microglia to an active "amoebic" morphology was observed (Gudi et al., 2014; Praet et al., 2014; Sen et al., 2020; S. E. Taylor, Morganti-Kossmann, Lifshitz, & Ziebell, 2014; Ziebell, Taylor, Cao, Harrison, & Lifshitz, 2012).

In terms of microglial activity state, a classification system originally devised for macrophages has been adapted for the microglial cells (Orihuela, McPherson, & Harry,

2016). This system is based on polarization into a detrimental (M1) or beneficial (M2) state in response to CNS injury states. M1 microglia are predominantly present as activated cells in pro-inflammatory situations, releasing pro-inflammatory cytokines. In contrast, M2 microglia represent activated cells that, unlike M1, tend to suppress inflammation and initiate repair of injured tissue, secreting mainly anti-inflammatory mediators to restore homeostasis (Aguilera, Colín-González, Rangel-López, Chavarría, & Santamaría, 2018; Gudi et al., 2014; Lassmann & van Horssen, 2016; Praet et al., 2014; Rossi et al., 2014; Wang, Yang, Weng, & He, 2019; Zheng & Wong, 2019).

Since the model can be similarly applied to astrocytes, dividing them into harmful (A1) and helpful (A2) reactive states (Liddelow & Barres, 2017; Liddelow et al., 2017) the GFAP and Iba1 immunohistochemistry findings can be placed in greater context. As in this study, the counting of microglia cells in the optic nerve only showed tendencies of increase after cuprizone diet, it is crucial to obtain further information on the presence of these specific microglia. Although they may exhibit the same numbers after undergoing cuprizone treatment as in the control animals, it cannot be ruled out that microglia functions would be different, given their exposure to toxins and tissue damage. A detailed examination of their morphology and characteristics could assist in identifying their role in the remyelination phase of the *GABA_{knockout}* mice alongside astrocytes.

4.7 Corpus callosum and other brain areas reconfirming neuronal changes with astroglial and microglial activity

In order to get the optic nerve findings into a broader context, I additionally examined different brain areas of the *GABA_{knockout}* mice. Similarly, I aimed to demonstrate the efficacy of the new cuprizone diet for these areas of the CNS. Therefore, immunohistochemical staining was conducted and assayed in the areas of the corpus callosum, cortex, striatum, and thalamus. As for the optic nerve investigations, I was interested in the proteins MBP, GFAP and Iba1. Here, I especially anticipated significant results on myelin level reduction to show the cuprizone effect of the modified treatment protocol.

In terms of MBP no change could be detected. However, strong variation in the fluorescence intensity was observed in all cohorts and areas. The MBP staining ought to be a consistent standard practice, particularly with respect to the corpus callosum. Although strong demyelination was not captured in the quantification, the histological images present a lack of MBP fluorescence intensity, specifically in the corpus callosum and cortex. In the corpus callosum, this was identifiable by the absence of staining and a subsequent void in the single slice (Fig. 18 B1-4). The quantification of all animals showed only a slight trend in the cuprizone treated animals. It is still unclear as to why the animals showed such variability in values and no decreased myelin at the age of 13 weeks. In any case, the small size of the individual cohorts presents a predicament, this must certainly be expanded in order to obtain significant results. Especially since members of the CIPMM department already demonstrated strong myelin reduction with the same cuprizone diet. On the other hand, it is worth considering whether the cuprizone powder food formulation provides sufficient duration and intensity of treatment. Additionally, it is important to determine whether the de- and remyelination time points could vary with the new diet protocol and whether the investigation should include different observation time points, especially since the *GABA_{knockout}* cohort represents a period of remyelination with an already proceed regain of myelin (Gudi et al., 2014). Therefore, it should be considered not only to study larger groups of mice in future investigations, but also to extend the studies to different time points during and after cuprizone treatment.

However, my studies of astroglial and microglial activity showed a significant increase after the cuprizone diet. The GFAP fluorescence intensity was about twice as high in the cuprizone treated cohorts in the callosal, cortical and thalamic area. But also the striatum showed the same tendencies and especially the single slice consideration underlined a similar activation

of astroglial cells (Fig. 19). The Iba1⁺ cells on the other hand tripled their cell count in the corpus callosum manifesting a strong increase. The cortical, striatal and thalamic area did not show any change in the cell count, but indeed presented a changed, enlarged cell morphology in the single slice examination (Fig. 20). These changes could also suggest an altered environment at the oligodendroglial level.

In general, insufficient microglial and astrocyte activity, particularly in the context of impaired phagocytosis of myelin debris and secretion of toxic mediators, may contribute to inadequate remyelination (Franklin, 2002; Lampron et al., 2015; Lubetzki, Zalc, Williams, Stadelmann, & Stankoff, 2020; Rawji, Gonzalez Martinez, Sharma, & Franklin, 2020; Town, Nikolic, & Tan, 2005). Particularly astrocytes showed an increase in activity in several brain regions (corpus callosum, cortex and thalamus), which could indicate ongoing repair processes. Furthermore, the histological images of the GFAP staining revealed a clear increase in the number of activated astrocytes in all observed brain areas after cuprizone treatment. Whereas there were visually no astrocytes in the cuprizone control cohorts, a large number of activated, vigorous astrocytes were seen after the cuprizone diet. This has already been frequently demonstrated in several studies with different cuprizone protocols (Hibbits et al., 2012; Sen et al., 2020; Skripuletz et al., 2013). Generally, as already described for the optic nerve, an astrocyte diversity is also reflected in different brain regions (Batiuk et al., 2020; Mazumder et al., 2022).

While microglia cells quantification only showed an increase in the corpus callosum, astroglial activation increased in multiple areas. It should be acknowledged that while the number of microglial cells may not have increased, their morphology certainly did. The histological images demonstrate that treatment with cuprizone altered cells in all areas of the brain. Cell bodies increased in size and extensions strengthened (Fig. 20 B7-8, 11-12, 15-16). These morphological changes are characteristic for cuprizone induced changes and have been described frequently (Gudi et al., 2014; Sen et al., 2020; Skripuletz et al., 2011; S. E. Taylor et al., 2014; Ziebell et al., 2012). Anyhow, regarding the microglial findings, further studies should be carried out at different time points after cuprizone treatment to see whether the microglial cell count in the cortex, striatum and thalamus will increase other observation time points. The diversity of astrocytes, on the other hand, has already been addressed many times in this study and also offers a broad approach for brain areas to gain further insights, e.g. through single-cell sequencing (Batiuk et al., 2020; Bayraktar et al., 2020). This would help to improve classifying the astroglial activity shown in my studies and to better understand the activity patterns in the cuprizone model and ultimately in the clinical picture of MS.

The loss of oligodendroglial GABA_B receptors, on the other hand, did not show an effect on the activity of astrocytes and microglia cells two weeks after ending the cuprizone diet. The knockout animals presented the same immunohistochemical values as their age related genetic control mice. At the same time, previous spinal cord data from the department showed an increase in astrocytes and microglia in the GABA_B receptor knockout groups after the cuprizone diet (Braun, 2020, Bachelor Thesis). Meanwhile, laboratory data from the same period in LPC models of the spinal cord also showed no differences due to the loss of the GABA_B receptor in the white matter (Dallorto, 2021, Master Thesis). To make further statements, larger cohorts at different time points of demyelination and remyelination should be studied.

4.8 Further insights of the experimental design

4.8.1 Conditional inducibility of the GABA_B receptor knockout

This study demonstrated a change in the optic nerve of the *GABA_Bknockout* mice due to the loss of the GABA_B receptor. This was seen in the cuprizone control mice at 13 weeks of age, where myelin level was higher in the knockout mice. However, the overall results did not provide further insight into the effects of the GABA_B receptor loss, especially with regards to the cuprizone diet. On the other hand, stand the *Non-induced_{ctl}* cohort, in which, as the name suggests, the knockout was not induced. However, it is the same mouse line as the *GABA_Bknockout* cohort but studied at a different time point. So the *Non-induced_{ctl}* mice also expressed the genetic predisposition for the GABA_B receptor knockout that was just not induced or rather activated by the tamoxifen injections. My studies could therefore simultaneously demonstrate the conditional inducibility of the knockout. Part of the *Non-induced_{ctl}* cohort therefore consists of genetic controls and the other half of potential but uninduced knockout animals. In both the immunohistochemistry results and the Western blot analyses, there were no noticeable differences in the measured values between the genetic controls and the non-induced knockout animals. This displayed a confirmation of the viability of knockout induction via tamoxifen and showed that the absence of tamoxifen administration was equivalent to genetically unaltered control mice. As the technical knockout animals were not split 1:1 between western blot analysis and immunofluorescence measurements or between cuprizone and cuprizone control groups, it is difficult to draw statistics from this. To investigate this further, a larger cohort should be used, e.g. for immunohistochemistry, and the genetic knockout animals should be compared with the genetic control animals, both with and without cuprizone.

4.8.2 Gender distribution

Another issue raised was the gender distribution. It is known that MS is more than twice as common in women as in men (Harbo, Gold, & Tintoré, 2013; The Multiple Sclerosis International Federation, 2020). It is not known what causes this difference in distribution, but there seem to be a number of factors involved, including hormonal and genetic influences (Russi, Ebel, Yang, & Brown, 2018; Voskuhl, Sawalha, & Itoh, 2018). The general question is whether this difference is at all detectable in the cuprizone model. The CIPMM laboratory had

recently performed spinal cord studies on animals treated with the same cuprizone protocol and found no sex differences (Dallorto, 2021, Master Thesis). Similarly, previous studies showed that male and female mice (C57BL/6) had analogous patterns of demyelination and equal level of oligodendrocytes and other glial cells after cuprizone treatment. Also, there has been evidence that cuprizone treatment has an effect on the oestrogen cycle making it difficult to examine specific differences (L. C. Taylor, Gilmore, Ting, & Matsushima, 2010). Which might be why often only male mice are used and systematic comparison is rarely done (Sen, Mahns, Coorssen, & Shortland, 2019). In this study, too, there were no differences seen between male and female mice neither for the optic nerve nor the brain results. The situation is different in the MS model of EAE, which is also widely used. Here, there are indeed sex differences that vary depending on the strain of animal, indicating a genetic influence. It was shown that female SJL mice, which are often used in EAE studies, have a higher incidence and severity of disease and suffer more frequent relapses than male mice (Bebo, Schuster, Vandenbark, & Offner, 1998; Bebo, Vandenbark, & Offner, 1996; Papenfuss et al., 2004; Voskuhl, Pitchejian-Halabi, MacKenzie-Graham, McFarland, & Raine, 1996). Furthermore, in the ethidium bromide model, another toxin-based demyelination model, it was shown that in rats, females remyelinated more efficiently than males (W. W. Li, Penderis, Zhao, Schumacher, & Franklin, 2006). For the precise classification of differences in de- and remyelination between female and male mice, it's important not to disregard hormonal differences, particularly since these factors may be involved in the development of MS (Russi et al., 2018). Therefore, female mice should be examined at the corresponding time of the menstrual cycle (Byers, Wiles, Dunn, & Taft, 2012; Goldman, Murr, & Cooper, 2007). In my experimental framework, such precise classification and differentiation were unfeasible. Nonetheless, it would be crucial to include the differentiation between male and female animals more extensively in medical research, particularly in diseases such as MS, which predominantly affect women and currently have no cure. Therefore, it is also imperative that national healthcare systems, registries, researchers, and MS organizations gather gender-specific data to substantiate the presentation of concrete evidence on these variances (The Multiple Sclerosis International Federation, 2020).

5. Conclusion

In this study, the alterations of glial cells in the optic nerve in MS were demonstrated. Murine oligodendrocytes, astrocytes, and microglia were observed following the administration of cuprizone powder chow, a toxin-induced demyelination and remyelination model. Two cohorts were utilized: the *Non-induced_{ctl}* cohort and the *GABA_{knockout}* cohort, both of which had the same genetic lineage and underwent the same Cuprizone protocol. The former was examined during the initial demyelinating phase immediately following cuprizone treatment, while the latter was analyzed two weeks after ending the diet during the remyelinating phase. To establish a conclusive link between the results of the optic nerves and the CNS, the corpus callosum, cortex, striatum and thalamus of the mice were additionally examined. Furthermore, in the *GABA_{knockout}* group, the loss of oligodendroglial GABA_B receptors and the possible impact on glial cells was investigated. Silencing these GABA_B receptors led to an increase in myelin level without the contribution of cuprizone. This again supported the idea of a protective knockout effect on myelin. Astrocytes in the *GABA_{knockout}* cohort showed striking increase in activity post cuprizone treatment during the remyelination phase. The rise in activity was also evident in the brain areas corpus callosum, cortex, and thalamus. Microglial cells, on the other hand, demonstrated an increase exclusively in the corpus callosum, with only indications observable in the optic nerves. Overall, the cuprizone treatment resulted in a substantial increase in the scatter of the individual values. However, the increase in the variation indicated that a change had occurred compared to the control animals. To conclude, the cuprizone model is a powerful tool for studying demyelinating diseases. The modified dietary regimen is capable of illuminating precise molecular pathways in the optic nerve, potentially leading to inflammatory processes as seen in optic neuritis and MS.

References

1. Adamus, G., Brown, L., Andrew, S., Meza-Romero, R., Burrows, G. G., & Vandenberg, A. A. (2012). Neuroprotective effects of recombinant T-cell receptor ligand in autoimmune optic neuritis in HLA-DR2 mice. *Invest Ophthalmol Vis Sci*, *53*(1), 406-412. doi:10.1167/iovs.11-8419
2. Aggarwal, S., Yurlova, L., & Simons, M. (2011). Central nervous system myelin: structure, synthesis and assembly. *Trends Cell Biol*, *21*(10), 585-593. doi:10.1016/j.tcb.2011.06.004
3. Agostini, S., Mancuso, R., Guerini, F. R., D'Alfonso, S., Agliardi, C., Hernis, A., . . . Clerici, M. (2018). HLA alleles modulate EBV viral load in multiple sclerosis. *J Transl Med*, *16*(1), 80. doi:10.1186/s12967-018-1450-6
4. Aguilera, G., Colín-González, A. L., Rangel-López, E., Chavarría, A., & Santamaría, A. (2018). Redox Signaling, Neuroinflammation, and Neurodegeneration. *Antioxid Redox Signal*, *28*(18), 1626-1651. doi:10.1089/ars.2017.7099
5. Ahmed, Z., Shaw, G., Sharma, V. P., Yang, C., McGowan, E., & Dickson, D. W. (2007). Actin-binding proteins coronin-1a and IBA-1 are effective microglial markers for immunohistochemistry. *J Histochem Cytochem*, *55*(7), 687-700. doi:10.1369/jhc.6A7156.2007
6. Ameer, A., Zaghlool, A., Halvardson, J., Wetterbom, A., Gyllensten, U., Cavelier, L., & Feuk, L. (2011). Total RNA sequencing reveals nascent transcription and widespread co-transcriptional splicing in the human brain. *Nat Struct Mol Biol*, *18*(12), 1435-1440. doi:10.1038/nsmb.2143
7. Anan'ina, T., Kisel, A., Kudabaeva, M., Chernysheva, G., Smolyakova, V., Usov, K., . . . Khodanovich, M. (2020). Neurodegeneration, Myelin Loss and Glial Response in the Three-Vessel Global Ischemia Model in Rat. *Int J Mol Sci*, *21*(17). doi:10.3390/ijms21176246
8. Angulo, M. C., Le Meur, K., Kozlov, A. S., Charpak, S., & Audinat, E. (2008). GABA, a forgotten gliotransmitter. *Prog Neurobiol*, *86*(3), 297-303. doi:10.1016/j.pneurobio.2008.08.002
9. Armstrong, R. C., Le, T. Q., Frost, E. E., Borke, R. C., & Vana, A. C. (2002). Absence of fibroblast growth factor 2 promotes oligodendroglial repopulation of demyelinated white matter. *J Neurosci*, *22*(19), 8574-8585.
10. Bagchi, B., Al-Sabi, A., Kaza, S., Scholz, D., O'Leary, V. B., Dolly, J. O., & Ovsepian, S. V. (2014). Disruption of myelin leads to ectopic expression of K(V)1.1 channels with abnormal conductivity of optic nerve axons in a cuprizone-induced model of demyelination. *PLoS One*, *9*(2), e87736. doi:10.1371/journal.pone.0087736

11. Bai, X., Kirchhoff, F., & Scheller, A. (2021). Oligodendroglial GABAergic Signaling: More Than Inhibition! *Neurosci Bull*, *37*(7), 1039-1050. doi:10.1007/s12264-021-00693-w
12. Barnett, M. H., & Prineas, J. W. (2004). Relapsing and remitting multiple sclerosis: pathology of the newly forming lesion. *Ann Neurol*, *55*(4), 458-468. doi:10.1002/ana.20016
13. Baron, W., Metz, B., Bansal, R., Hoekstra, D., & de Vries, H. (2000). PDGF and FGF-2 signaling in oligodendrocyte progenitor cells: regulation of proliferation and differentiation by multiple intracellular signaling pathways. *Mol Cell Neurosci*, *15*(3), 314-329. doi:10.1006/mcne.1999.0827
14. Batiuk, M. Y., Martirosyan, A., Wahis, J., de Vin, F., Marneffe, C., Kusserow, C., . . . Holt, M. G. (2020). Identification of region-specific astrocyte subtypes at single cell resolution. *Nat Commun*, *11*(1), 1220. doi:10.1038/s41467-019-14198-8
15. Baumann, N., & Pham-Dinh, D. (2001). Biology of oligodendrocyte and myelin in the mammalian central nervous system. *Physiol Rev*, *81*(2), 871-927.
16. Bayraktar, O. A., Bartels, T., Holmqvist, S., Kleshchevnikov, V., Martirosyan, A., Polioudakis, D., . . . Rowitch, D. H. (2020). Astrocyte layers in the mammalian cerebral cortex revealed by a single-cell in situ transcriptomic map. *Nat Neurosci*, *23*(4), 500-509. doi:10.1038/s41593-020-0602-1
17. Bebo, B. F., Schuster, J. C., Vandenbark, A. A., & Offner, H. (1998). Gender differences in experimental autoimmune encephalomyelitis develop during the induction of the immune response to encephalitogenic peptides. *J Neurosci Res*, *52*(4), 420-426. doi:10.1002/(SICI)1097-4547(19980515)52:4<420::AID-JNR5>3.0.CO;2-B
18. Bebo, B. F., Vandenbark, A. A., & Offner, H. (1996). Male SJL mice do not relapse after induction of EAE with PLP 139-151. *J Neurosci Res*, *45*(6), 680-689. doi:10.1002/(SICI)1097-4547(19960915)45:6<680::AID-JNR4>3.0.CO;2-4
19. Bentley, D. L. (2014). Coupling mRNA processing with transcription in time and space. *Nat Rev Genet*, *15*(3), 163-175. doi:10.1038/nrg3662
20. Bercury, K. K., & Macklin, W. B. (2015). Dynamics and mechanisms of CNS myelination. *Dev Cell*, *32*(4), 447-458. doi:10.1016/j.devcel.2015.01.016
21. Bernstein, S. L., Guo, Y., Kerr, C., Fawcett, R. J., Stern, J. H., Temple, S., & Mehrabian, Z. (2020). The optic nerve lamina region is a neural progenitor cell niche. *Proc Natl Acad Sci U S A*, *117*(32), 19287-19298. doi:10.1073/pnas.2001858117
22. Bettler, B., Kaupmann, K., Mosbacher, J., & Gassmann, M. (2004). Molecular structure and physiological functions of GABA(B) receptors. *Physiol Rev*, *84*(3), 835-867. doi:10.1152/physrev.00036.2003
23. Bhat, R. V., Axt, K. J., Fosnaugh, J. S., Smith, K. J., Johnson, K. A., Hill, D. E., . . . Baraban, J. M. (1996). Expression of the APC tumor suppressor protein in

- oligodendroglia. *Glia*, 17(2), 169-174. doi:10.1002/(SICI)1098-1136(199606)17:2<169::AID-GLIA8>3.0.CO;2-Y
24. Bjornevik, K., Cortese, M., Healy, B. C., Kuhle, J., Mina, M. J., Leng, Y., . . . Ascherio, A. (2022). Longitudinal analysis reveals high prevalence of Epstein-Barr virus associated with multiple sclerosis. *Science*, 375(6578), 296-301. doi:10.1126/science.abj8222
 25. Boggs, J. M. (2006). Myelin basic protein: a multifunctional protein. *Cell Mol Life Sci*, 63(17), 1945-1961. doi:10.1007/s00018-006-6094-7
 26. Borisy, G., Heald, R., Howard, J., Janke, C., Musacchio, A., & Nogales, E. (2016). Microtubules: 50 years on from the discovery of tubulin. *Nat Rev Mol Cell Biol*, 17(5), 322-328. doi:10.1038/nrm.2016.45
 27. Bork, P., Sander, C., & Valencia, A. (1992). An ATPase domain common to prokaryotic cell cycle proteins, sugar kinases, actin, and hsp70 heat shock proteins. *Proc Natl Acad Sci U S A*, 89(16), 7290-7294. doi:10.1073/pnas.89.16.7290
 28. Braun, L. (2020, Bachelor Thesis). *Influence of oligendroglial GAGAG receptors on de- and remyelination in the murine spinal cord*. Hochschule Kaiserslautern, University of Applied Sciences, Kaiserslautern.
 29. Browne, P., Chandraratna, D., Angood, C., Tremlett, H., Baker, C., Taylor, B. V., & Thompson, A. J. (2014). Atlas of Multiple Sclerosis 2013: A growing global problem with widespread inequity. *Neurology*, 83(11), 1022-1024. doi:10.1212/WNL.0000000000000768
 30. Buschmann, J. P., Berger, K., Awad, H., Clarner, T., Beyer, C., & Kipp, M. (2012). Inflammatory response and chemokine expression in the white matter corpus callosum and gray matter cortex region during cuprizone-induced demyelination. *J Mol Neurosci*, 48(1), 66-76. doi:10.1007/s12031-012-9773-x
 31. Butt, A. M., Pugh, M., Hubbard, P., & James, G. (2004). Functions of optic nerve glia: axoglial signalling in physiology and pathology. *Eye (Lond)*, 18(11), 1110-1121. doi:10.1038/sj.eye.6701595
 32. Byers, S. L., Wiles, M. V., Dunn, S. L., & Taft, R. A. (2012). Mouse estrous cycle identification tool and images. *PLoS One*, 7(4), e35538. doi:10.1371/journal.pone.0035538
 33. Calabresi, P. A. (2004). Diagnosis and management of multiple sclerosis. *Am Fam Physician*, 70(10), 1935-1944.
 34. Calkins, E., Pocius, E., Marracci, G., & Chaudhary, P. (2020). A microwave method for plastic embedding of nervous tissue for light and electron microscopy. *Heliyon*, 6(1), e03036. doi:10.1016/j.heliyon.2019.e03036

35. Calver, A. R., Hall, A. C., Yu, W. P., Walsh, F. S., Heath, J. K., Betsholtz, C., & Richardson, W. D. (1998). Oligodendrocyte population dynamics and the role of PDGF in vivo. *Neuron*, *20*(5), 869-882. doi:10.1016/s0896-6273(00)80469-9
36. Carlton, W. W. (1967). Studies on the induction of hydrocephalus and spongy degeneration by cuprizone feeding and attempts to antidote the toxicity. *Life Sci*, *6*(1), 11-19. doi:10.1016/0024-3205(67)90356-6
37. Carriel, V., Campos, A., Alaminos, M., Raimondo, S., & Geuna, S. (2017). Staining Methods for Normal and Regenerative Myelin in the Nervous System. *Methods Mol Biol*, *1560*, 207-218. doi:10.1007/978-1-4939-6788-9_15
38. Carriel, V., Garrido-Gómez, J., Hernández-Cortés, P., Garzón, I., García-García, S., Sáez-Moreno, J. A., . . . Alaminos, M. (2013). Combination of fibrin-agarose hydrogels and adipose-derived mesenchymal stem cells for peripheral nerve regeneration. *J Neural Eng*, *10*(2), 026022. doi:10.1088/1741-2560/10/2/026022
39. Carriel, V., Garzón, I., Alaminos, M., & Campos, A. (2011). Evaluation of myelin sheath and collagen reorganization pattern in a model of peripheral nerve regeneration using an integrated histochemical approach. *Histochem Cell Biol*, *136*(6), 709-717. doi:10.1007/s00418-011-0874-3
40. Carriel, V., Garzón, I., Alaminos, M., & Cornelissen, M. (2014). Histological assessment in peripheral nerve tissue engineering. *Neural Regen Res*, *9*(18), 1657-1660. doi:10.4103/1673-5374.141798
41. Cherubini, E., Gaiarsa, J. L., & Ben-Ari, Y. (1991). GABA: an excitatory transmitter in early postnatal life. *Trends Neurosci*, *14*(12), 515-519. doi:10.1016/0166-2236(91)90003-d
42. Chiaravalloti, N. D., & DeLuca, J. (2008). Cognitive impairment in multiple sclerosis. *Lancet Neurol*, *7*(12), 1139-1151. doi:10.1016/S1474-4422(08)70259-X
43. Compston, A., & Coles, A. (2002). Multiple sclerosis. *Lancet*, *359*(9313), 1221-1231. doi:10.1016/S0140-6736(02)08220-X
44. Confavreux, C., Aimard, G., & Devic, M. (1980). Course and prognosis of multiple sclerosis assessed by the computerized data processing of 349 patients. *Brain*, *103*(2), 281-300. doi:10.1093/brain/103.2.281
45. Cortese, R., Prados Carrasco, F., Tur, C., Bianchi, A., Brownlee, W., De Angelis, F., . . . Ciccarelli, O. (2023). Differentiating Multiple Sclerosis From AQP4-Neuromyelitis Optica Spectrum Disorder and MOG-Antibody Disease With Imaging. *Neurology*, *100*(3), e308-e323. doi:10.1212/WNL.0000000000201465
46. Crewe, H. K., Ellis, S. W., Lennard, M. S., & Tucker, G. T. (1997). Variable contribution of cytochromes P450 2D6, 2C9 and 3A4 to the 4-hydroxylation of tamoxifen by human liver microsomes. *Biochem Pharmacol*, *53*(2), 171-178. doi:10.1016/s0006-2952(96)00650-8

47. Dallorto, E. (2021, Master Thesis). *Comparative analysis of systemic and focal demyelination models of multiple sclerosis on murine spinal interneurons and glial cells*. University of Torino,
48. Daltrozzo, T., Hapfelmeier, A., Donnachie, E., Schneider, A., & Hemmer, B. (2018). A Systematic Assessment of Prevalence, Incidence and Regional Distribution of Multiple Sclerosis in Bavaria From 2006 to 2015. *Front Neurol*, 9, 871. doi:10.3389/fneur.2018.00871
49. Damo, E. (2019, Master Thesis). *Impact of cuprizone in de- and remyelination on murine spinal glial cells*.
50. Dawson, M. R., Polito, A., Levine, J. M., & Reynolds, R. (2003). NG2-expressing glial progenitor cells: an abundant and widespread population of cycling cells in the adult rat CNS. *Mol Cell Neurosci*, 24(2), 476-488. doi:10.1016/s1044-7431(03)00210-0
51. Dehghan, S., Aref, E., Raoufy, M. R., & Javan, M. (2021). An optimized animal model of lysolecithin induced demyelination in optic nerve; more feasible, more reproducible, promising for studying the progressive forms of multiple sclerosis. *J Neurosci Methods*, 352, 109088. doi:10.1016/j.jneumeth.2021.109088
52. Dehghan, S., Hesaraki, M., Soleimani, M., Mirnajafi-Zadeh, J., Fathollahi, Y., & Javan, M. (2016). Oct4 transcription factor in conjunction with valproic acid accelerates myelin repair in demyelinated optic chiasm in mice. *Neuroscience*, 318, 178-189. doi:10.1016/j.neuroscience.2016.01.028
53. Deiters, O. F. C. (1865). *Untersuchungen über Gehirn und Rückenmark des Menschen und der Säugetiere*. In. Braunschweig.
54. Del Rio-Hortega, P. (1920). *La microglia y su transformación en células en bastoncito y cuerpos gránulo-adiposos*. In. Madrid.
55. Del Rio-Hortega, P. (1933). *Arte y artificio de la ciencia histológica*. In.
56. Denic, A., Johnson, A. J., Bieber, A. J., Warrington, A. E., Rodriguez, M., & Pirko, I. (2011). The relevance of animal models in multiple sclerosis research. *Pathophysiology*, 18(1), 21-29. doi:10.1016/j.pathophys.2010.04.004
57. Dittmer, A., & Dittmer, J. (2006). Beta-actin is not a reliable loading control in Western blot analysis. *Electrophoresis*, 27(14), 2844-2845. doi:10.1002/elps.200500785
58. Eaton, S. L., Roche, S. L., Llaveró Hurtado, M., Oldknow, K. J., Farquharson, C., Gillingwater, T. H., & Wishart, T. M. (2013). Total protein analysis as a reliable loading control for quantitative fluorescent Western blotting. *PLoS One*, 8(8), e72457. doi:10.1371/journal.pone.0072457
59. El Waly, B., Buttigieg, E., Karakus, C., Brustlein, S., & Debarbieux, F. (2020). Longitudinal Intravital Microscopy Reveals Axon Degeneration Concomitant With Inflammatory Cell

- Infiltration in an LPC Model of Demyelination. *Front Cell Neurosci*, 14, 165. doi:10.3389/fncel.2020.00165
60. Elkon, R., Ugalde, A. P., & Agami, R. (2013). Alternative cleavage and polyadenylation: extent, regulation and function. *Nat Rev Genet*, 14(7), 496-506. doi:10.1038/nrg3482
 61. Eng, L. F., & Ghimikar, R. S. (1994). GFAP and astrogliosis. *Brain Pathol*, 4(3), 229-237.
 62. Eng, L. F., Ghimikar, R. S., & Lee, Y. L. (2000). Glial fibrillary acidic protein: GFAP-thirty-one years (1969-2000). *Neurochem Res*, 25(9-10), 1439-1451. doi:10.1023/a:1007677003387
 63. Eng, L. F., Vanderhaeghen, J. J., Bignami, A., & Gerstl, B. (1971). An acidic protein isolated from fibrous astrocytes. *Brain Res*, 28(2), 351-354. doi:10.1016/0006-8993(71)90668-8
 64. Eriksson, J. E., Dechat, T., Grin, B., Helfand, B., Mendez, M., Pallari, H. M., & Goldman, R. D. (2009). Introducing intermediate filaments: from discovery to disease. *J Clin Invest*, 119(7), 1763-1771. doi:10.1172/JCI38339
 65. Faiss, J. H. W., H. (2011). Multiple Sklerose. In P. Berlit (Ed.), *Klinische Neurologie*.
 66. Farrant, M., & Nusser, Z. (2005). Variations on an inhibitory theme: phasic and tonic activation of GABA(A) receptors. *Nat Rev Neurosci*, 6(3), 215-229. doi:10.1038/nrn1625
 67. Feil, R., Brocard, J., Mascrez, B., LeMeur, M., Metzger, D., & Chambon, P. (1996). Ligand-activated site-specific recombination in mice. *Proc Natl Acad Sci U S A*, 93(20), 10887-10890.
 68. Fields, R. D. (2008). White matter in learning, cognition and psychiatric disorders. *Trends Neurosci*, 31(7), 361-370. doi:10.1016/j.tins.2008.04.001
 69. Frangaj, A., & Fan, Q. R. (2018). Structural biology of GABA. *Neuropharmacology*, 136(Pt A), 68-79. doi:10.1016/j.neuropharm.2017.10.011
 70. Franklin, R. J. (2002). Why does remyelination fail in multiple sclerosis? *Nat Rev Neurosci*, 3(9), 705-714. doi:10.1038/nrn917
 71. Galvez, T., Duthey, B., Kniazeff, J., Blahos, J., Rovelli, G., Bettler, B., . . . Pin, J. P. (2001). Allosteric interactions between GB1 and GB2 subunits are required for optimal GABA(B) receptor function. *EMBO J*, 20(9), 2152-2159. doi:10.1093/emboj/20.9.2152
 72. Gautier, H. O., Evans, K. A., Volbracht, K., James, R., Sitnikov, S., Lundgaard, I., . . . Káradóttir, R. T. (2015). Neuronal activity regulates remyelination via glutamate signalling to oligodendrocyte progenitors. *Nat Commun*, 6, 8518. doi:10.1038/ncomms9518
 73. GBD. (2016). Multiple Sclerosis Collaborators. Global, regional, and national burden of multiple sclerosis 1990-2016: a systematic analysis for the Global Burden of Disease Study 2016. In: *Lancet Neurol*, 2019.

74. Geisler, N., & Weber, K. (1983). Amino acid sequence data on glial fibrillary acidic protein (GFA); implications for the subdivision of intermediate filaments into epithelial and non-epithelial members. *EMBO J*, 2(11), 2059-2063. doi:10.1002/j.1460-2075.1983.tb01700.x
75. Giacci, M. K., Bartlett, C. A., Huynh, M., Kilburn, M. R., Dunlop, S. A., & Fitzgerald, M. (2018). Three dimensional electron microscopy reveals changing axonal and myelin morphology along normal and partially injured optic nerves. *Sci Rep*, 8(1), 3979. doi:10.1038/s41598-018-22361-2
76. Gilda, J. E., Ghosh, R., Cheah, J. X., West, T. M., Bodine, S. C., & Gomes, A. V. (2015). Western Blotting Inaccuracies with Unverified Antibodies: Need for a Western Blotting Minimal Reporting Standard (WBMRS). *PLoS One*, 10(8), e0135392. doi:10.1371/journal.pone.0135392
77. Gilda, J. E., & Gomes, A. V. (2013). Stain-Free total protein staining is a superior loading control to β -actin for Western blots. *Anal Biochem*, 440(2), 186-188. doi:10.1016/j.ab.2013.05.027
78. Ginhoux, F., Greter, M., Leboeuf, M., Nandi, S., See, P., Gokhan, S., . . . Merad, M. (2010). Fate mapping analysis reveals that adult microglia derive from primitive macrophages. *Science*, 330(6005), 841-845. doi:10.1126/science.1194637
79. Goasdoue, K., Awabdy, D., Bjorkman, S. T., & Miller, S. (2016). Standard loading controls are not reliable for Western blot quantification across brain development or in pathological conditions. *Electrophoresis*, 37(4), 630-634. doi:10.1002/elps.201500385
80. Gold, R., Wolinsky, J. S., Amato, M. P., & Comi, G. (2010). Evolving expectations around early management of multiple sclerosis. *Ther Adv Neurol Disord*, 3(6), 351-367. doi:10.1177/1756285610385608
81. Goldberg, M. P., & Ransom, B. R. (2003). New light on white matter. *Stroke*, 34(2), 330-332. doi:10.1161/01.str.0000054048.22626.b9
82. Goldman, J. M., Murr, A. S., & Cooper, R. L. (2007). The rodent estrous cycle: characterization of vaginal cytology and its utility in toxicological studies. *Birth Defects Res B Dev Reprod Toxicol*, 80(2), 84-97. doi:10.1002/bdrb.20106
83. Golgi, C. (1885). Sulla Fina Anatomia Degli Organi Centrali del Sistema Nervoso. In. Milano.
84. Gross, A., Schoendube, J., Zimmermann, S., Steeb, M., Zengerle, R., & Koltay, P. (2015). Technologies for Single-Cell Isolation. *Int J Mol Sci*, 16(8), 16897-16919. doi:10.3390/ijms160816897
85. Gudi, V., Gingele, S., Skripuletz, T., & Stangel, M. (2014). Glial response during cuprizone-induced de- and remyelination in the CNS: lessons learned. *Front Cell Neurosci*, 8, 73. doi:10.3389/fncel.2014.00073

86. Gudi, V., Moharreggh-Khiabani, D., Skripuletz, T., Koutsoudaki, P. N., Kotsiari, A., Skuljec, J., . . . Stangel, M. (2009). Regional differences between grey and white matter in cuprizone induced demyelination. *Brain Res*, *1283*, 127-138. doi:10.1016/j.brainres.2009.06.005
87. Hainz, N., Becker, P., Rapp, D., Wagenpfeil, S., Wonenberg, B., Beisswenger, C., . . . Meier, C. (2017). Probenecid-treatment reduces demyelination induced by cuprizone feeding. *J Chem Neuroanat*, *85*, 21-26. doi:10.1016/j.jchemneu.2017.06.003
88. Harbo, H. F., Gold, R., & Tintoré, M. (2013). Sex and gender issues in multiple sclerosis. *Ther Adv Neurol Disord*, *6*(4), 237-248. doi:10.1177/1756285613488434
89. Hart, F. M., & Bainbridge, J. (2016). Current and emerging treatment of multiple sclerosis. *Am J Manag Care*, *22*(6 Suppl), s159-170.
90. Hartline, D. K., & Colman, D. R. (2007). Rapid conduction and the evolution of giant axons and myelinated fibers. *Curr Biol*, *17*(1), R29-35. doi:10.1016/j.cub.2006.11.042
91. Hedderich, J., & Sachs, L. (2021). Angewandte Statistik - Methodensammlung mit R. In. Berlin/Heidelberg: Springer Spektrum.
92. Hemmer, B. e. a. (2023). Diagnose und Therapie der Multiplen Sklerose, Neuromyelitis-optica-Spektrum-Erkrankungen und MOG-IgG-assoziierten Erkrankungen, S2k-Leitlinie, 2023. In: Deutsche Gesellschaft für Neurologie (Hrsg.), Leitlinien für Diagnostik und Therapie in der Neurologie. Online: www.dgn.org/leitlinien (abgerufen am 29.06.2023).
93. Herzel, L., Ottoz, D. S. M., Alpert, T., & Neugebauer, K. M. (2017). Splicing and transcription touch base: co-transcriptional spliceosome assembly and function. *Nat Rev Mol Cell Biol*, *18*(10), 637-650. doi:10.1038/nrm.2017.63
94. Herzenberg, L. A., & Sweet, R. G. (1976). Fluorescence-activated cell sorting. *Sci Am*, *234*(3), 108-117. doi:10.1038/scientificamerican0376-108
95. Hibbits, N., Yoshino, J., Le, T. Q., & Armstrong, R. C. (2012). Astroglialosis during acute and chronic cuprizone demyelination and implications for remyelination. *ASN Neuro*, *4*(6), 393-408. doi:10.1042/AN20120062
96. Hildebrand, C., & Mohseni, S. (2005). The Structure of Myelinated Axons in the CNS. In *Multiple Sclerosis as A Neuronal Disease*. Amsterdam: Elsevier Inc, DOI: 10.1016/B978-012738761-1/50002-X.
97. Hiremath, M. M., Chen, V. S., Suzuki, K., Ting, J. P., & Matsushima, G. K. (2008). MHC class II exacerbates demyelination in vivo independently of T cells. *J Neuroimmunol*, *203*(1), 23-32. doi:10.1016/j.jneuroim.2008.06.034
98. Hochstrasser, T., Exner, G. L., Nyamoya, S., Schmitz, C., & Kipp, M. (2017). Cuprizone-Containing Pellets Are Less Potent to Induce Consistent Demyelination in the Corpus Callosum of C57BL/6 Mice. *J Mol Neurosci*, *61*(4), 617-624. doi:10.1007/s12031-017-0903-3

99. Holstiege, J., Akmatov, M. K., Klimke, K., Dammertz, L., Kohring, C., Marx, C., . . . Bätzing, J. (2022). Trends in administrative prevalence of multiple sclerosis and utilization patterns of disease modifying drugs in Germany. *Mult Scler Relat Disord*, *59*, 103534. doi:10.1016/j.msard.2022.103534
100. Holstiege, J., Steffen, A., Goffrier, B., & Bätzing, J. (2017). Epidemiologie der Multiplen Sklerose – eine populationsbasierte deutschlandweite Studie. In. Berlin: Zentralinstitut für die kassenärztliche Versorgung in Deutschland, versorgungsatlas.de.
101. Hoppe, D., & Kettenmann, H. (1989). GABA triggers a Cl⁻ efflux from cultured mouse oligodendrocytes. *Neurosci Lett*, *97*(3), 334-339. doi:10.1016/0304-3940(89)90620-4
102. Horner, P. J., Power, A. E., Kempermann, G., Kuhn, H. G., Palmer, T. D., Winkler, J., . . . Gage, F. H. (2000). Proliferation and differentiation of progenitor cells throughout the intact adult rat spinal cord. *J Neurosci*, *20*(6), 2218-2228.
103. Horstmann, L., Kuehn, S., Pedreiturria, X., Haak, K., Pfarrer, C., Dick, H. B., . . . Joachim, S. C. (2016). Microglia response in retina and optic nerve in chronic experimental autoimmune encephalomyelitis. *J Neuroimmunol*, *298*, 32-41. doi:10.1016/j.jneuroim.2016.06.008
104. Horstmann, L., Schmid, H., Heinen, A. P., Kurschus, F. C., Dick, H. B., & Joachim, S. C. (2013). Inflammatory demyelination induces glia alterations and ganglion cell loss in the retina of an experimental autoimmune encephalomyelitis model. *J Neuroinflammation*, *10*, 120. doi:10.1186/1742-2094-10-120
105. Hu, P., Zhang, W., Xin, H., & Deng, G. (2016). Single Cell Isolation and Analysis. *Front Cell Dev Biol*, *4*, 116. doi:10.3389/fcell.2016.00116
106. Huang, W., Bai, X., Stopper, L., Catalin, B., Cartarozzi, L. P., Scheller, A., & Kirchhoff, F. (2018). During Development NG2 Glial Cells of the Spinal Cord are Restricted to the Oligodendrocyte Lineage, but Generate Astrocytes upon Acute Injury. *Neuroscience*, *385*, 154-165. doi:10.1016/j.neuroscience.2018.06.015
107. Ibrahim, S. F., & van den Engh, G. (2003). High-speed cell sorting: fundamentals and recent advances. *Curr Opin Biotechnol*, *14*(1), 5-12. doi:10.1016/s0958-1669(02)00009-5
108. Ishibashi, T., Dakin, K. A., Stevens, B., Lee, P. R., Kozlov, S. V., Stewart, C. L., & Fields, R. D. (2006). Astrocytes promote myelination in response to electrical impulses. *Neuron*, *49*(6), 823-832. doi:10.1016/j.neuron.2006.02.006
109. Itoh, N., Itoh, Y., Tassoni, A., Ren, E., Kaito, M., Ohno, A., . . . Voskuhl, R. R. (2018). Cell-specific and region-specific transcriptomics in the multiple sclerosis model: Focus on astrocytes. *Proc Natl Acad Sci U S A*, *115*(2), E302-E309. doi:10.1073/pnas.1716032115
110. Jahn, H. M., Kasakow, C. V., Helfer, A., Michely, J., Verkhatsky, A., Maurer, H. H., . . . Kirchhoff, F. (2018). Refined protocols of tamoxifen injection for inducible DNA recombination in mouse astroglia. *Sci Rep*, *8*(1), 5913. doi:10.1038/s41598-018-24085-9

111. Jeffery, N. D., & Blakemore, W. F. (1995). Remyelination of mouse spinal cord axons demyelinated by local injection of lysolecithin. *J Neurocytol*, 24(10), 775-781. doi:10.1007/BF01191213
112. Kaiser, M., Maletzki, I., Huelsmann, S., Holtmann, B., Schulz-Schaeffer, W., Kirchhoff, F., . . . Neusch, C. (2006). Progressive loss of a glial potassium channel (KCNJ10) in the spinal cord of the SOD1 (G93A) transgenic mouse model of amyotrophic lateral sclerosis. *Journal of Neurochemistry*, 99(3), 900-912. doi:10.1111/j.1471-4159.2006.04131.x
113. Kalman, B., Laitinen, K., & Komoly, S. (2007). The involvement of mitochondria in the pathogenesis of multiple sclerosis. *J Neuroimmunol*, 188(1-2), 1-12. doi:10.1016/j.jneuroim.2007.03.020
114. Kashani, I. R., Hedayatpour, A., Pasbakhsh, P., Kafami, L., Khallaghi, B., & Malek, F. (2015). Progesterone Enhanced Remyelination in the Mouse Corpus Callosum after Cuprizone Induced Demyelination. *Iran J Med Sci*, 40(6), 507-514.
115. Kaupmann, K., Schuler, V., Mosbacher, J., Bischoff, S., Bittiger, H., Heid, J., . . . Bettler, B. (1998). Human gamma-aminobutyric acid type B receptors are differentially expressed and regulate inwardly rectifying K⁺ channels. *Proc Natl Acad Sci U S A*, 95(25), 14991-14996.
116. Khakh, B. S., & Deneen, B. (2019). The Emerging Nature of Astrocyte Diversity. *Annu Rev Neurosci*, 42, 187-207. doi:10.1146/annurev-neuro-070918-050443
117. Khan, S. U., & Khan, M. U. (2021). Recent Developments and Applications of Single-Cell RNA Sequencing
118. Technology in Cell Classification. In: Journal of Biomedical Research & Environmental Sciences.
119. Kipp, M., Nyamoya, S., Hochstrasser, T., & Amor, S. (2017). Multiple sclerosis animal models: a clinical and histopathological perspective. *Brain Pathol*, 27(2), 123-137. doi:10.1111/bpa.12454
120. Kiray, H., Lindsay, S. L., Hosseinzadeh, S., & Barnett, S. C. (2016). The multifaceted role of astrocytes in regulating myelination. *Exp Neurol*. doi:10.1016/j.expneurol.2016.03.009
121. Kirchhoff, F., & Kettenmann, H. (1992). GABA Triggers a [Ca²⁺]_i Increase in Murine Precursor Cells of the Oligodendrocyte Lineage. *Eur J Neurosci*, 4(11), 1049-1058. doi:10.1111/j.1460-9568.1992.tb00131.x
122. Kluver, H., & Barrera, E. (1953). A method for the combined staining of cells and fibers in the nervous system. *J Neuropathol Exp Neurol*, 12(4), 400-403. doi:10.1097/00005072-195312040-00008

123. Kraft, R. H., Mitchell, O. R., Languis, M. L., & Wheatley, G. H. (1980). Hemispheric asymmetries during six- to eight-year-olds performance of Piagetian conservation and reading tasks. *Neuropsychologia*, *18*(6), 637-643. doi:10.1016/0028-3932(80)90103-7
124. Kroepfl, J. F., Viise, L. R., Charron, A. J., Linington, C., & Gardinier, M. V. (1996). Investigation of myelin/oligodendrocyte glycoprotein membrane topology. *J Neurochem*, *67*(5), 2219-2222. doi:10.1046/j.1471-4159.1996.67052219.x
125. Kuhn, S., Gritti, L., Crooks, D., & Dombrowski, Y. (2019). Oligodendrocytes in Development, Myelin Generation and Beyond. *Cells*, *8*(11). doi:10.3390/cells8111424
126. Kuypers, N. J., Bankston, A. N., Howard, R. M., Beare, J. E., & Whittemore, S. R. (2016). Remyelinating Oligodendrocyte Precursor Cell miRNAs from the Sfmbt2 Cluster Promote Cell Cycle Arrest and Differentiation. *J Neurosci*, *36*(5), 1698-1710. doi:10.1523/JNEUROSCI.1240-15.2016
127. Kwon, H. S., Nakaya, N., Abu-Asab, M., Kim, H. S., & Tomarev, S. I. (2014). Myocilin is involved in NgR1/Lingo-1-mediated oligodendrocyte differentiation and myelination of the optic nerve. *J Neurosci*, *34*(16), 5539-5551. doi:10.1523/JNEUROSCI.4731-13.2014
128. Laflamme, N., Cisbani, G., Préfontaine, P., Srour, Y., Bernier, J., St-Pierre, M. K., . . . Rivest, S. (2018). mCSF-Induced Microglial Activation Prevents Myelin Loss and Promotes Its Repair in a Mouse Model of Multiple Sclerosis. *Front Cell Neurosci*, *12*, 178. doi:10.3389/fncel.2018.00178
129. Lampron, A., Larochelle, A., Laflamme, N., Préfontaine, P., Plante, M. M., Sánchez, M. G., . . . Rivest, S. (2015). Inefficient clearance of myelin debris by microglia impairs remyelinating processes. *J Exp Med*, *212*(4), 481-495. doi:10.1084/jem.20141656
130. Langer-Gould, A. (2014). The incidence of clinically isolated syndrome in a multi-ethnic cohort.
131. Lassmann, H. (2014). Multiple sclerosis: lessons from molecular neuropathology. *Exp Neurol*, *262 Pt A*, 2-7. doi:10.1016/j.expneurol.2013.12.003
132. Lassmann, H., Brück, W., & Lucchinetti, C. F. (2007). The immunopathology of multiple sclerosis: an overview. *Brain Pathol*, *17*(2), 210-218. doi:10.1111/j.1750-3639.2007.00064.x
133. Lassmann, H., & van Horssen, J. (2016). Oxidative stress and its impact on neurons and glia in multiple sclerosis lesions. *Biochim Biophys Acta*, *1862*(3), 506-510. doi:10.1016/j.bbadis.2015.09.018
134. Ledbetter, M. C., & Porter, K. R. (1963). A "MICROTUBULE" IN PLANT CELL FINE STRUCTURE. *J Cell Biol*, *19*(1), 239-250. doi:10.1083/jcb.19.1.239
135. Lee, S. E., Lee, Y., & Lee, G. H. (2019). The regulation of glutamic acid decarboxylases in GABA neurotransmission in the brain. *Arch Pharm Res*, *42*(12), 1031-1039. doi:10.1007/s12272-019-01196-z

136. Leppert, D., Watanabe, M., Schaedelin, S., Piehl, F., Furlan, R., Gastaldi, M., . . . Kuhle, J. (2023). Granulocyte activation markers in cerebrospinal fluid differentiate acute neuromyelitis spectrum disorder from multiple sclerosis. *J Neurol Neurosurg Psychiatry*, *94*(9), 726-737. doi:10.1136/jnnp-2022-330796
137. Li, Q., & Barres, B. A. (2018). Microglia and macrophages in brain homeostasis and disease. *Nat Rev Immunol*, *18*(4), 225-242. doi:10.1038/nri.2017.125
138. Li, W. W., Penderis, J., Zhao, C., Schumacher, M., & Franklin, R. J. (2006). Females remyelinate more efficiently than males following demyelination in the aged but not young adult CNS. *Exp Neurol*, *202*(1), 250-254. doi:10.1016/j.expneurol.2006.05.012
139. Liddelow, S. A., & Barres, B. A. (2017). Reactive Astrocytes: Production, Function, and Therapeutic Potential. *Immunity*, *46*(6), 957-967. doi:10.1016/j.immuni.2017.06.006
140. Liddelow, S. A., Guttenplan, K. A., Clarke, L. E., Bennett, F. C., Bohlen, C. J., Schirmer, L., . . . Barres, B. A. (2017). Neurotoxic reactive astrocytes are induced by activated microglia. *Nature*. doi:10.1038/nature21029
141. Lin, Z., Gasic, I., Chandrasekaran, V., Peters, N., Shao, S., Mitchison, T. J., & Hegde, R. S. (2020). TTC5 mediates autoregulation of tubulin via mRNA degradation. *Science*, *367*(6473), 100-104. doi:10.1126/science.aaz4352
142. Linder, M. C., & Hazegh-Azam, M. (1996). Copper biochemistry and molecular biology. *Am J Clin Nutr*, *63*(5), 797S-811S. doi:10.1093/ajcn/63.5.797
143. Lindner, M., Fokuhl, J., Linsmeier, F., Trebst, C., & Stangel, M. (2009). Chronic toxic demyelination in the central nervous system leads to axonal damage despite remyelination. *Neurosci Lett*, *453*(2), 120-125. doi:10.1016/j.neulet.2009.02.004
144. Lindner, M., Heine, S., Haastert, K., Garde, N., Fokuhl, J., Linsmeier, F., . . . Stangel, M. (2008). Sequential myelin protein expression during remyelination reveals fast and efficient repair after central nervous system demyelination. *Neuropathol Appl Neurobiol*, *34*(1), 105-114. doi:10.1111/j.1365-2990.2007.00879.x
145. Litovchick, L. (2020a). Staining the Blot for Total Protein with Ponceau S. *Cold Spring Harb Protoc*, *2020*(3), 098459. doi:10.1101/pdb.prot098459
146. Litovchick, L. (2020b). Stripping of the Immunoblot for Reprobing. *Cold Spring Harb Protoc*, *2020*(3), 098491. doi:10.1101/pdb.prot098491
147. Liu, Y., Cai, Y., & Zhang, X. (2003). Induction of caspase-dependent apoptosis in cultured rat oligodendrocytes by murine coronavirus is mediated during cell entry and does not require virus replication. *J Virol*, *77*(22), 11952-11963. doi:10.1128/jvi.77.22.11952-11963.2003
148. Lubetzki, C., Zalc, B., Williams, A., Stadelmann, C., & Stankoff, B. (2020). Remyelination in multiple sclerosis: from basic science to clinical translation. *Lancet Neurol*, *19*(8), 678-688. doi:10.1016/S1474-4422(20)30140-X

149. Lublin, F. D., & Reingold, S. C. (1996). Defining the clinical course of multiple sclerosis. *Neurology*, *46*(4), 907. doi:10.1212/WNL.46.4.907
150. Lublin, F. D., Reingold, S. C., Cohen, J. A., Cutter, G. R., Sørensen, P. S., Thompson, A. J., . . . Polman, C. H. (2014). Defining the clinical course of multiple sclerosis: the 2013 revisions. *Neurology*, *83*(3), 278-286. doi:10.1212/WNL.0000000000000560
151. Lucchinetti, C., Brück, W., Parisi, J., Scheithauer, B., Rodriguez, M., & Lassmann, H. (2000). Heterogeneity of multiple sclerosis lesions: implications for the pathogenesis of demyelination. *Ann Neurol*, *47*(6), 707-717. doi:10.1002/1531-8249(200006)47:6<707::aid-ana3>3.0.co;2-q
152. Luyt, K., Slade, T. P., Dorward, J. J., Durant, C. F., Wu, Y., Shigemoto, R., . . . Molnár, E. (2007). Developing oligodendrocytes express functional GABA(B) receptors that stimulate cell proliferation and migration. *J Neurochem*, *100*(3), 822-840. doi:10.1111/j.1471-4159.2006.04255.x
153. Lüllmann-Rauch, R., & Asan, E. *Taschenlehrbuch Histologie* (6., vollständig überarbeitete Auflage ed.).
154. Marena, S., Huang, S. C., Castoldi, V., d'Isa, R., Costa, G. D., Comi, G., & Leocani, L. (2020). Functional evolution of visual involvement in experimental autoimmune encephalomyelitis. *Mult Scler J Exp Transl Clin*, *6*(4), 2055217320963474. doi:10.1177/2055217320963474
155. Marena, S., Huang, S. C., Dalla Costa, G., d'Isa, R., Castoldi, V., Rossi, E., . . . Leocani, L. (2022). Visual Evoked Potentials to Monitor Myelin Cuprizone-Induced Functional Changes. *Front Neurosci*, *16*, 820155. doi:10.3389/fnins.2022.820155
156. Matsushima, G. K., & Morell, P. (2001). The neurotoxicant, cuprizone, as a model to study demyelination and remyelination in the central nervous system. *Brain Pathol*, *11*(1), 107-116.
157. Matute, C., & Pérez-Cerdá, F. (2005). Multiple sclerosis: novel perspectives on newly forming lesions. *Trends Neurosci*, *28*(4), 173-175. doi:10.1016/j.tins.2005.01.006
158. Mayo, L., Quintana, F. J., & Weiner, H. L. (2012). The innate immune system in demyelinating disease. *Immunol Rev*, *248*(1), 170-187. doi:10.1111/j.1600-065X.2012.01135.x
159. Mazumder, A. G., Julé, A. M., Cullen, P. F., & Sun, D. (2022). Astrocyte heterogeneity within white matter tracts and a unique subpopulation of optic nerve head astrocytes. *iScience*, *25*(12), 105568. doi:10.1016/j.isci.2022.105568
160. McMurran, C. E., Zhao, C., & Franklin, R. J. M. (2019). Toxin-Based Models to Investigate Demyelination and Remyelination. *Methods Mol Biol*, *1936*, 377-396. doi:10.1007/978-1-4939-9072-6_21

161. Melling, M., Karimian-Teherani, D., Mostler, S., & Hochmeister, S. (2005). Three-dimensional morphological characterization of optic nerve fibers by atomic force microscopy and by scanning electron microscopy. *Microsc Microanal*, 11(4), 333-340. doi:10.1017/S1431927605050245
162. Menichella, D. M., Goodenough, D. A., Sirkowski, E., Scherer, S. S., & Paul, D. L. (2003). Connexins are critical for normal myelination in the CNS. *J Neurosci*, 23(13), 5963-5973.
163. Messing, A., & Brenner, M. (2020). GFAP at 50. *ASN Neuro*, 12, 1759091420949680. doi:10.1177/1759091420949680
164. Miller, D., Barkhof, F., Montalban, X., Thompson, A., & Filippi, M. (2005). Clinically isolated syndromes suggestive of multiple sclerosis, part I: natural history, pathogenesis, diagnosis, and prognosis. *Lancet Neurol*, 4(5), 281-288. doi:10.1016/S1474-4422(05)70071-5
165. Miller, D. H., Chard, D. T., & Ciccarelli, O. (2012). Clinically isolated syndromes. *Lancet Neurol*, 11(2), 157-169. doi:10.1016/S1474-4422(11)70274-5
166. Miller, D. H., Weinshenker, B. G., Filippi, M., Banwell, B. L., Cohen, J. A., Freedman, M. S., . . . Polman, C. H. (2008). Differential diagnosis of suspected multiple sclerosis: a consensus approach. *Mult Scler*, 14(9), 1157-1174. doi:10.1177/1352458508096878
167. Min, Y., Kristiansen, K., Boggs, J. M., Husted, C., Zasadzinski, J. A., & Israelachvili, J. (2009). Interaction forces and adhesion of supported myelin lipid bilayers modulated by myelin basic protein. *Proc Natl Acad Sci U S A*, 106(9), 3154-3159. doi:10.1073/pnas.0813110106
168. Mohamed, A., Al-Kafaji, G., Almahroos, A., Almosawi, Z., Alalwan, H., Abdulla, R., . . . Kamal, A. (2019). Effects of enhanced environment and induced depression on cuprizone mouse model of demyelination. *Exp Ther Med*, 18(1), 566-572. doi:10.3892/etm.2019.7654
169. Moore, C. S., Abdullah, S. L., Brown, A., Arulpragasam, A., & Crocker, S. J. (2011). How factors secreted from astrocytes impact myelin repair. *J Neurosci Res*, 89(1), 13-21. doi:10.1002/jnr.22482
170. Moritz, C. P. (2017). Tubulin or Not Tubulin: Heading Toward Total Protein Staining as Loading Control in Western Blots. *Proteomics*, 17(20). doi:10.1002/pmic.201600189
171. Moscarello, M. A. (1997). Myelin Basic Protein, the "Executive" Molecule of the Myelin Membrane. In *Cell Biology and Pathology of Myelin* (pp. 13-25). New York: Juurlink, B.H.J., Devon, R.M., Doucette, J.R., Nazarali, A.J., Schreyer, D.J., Verge, V.M.K. (eds).
172. Moskowitz, P. F., & Oblinger, M. M. (1995). Transcriptional and post-transcriptional mechanisms regulating neurofilament and tubulin gene expression during normal development of the rat brain. *Brain Res Mol Brain Res*, 30(2), 211-222. doi:10.1016/0169-328x(95)00006-e

173. Mozafari, S., Javan, M., Sherafat, M. A., Mirnajafi-Zadeh, J., Heibatollahi, M., Pour-Beiranvand, S., . . . Ahmadiani, A. (2011). Analysis of structural and molecular events associated with adult rat optic chiasm and nerves demyelination and remyelination: possible role for 3rd ventricle proliferating cells. *Neuromolecular Med*, *13*(2), 138-150. doi:10.1007/s12017-011-8143-0
174. Nair, A., Frederick, T. J., & Miller, S. D. (2008). Astrocytes in multiple sclerosis: a product of their environment. *Cell Mol Life Sci*, *65*(17), 2702-2720. doi:10.1007/s00018-008-8059-5
175. Nakahara, J., Aiso, S., & Suzuki, N. (2010). Autoimmune versus oligodendroglipathy: the pathogenesis of multiple sclerosis. *Arch Immunol Ther Exp (Warsz)*, *58*(5), 325-333. doi:10.1007/s00005-010-0094-x
176. Namekata, K., Kimura, A., Harada, C., Yoshida, H., Matsumoto, Y., & Harada, T. (2014). Dock3 protects myelin in the cuprizone model for demyelination. *Cell Death Dis*, *5*(8), e1395. doi:10.1038/cddis.2014.357
177. Nguyen, J. V., Soto, I., Kim, K. Y., Bushong, E. A., Oglesby, E., Valiente-Soriano, F. J., . . . Marsh-Armstrong, N. (2011). Myelination transition zone astrocytes are constitutively phagocytic and have synuclein dependent reactivity in glaucoma. *Proc Natl Acad Sci U S A*, *108*(3), 1176-1181. doi:10.1073/pnas.1013965108
178. Noseworthy, J. H. (1999). Progress in determining the causes and treatment of multiple sclerosis. *Nature*, *399*(6738 Suppl), A40-47. doi:10.1038/399a040
179. Noyes, K., & Weinstock-Guttman, B. (2013). Impact of diagnosis and early treatment on the course of multiple sclerosis. *Am J Manag Care*, *19*(17 Suppl), s321-331.
180. Odermatt, B., Wellershaus, K., Wallraff, A., Seifert, G., Degen, J., Euwens, C., . . . Willecke, K. (2003). Connexin 47 (Cx47)-deficient mice with enhanced green fluorescent protein reporter gene reveal predominant oligodendrocytic expression of Cx47 and display vacuolized myelin in the CNS. *J Neurosci*, *23*(11), 4549-4559.
181. Ono, K., Gotoh, H., Nomura, T., Morita, T., Baba, O., Matsumoto, M., . . . Ohno, N. (2022). Ultrastructural characteristics of oligodendrocyte precursor cells in the early postnatal mouse optic nerve observed by serial block-face scanning electron microscopy. *PLoS One*, *17*(12), e0278118. doi:10.1371/journal.pone.0278118
182. Orihuela, R., McPherson, C. A., & Harry, G. J. (2016). Microglial M1/M2 polarization and metabolic states. *Br J Pharmacol*, *173*(4), 649-665. doi:10.1111/bph.13139
183. Orthmann-Murphy, J. L., Abrams, C. K., & Scherer, S. S. (2008). Gap junctions couple astrocytes and oligodendrocytes. *J Mol Neurosci*, *35*(1), 101-116. doi:10.1007/s12031-007-9027-5

184. Pajooesh-Ganji, A., & Miller, R. H. (2020). Targeted Oligodendrocyte Apoptosis in Optic Nerve Leads to Persistent Demyelination. *Neurochem Res*, *45*(3), 580-590. doi:10.1007/s11064-019-02754-z
185. Papenfuss, T. L., Rogers, C. J., Gienapp, I., Yurrita, M., McClain, M., Damico, N., . . . Whitacre, C. C. (2004). Sex differences in experimental autoimmune encephalomyelitis in multiple murine strains. *J Neuroimmunol*, *150*(1-2), 59-69. doi:10.1016/j.jneuroim.2004.01.018
186. Penderis, J., Shields, S. A., & Franklin, R. J. (2003). Impaired remyelination and depletion of oligodendrocyte progenitors does not occur following repeated episodes of focal demyelination in the rat central nervous system. *Brain*, *126*(Pt 6), 1382-1391. doi:10.1093/brain/awg126
187. Pestana, F., Edwards-Faret, G., Belgard, T. G., Martirosyan, A., & Holt, M. G. (2020). No Longer Underappreciated: The Emerging Concept of Astrocyte Heterogeneity in Neuroscience. *Brain Sciences*, *10*(3), 168. doi:10.3390/brainsci10030168
188. Petrikowski, L., Reinehr, S., Hauptelshofer, S., Deppe, L., Graz, F., Kleiter, I., . . . Joachim, S. C. (2021). Progressive Retinal and Optic Nerve Damage in a Mouse Model of Spontaneous Opticospinal Encephalomyelitis. *Front Immunol*, *12*, 759389. doi:10.3389/fimmu.2021.759389
189. Pin, J. P., & Bettler, B. (2016). Organization and functions of mGlu and GABAB receptor complexes. *Nature*, *540*(7631), 60-68. doi:10.1038/nature20566
190. Plantone, D., De Angelis, F., Doshi, A., & Chataway, J. (2016). Secondary Progressive Multiple Sclerosis: Definition and Measurement. *CNS Drugs*, *30*(6), 517-526. doi:10.1007/s40263-016-0340-9
191. Plemel, J. R., Michaels, N. J., Weishaupt, N., Caprariello, A. V., Keough, M. B., Rogers, J. A., . . . Yong, V. W. (2018). Mechanisms of lysophosphatidylcholine-induced demyelination: A primary lipid disrupting myelinopathy. *Glia*, *66*(2), 327-347. doi:10.1002/glia.23245
192. Polman, C. H., Reingold, S. C., Banwell, B., Clanet, M., Cohen, J. A., Filippi, M., . . . Wolinsky, J. S. (2011). Diagnostic criteria for multiple sclerosis: 2010 revisions to the McDonald criteria. *Ann Neurol*, *69*(2), 292-302. doi:10.1002/ana.22366
193. Ponath, G., Park, C., & Pitt, D. (2018). The Role of Astrocytes in Multiple Sclerosis. *Front Immunol*, *9*, 217. doi:10.3389/fimmu.2018.00217
194. Praet, J., Guglielmetti, C., Berneman, Z., Van der Linden, A., & Ponsaerts, P. (2014). Cellular and molecular neuropathology of the cuprizone mouse model: clinical relevance for multiple sclerosis. *Neurosci Biobehav Rev*, *47*, 485-505. doi:10.1016/j.neubiorev.2014.10.004

195. Pujol, J., Soriano-Mas, C., Ortiz, H., Sebastián-Gallés, N., Losilla, J. M., & Deus, J. (2006). Myelination of language-related areas in the developing brain. *Neurology*, *66*(3), 339-343. doi:10.1212/01.wnl.0000201049.66073.8d
196. Qu, J., & Jakobs, T. C. (2013). The Time Course of Gene Expression during Reactive Gliosis in the Optic Nerve. *PLoS One*, *8*(6), e67094. doi:10.1371/journal.pone.0067094
197. Quarles, R. H. (2007). Myelin-associated glycoprotein (MAG): past, present and beyond. *J Neurochem*, *100*(6), 1431-1448. doi:10.1111/j.1471-4159.2006.04319.x
198. Radu, R., Petrescu, G. E. D., Gorgan, R. M., & Brehar, F. M. (2022). GFAP δ : A Promising Biomarker and Therapeutic Target in Glioblastoma. *Front Oncol*, *12*, 859247. doi:10.3389/fonc.2022.859247
199. Ransohoff, R. M. (2012). Animal models of multiple sclerosis: the good, the bad and the bottom line. *Nat Neurosci*, *15*(8), 1074-1077. doi:10.1038/nn.3168
200. Ransohoff, R. M. (2016). A polarizing question: do M1 and M2 microglia exist? *Nat Neurosci*, *19*(8), 987-991. doi:10.1038/nn.4338
201. Rash, J. E. (2010). Molecular disruptions of the panglial syncytium block potassium siphoning and axonal saltatory conduction: pertinence to neuromyelitis optica and other demyelinating diseases of the central nervous system. *Neuroscience*, *168*(4), 982-1008. doi:10.1016/j.neuroscience.2009.10.028
202. Rawji, K. S., Gonzalez Martinez, G. A., Sharma, A., & Franklin, R. J. M. (2020). The Role of Astrocytes in Remyelination. *Trends Neurosci*, *43*(8), 596-607. doi:10.1016/j.tins.2020.05.006
203. Rieder, P. (2023, PhD Thesis). *Glial Ca²⁺ signaling in the spinal cord and the myelin-protective effect of the GABA_B receptor in oligodendrocyte precursor cells.*
204. Roberts, E., & Frankel, S. (1950). gamma-Aminobutyric acid in brain: its formation from glutamic acid. *J Biol Chem*, *187*(1), 55-63.
205. Ronchi, G., Jager, S. B., Vaegter, C. B., Raimondo, S., Giacobini-Robecchi, M. G., & Geuna, S. (2014). Discrepancies in quantitative assessment of normal and regenerated peripheral nerve fibers between light and electron microscopy. *J Peripher Nerv Syst*, *19*(3), 224-233. doi:10.1111/jns.12090
206. Rossi, S., Motta, C., Studer, V., Barbieri, F., Buttari, F., Bergami, A., . . . Centonze, D. (2014). Tumor necrosis factor is elevated in progressive multiple sclerosis and causes excitotoxic neurodegeneration. *Mult Scler*, *20*(3), 304-312. doi:10.1177/1352458513498128
207. Russi, A. E., Ebel, M. E., Yang, Y., & Brown, M. A. (2018). Male-specific IL-33 expression regulates sex-dimorphic EAE susceptibility. *Proc Natl Acad Sci U S A*, *115*(7), E1520-E1529. doi:10.1073/pnas.1710401115

208. Sander, H., Wallace, S., Plouse, R., Tiwari, S., & Gomes, A. V. (2019). Ponceau S waste: Ponceau S staining for total protein normalization. *Anal Biochem*, *575*, 44-53. doi:10.1016/j.ab.2019.03.010
209. Saunders, A., Macosko, E. Z., Wysoker, A., Goldman, M., Krienen, F. M., de Rivera, H., . . . McCarroll, S. A. (2018). Molecular Diversity and Specializations among the Cells of the Adult Mouse Brain. *Cell*, *174*(4), 1015-1030.e1016. doi:10.1016/j.cell.2018.07.028
210. Schablowski, M. J. (2019, Bachelor Thesis). *The effect of cuprizone induced de- and remyelination on spinal glial cells*. Saarland University, Germany,
211. Sen, M. K., Almuslehi, M. S. M., Coorsen, J. R., Mahns, D. A., & Shortland, P. J. (2020). anlyioural and histological changes in cuprizone-fed mice. *Brain Behav Immun*, *87*, 508-523. doi:10.1016/j.bbi.2020.01.021
212. Sen, M. K., Mahns, D. A., Coorsen, J. R., & Shortland, P. J. (2019). Behavioural phenotypes in the cuprizone model of central nervous system demyelination. *Neurosci Biobehav Rev*, *107*, 23-46. doi:10.1016/j.neubiorev.2019.08.008
213. Sequerra, E. B., Gardino, P., Hedin-Pereira, C., & de Mello, F. G. (2007). Putrescine as an important source of GABA in the postnatal rat subventricular zone. *Neuroscience*, *146*(2), 489-493. doi:10.1016/j.neuroscience.2007.01.062
214. Serrano-Regal, M. P., Luengas-Escuza, I., Bayón-Cordero, L., Ibarra-Aizpurua, N., Alberdi, E., Pérez-Samartín, A., . . . Sánchez-Gómez, M. V. (2019). Oligodendrocyte Differentiation and Myelination Is Potentiated via GABA. *Neuroscience*. doi:10.1016/j.neuroscience.2019.07.014
215. Serrano-Regal, M. P., Luengas-Escuza, I., Bayón-Cordero, L., Ibarra-Aizpurua, N., Alberdi, E., Pérez-Samartín, A., . . . Sánchez-Gómez, M. V. (2020). Oligodendrocyte Differentiation and Myelination Is Potentiated via GABA. *Neuroscience*, *439*, 163-180. doi:10.1016/j.neuroscience.2019.07.014
216. Shikishima, K., Mizuno, A., Kawai, K., & Matsuzaki, H. (1985). Focal experimental demyelination in monkey optic nerve by lysophosphatidylcholine. *Jpn J Ophthalmol*, *29*(4), 429-433.
217. Siu, K. F., Cheung, H. C., & Wong, J. (1986). Shrinkage of the esophagus after resection for carcinoma. *Ann Surg*, *203*(2), 173-176. doi:10.1097/00000658-198602000-00011
218. Skripuletz, T., Bussmann, J. H., Gudi, V., Koutsoudaki, P. N., Pul, R., Moharreggh-Khiabani, D., . . . Stangel, M. (2010). Cerebellar cortical demyelination in the murine cuprizone model. *Brain Pathol*, *20*(2), 301-312. doi:10.1111/j.1750-3639.2009.00271.x
219. Skripuletz, T., Gudi, V., Hackstette, D., & Stangel, M. (2011). De- and remyelination in the CNS white and grey matter induced by cuprizone: the old, the new, and the unexpected. *Histol Histopathol*, *26*(12), 1585-1597. doi:10.14670/HH-26.1585

220. Skripuletz, T., Hackstette, D., Bauer, K., Gudi, V., Pul, R., Voss, E., . . . Stangel, M. (2013). Astrocytes regulate myelin clearance through recruitment of microglia during cuprizone-induced demyelination. *Brain*, *136*(Pt 1), 147-167. doi:10.1093/brain/aws262
221. Slowik, A., Schmidt, T., Beyer, C., Amor, S., Clarner, T., & Kipp, M. (2015). The sphingosine 1-phosphate receptor agonist FTY720 is neuroprotective after cuprizone-induced CNS demyelination. *Br J Pharmacol*, *172*(1), 80-92. doi:10.1111/bph.12938
222. Snaidero, N., Möbius, W., Czopka, T., Hekking, L. H., Mathisen, C., Verkleij, D., . . . Simons, M. (2014). Myelin membrane wrapping of CNS axons by PI(3,4,5)P3-dependent polarized growth at the inner tongue. *Cell*, *156*(1-2), 277-290. doi:10.1016/j.cell.2013.11.044
223. Sofroniew, M. V., & Vinters, H. V. (2010). Astrocytes: biology and pathology. *Acta Neuropathol*, *119*(1), 7-35. doi:10.1007/s00401-009-0619-8
224. Soliven, B. (2001). Calcium signalling in cells of oligodendroglial lineage. *Microsc Res Tech*, *52*(6), 672-679. doi:10.1002/jemt.1051
225. Somjen, G. G. (1988). Nervenkit: notes on the history of the concept of neuroglia. *Glia*, *1*(1), 2-9.
226. Sorensen, P. S., Sellebjerg, F., Hartung, H. P., Montalban, X., Comi, G., & Tintoré, M. (2020). The apparently milder course of multiple sclerosis: changes in the diagnostic criteria, therapy and natural history. *Brain*, *143*(9), 2637-2652. doi:10.1093/brain/awaa145
227. Stevens, B., Porta, S., Haak, L. L., Gallo, V., & Fields, R. D. (2002). Adenosine: a neuroglial transmitter promoting myelination in the CNS in response to action potentials. *Neuron*, *36*(5), 855-868. doi:10.1016/s0896-6273(02)01067-x
228. Sun, D., Lye-Barthel, M., Masland, R. H., & Jakobs, T. C. (2009). The morphology and spatial arrangement of astrocytes in the optic nerve head of the mouse. *J Comp Neurol*, *516*(1), 1-19. doi:10.1002/cne.22058
229. Suzuki, H., Oku, H., Horie, T., Morishita, S., Tonari, M., Oku, K., . . . Ikeda, T. (2014). Changes in expression of aquaporin-4 and aquaporin-9 in optic nerve after crushing in rats. *PLoS One*, *9*(12), e114694. doi:10.1371/journal.pone.0114694
230. Tang, F., Barbacioru, C., Wang, Y., Nordman, E., Lee, C., Xu, N., . . . Surani, M. A. (2009). mRNA-Seq whole-transcriptome analysis of a single cell. *Nat Methods*, *6*(5), 377-382. doi:10.1038/nmeth.1315
231. Taylor, L. C., Gilmore, W., Ting, J. P., & Matsushima, G. K. (2010). Cuprizone induces similar demyelination in male and female C57BL/6 mice and results in disruption of the estrous cycle. *J Neurosci Res*, *88*(2), 391-402. doi:10.1002/jnr.22215
232. Taylor, S. E., Morganti-Kossmann, C., Lifshitz, J., & Ziebell, J. M. (2014). Rod microglia: a morphological definition. *PLoS One*, *9*(5), e97096. doi:10.1371/journal.pone.0097096

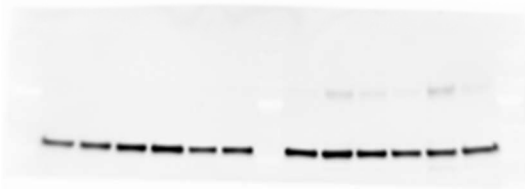
233. The Multiple Sclerosis International Federation, M. (2020). *Atlas of MS, 3rd Edition*.
234. Thompson, A. J., Baranzini, S. E., Geurts, J., Hemmer, B., & Ciccarelli, O. (2018). Multiple sclerosis. *Lancet*, *391*(10130), 1622-1636. doi:10.1016/S0140-6736(18)30481-1
235. Torkildsen, O., Brunborg, L. A., Myhr, K. M., & Bø, L. (2008). The cuprizone model for demyelination. *Acta Neurol Scand Suppl*, *188*, 72-76. doi:10.1111/j.1600-0404.2008.01036.x
236. Torre-Fuentes, L., Moreno-Jiménez, L., Pytel, V., Matías-Guiu, J. A., Gómez-Pinedo, U., & Matías-Guiu, J. (2020). Experimental models of demyelination and remyelination. *Neurologia (Engl Ed)*, *35*(1), 32-39. doi:10.1016/j.nrl.2017.07.002
237. Town, T., Nikolic, V., & Tan, J. (2005). The microglial "activation" continuum: from innate to adaptive responses. *J Neuroinflammation*, *2*, 24. doi:10.1186/1742-2094-2-24
238. Trapp, B. D., Peterson, J., Ransohoff, R. M., Rudick, R., Mörk, S., & Bö, L. (1998). Axonal transection in the lesions of multiple sclerosis. *N Engl J Med*, *338*(5), 278-285. doi:10.1056/NEJM199801293380502
239. van Bodegraven, E. J., Sluijs, J. A., Tan, A. K., Robe, P. A. J. T., & Hol, E. M. (2021). New GFAP splice isoform (GFAP μ) differentially expressed in glioma translates into 21 kDa N-terminal GFAP protein. *FASEB J*, *35*(3), e21389. doi:10.1096/fj.202001767R
240. van der Valk, P., & Amor, S. (2009). Preactive lesions in multiple sclerosis. *Curr Opin Neurol*, *22*(3), 207-213. doi:10.1097/WCO.0b013e32832b4c76
241. Vega-Riquer, J. M., Mendez-Victoriano, G., Morales-Luckie, R. A., & Gonzalez-Perez, O. (2019). Five Decades of Cuprizone, an Updated Model to Replicate Demyelinating Diseases. *Curr Neuropharmacol*, *17*(2), 129-141. doi:10.2174/1570159X15666170717120343
242. Virchow, R. (1856). *Gesammelte Abhandlungen zur Wissenschaftlichen Medicin*. In: Hamm, Frankfurt a.M.
243. Virchow, R. (1858). *Die Cellularpathologie in ihrer Begründung auf physiologische und pathologische Gewebelehre*. In: Berlin.
244. Voskuhl, R. R., Itoh, N., Tassoni, A., Matsukawa, M. A., Ren, E., Tse, V., . . . Itoh, Y. (2019). Gene expression in oligodendrocytes during remyelination reveals cholesterol homeostasis as a therapeutic target in multiple sclerosis. *Proc Natl Acad Sci U S A*, *116*(20), 10130-10139. doi:10.1073/pnas.1821306116
245. Voskuhl, R. R., Pitchekian-Halabi, H., MacKenzie-Graham, A., McFarland, H. F., & Raine, C. S. (1996). Gender differences in autoimmune demyelination in the mouse: implications for multiple sclerosis. *Ann Neurol*, *39*(6), 724-733. doi:10.1002/ana.410390608
246. Voskuhl, R. R., Sawalha, A. H., & Itoh, Y. (2018). Sex chromosome contributions to sex differences in multiple sclerosis susceptibility and progression. *Mult Scler*, *24*(1), 22-31. doi:10.1177/1352458517737394

247. Voss, E. V., Škuljec, J., Gudi, V., Skripuletz, T., Pul, R., Trebst, C., & Stangel, M. (2012). Characterisation of microglia during de- and remyelination: can they create a repair promoting environment? *Neurobiol Dis*, *45*(1), 519-528. doi:10.1016/j.nbd.2011.09.008
248. Wang, J., Yang, B., Weng, Q., & He, Q. (2019). Targeting Microglia and Macrophages: A Potential Treatment Strategy for Multiple Sclerosis. *Front Pharmacol*, *10*, 286. doi:10.3389/fphar.2019.00286
249. Weinschenker, B. G., Bass, B., Rice, G. P., Noseworthy, J., Carriere, W., Baskerville, J., & Ebers, G. C. (1989). The natural history of multiple sclerosis: a geographically based study. I. Clinical course and disability. *Brain*, *112* (Pt 1), 133-146. doi:10.1093/brain/112.1.133
250. Westergard, T., & Rothstein, J. D. (2020). Astrocyte Diversity: Current Insights and Future Directions. *Neurochem Res*, *45*(6), 1298-1305. doi:10.1007/s11064-020-02959-7
251. Wilhelm, H., & Schabet, M. (2015). The Diagnosis and Treatment of Optic Neuritis. *Deutsches Ärzteblatt International*, *112*(37), 616-625; quiz 626. doi:10.3238/arztebl.2015.0616
252. Williams, A., Piaton, G., & Lubetzki, C. (2007). Astrocytes--friends or foes in multiple sclerosis? *Glia*, *55*(13), 1300-1312. doi:10.1002/glia.20546
253. Williamson, A. V., Mellor, J. R., Grant, A. L., & Randall, A. D. (1998). Properties of GABA(A) receptors in cultured rat oligodendrocyte progenitor cells. *Neuropharmacology*, *37*(7), 859-873. doi:10.1016/s0028-3908(98)00016-1
254. Wolf, Y., Shemer, A., Levy-Efrati, L., Gross, M., Kim, J. S., Engel, A., . . . Jung, S. (2018). Microglial MHC class II is dispensable for experimental autoimmune encephalomyelitis and cuprizone-induced demyelination. *Eur J Immunol*, *48*(8), 1308-1318. doi:10.1002/eji.201847540
255. Wolswijk, G. (1998). Chronic stage multiple sclerosis lesions contain a relatively quiescent population of oligodendrocyte precursor cells. *J Neurosci*, *18*(2), 601-609.
256. Woodruff, R. H., Fruttiger, M., Richardson, W. D., & Franklin, R. J. (2004). Platelet-derived growth factor regulates oligodendrocyte progenitor numbers in adult CNS and their response following CNS demyelination. *Mol Cell Neurosci*, *25*(2), 252-262. doi:10.1016/j.mcn.2003.10.014
257. World Health Organization, W. (2008). Atlas multiple sclerosis resources in the world 2008
258. Yamout, B. I., & Alroughani, R. (2018). Multiple Sclerosis. *Semin Neurol*, *38*(2), 212-225. doi:10.1055/s-0038-1649502
259. Yperman, J., De Visscher, G., Holvoet, P., & Flameng, W. (2004). Beta-actin cannot be used as a control for gene expression in ovine interstitial cells derived from heart valves. *J Heart Valve Dis*, *13*(5), 848-853.

260. Yu, Y., Chen, Y., Kim, B., Wang, H., Zhao, C., He, X., . . . Lu, Q. R. (2013). Olig2 targets chromatin remodelers to enhancers to initiate oligodendrocyte differentiation. *Cell*, *152*(1-2), 248-261. doi:10.1016/j.cell.2012.12.006
261. Zamanian, J. L., Xu, L., Foo, L. C., Nouri, N., Zhou, L., Giffard, R. G., & Barres, B. A. (2012). Genomic analysis of reactive astrogliosis. *J Neurosci*, *32*(18), 6391-6410. doi:10.1523/JNEUROSCI.6221-11.2012
262. Zeisel, A., Hochgerner, H., Lönnerberg, P., Johnsson, A., Memic, F., van der Zwan, J., . . . Linnarsson, S. (2018). Molecular Architecture of the Mouse Nervous System. *Cell*, *174*(4), 999-1014.e1022. doi:10.1016/j.cell.2018.06.021
263. Zhan, J., Mann, T., Joost, S., Behrang, N., Frank, M., & Kipp, M. (2020). The Cuprizone Model: Dos and Do Nots. *Cells*, *9*(4). doi:10.3390/cells9040843
264. Zhang, Z., Ma, Z., Zou, W., Guo, H., Liu, M., Ma, Y., & Zhang, L. (2019). The Appropriate Marker for Astrocytes: Comparing the Distribution and Expression of Three Astrocytic Markers in Different Mouse Cerebral Regions. *Biomed Res Int*, *2019*, 9605265. doi:10.1155/2019/9605265
265. Zhao, Z., Li, T., Dong, X., Wang, X., Zhang, Z., Zhao, C., . . . Li, X. (2021). Untargeted Metabolomic Profiling of Cuprizone-Induced Demyelination in Mouse Corpus Callosum by UPLC-Orbitrap/MS Reveals Potential Metabolic Biomarkers of CNS Demyelination Disorders. *Oxid Med Cell Longev*, *2021*, 7093844. doi:10.1155/2021/7093844
266. Zheng, Z. V., & Wong, K. C. G. (2019). Microglial activation and polarization after subarachnoid hemorrhage. In: *Neuroimmunol Neuroinflammation*.
267. Ziebell, J. M., Taylor, S. E., Cao, T., Harrison, J. L., & Lifshitz, J. (2012). Rod microglia: elongation, alignment, and coupling to form trains across the somatosensory cortex after experimental diffuse brain injury. *J Neuroinflammation*, *9*, 247. doi:10.1186/1742-2094-9-247

Supplementary Figures

First run



Repetition

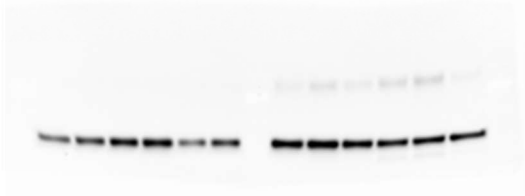


Figure 22. Optic nerve tubulin unedited Western blot gel documentary for *GABA_{knockout}*. First run and repetition of the Western blot.

First run



Repetition

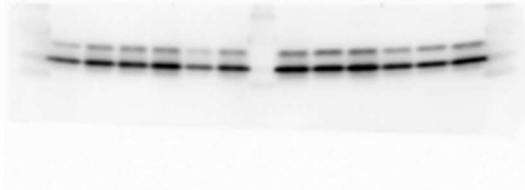
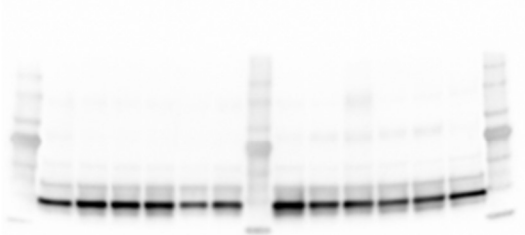


Figure 23. Optic nerve MBP unedited Western blot gel documentary for *GABA_{knockout}*. First run and repetition of the Western blot.

First run



Repetition



Figure 24. Optic nerve GFAP unedited Western blot gel documentary for *GABA_{knockout}*. First run and repetition of the Western blot.

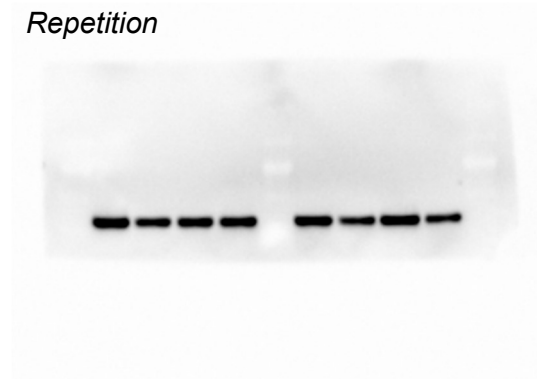
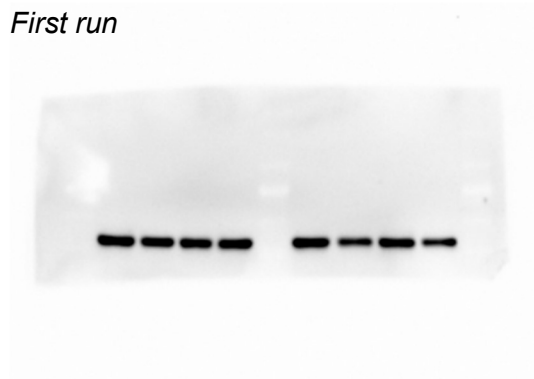


Figure 25. Optic nerve tubulin unedited Western blot gel documentary for Non-induced_{ctl}. First run and repetition of the Western blot.

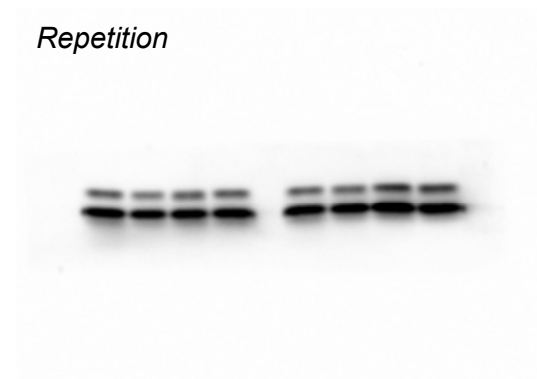
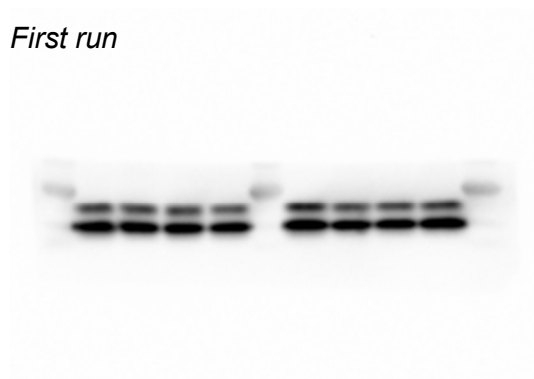


Figure 26. Optic nerve MBP unedited Western blot gel documentary for Non-induced_{ctl}. First run and repetition of the Western blot.

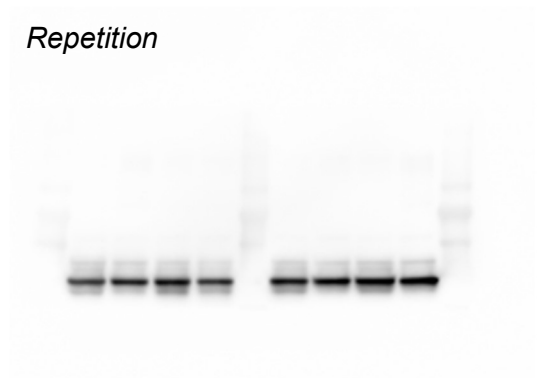
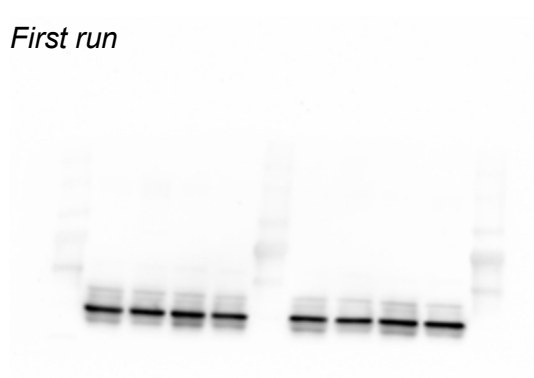


Figure 27. Optic nerve GFAP unedited Western blot gel documentary for Non-induced_{ctl}. First run and repetition of the Western blot.

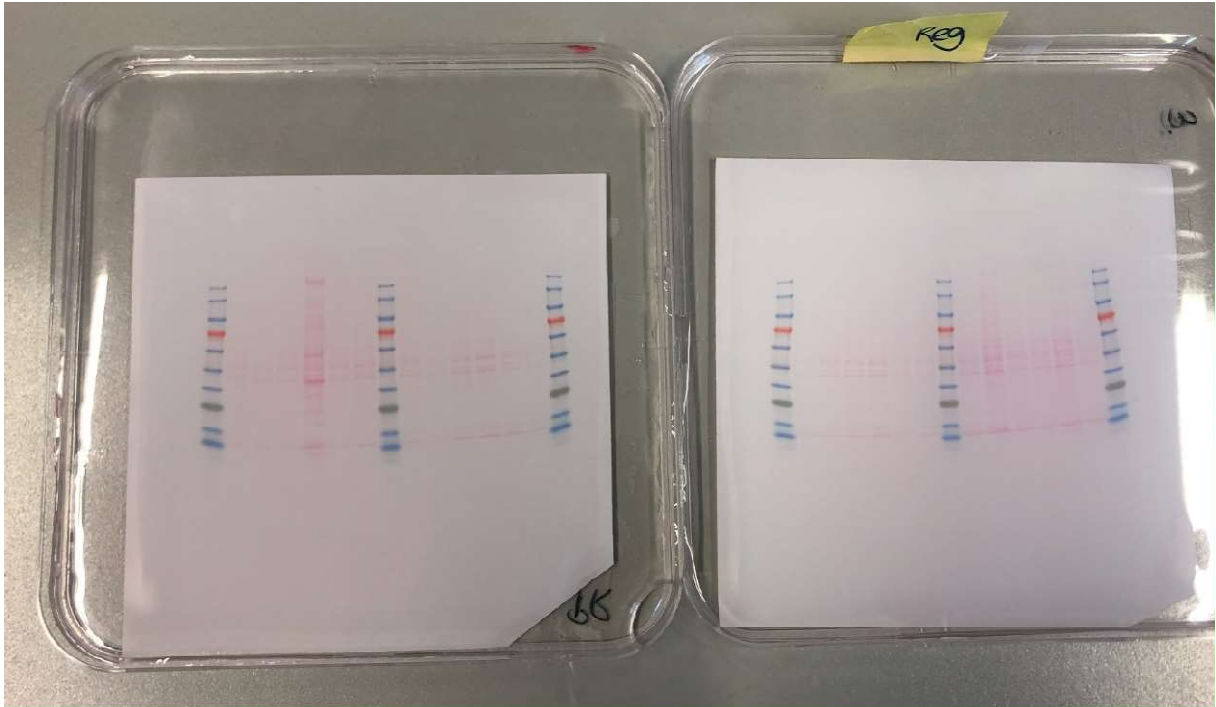


Figure 28. Nitrocellulose membrane showing Ponceau S staining. An exemplary Western blot from GABAknockout mice. After conducting electrophoresis and transferring the protein to the nitrocellulose membrane, staining with Ponceau S was conducted to verify the quality of the blot.

Appendix

Table 11. Descriptive statistical analyses for MBP fluorescence intensity in *GABA_{knockout}* group.

Individual mean values for each mouse. In light grey the mean value of the cohort. In dark grey the SEM value.

MBP			
	Mouse Mean	Cohort Mean	SEM
Genetic Control	4,98701084 5,30752904 5,44378615 7,03841168	5,694	0,3348
Knockout	6,5429133 6,99804392 9,68641846 8,23005816	7,864	0,5524
Genetic Control CPZ	6,21636126 9,43008175 4,43031176 7,93693947	7,003	0,6322
Knockout CPZ	7,91940367 9,92560119 4,99231978 4,5700225	6,572	0,6951

Table 12. Descriptive statistical analyses for dMBP fluorescence intensity in *GABA_{knockout}* group.

Individual mean values for each mouse. In light grey the mean value of the cohort. In dark grey the SEM value.

dMBP			
	Mouse Mean	Cohort Mean	SEM
Genetic Control	1,372850123 1,325805333 1,122114563 1,927738297	1,437	0,1168
Knockout	1,395015863 1,22242869 1,589056097 2,448388023	1,664	0,1481
Genetic Control CPZ	1,924718863 1,22231844 0,80282797 1,313173017	1,316	0,1250
Knockout CPZ	1,808668687 1,80963479 1,258853413 0,96344805	1,428	0,1258

Table 13. Descriptive statistical analyses for GFAP fluorescence intensity in GABA_{knockout} group.

Individual mean values for each mouse. In light grey the mean value of the cohort. In dark grey the SEM value.

GFAP			
	Mouse Mean	Cohort Mean	SEM
Genetic Control	1,870264981 1,586395294 1,933947471 2,034205642	1,856	0,09020
Knockout	2,156797317 1,572736995 2,208214851 2,197348484	2,034	0,1018
Genetic Control CPZ	1,769206129 2,355945704 2,026514187 2,892523398	2,261	0,1451
Knockout CPZ	1,439011615 3,279932966 3,45119194 1,64509709	2,454	0,2856

Table 14. Descriptive statistical analyses for Iba1 fluorescence intensity in GABA_{knockout} group.

Individual mean values for each mouse. In light grey the mean value of the cohort. In dark grey the SEM value.

Iba1			
	Mouse Mean	Cohort Mean	SEM
Genetic Control	153,946399 112,300995 175,942243 152,056505	148,6	13,25
Knockout	149,918709 141,42363 209,414518 183,454594	171,1	15,68
Genetic Control CPZ	199,640632 209,565846 159,705539	189,6	15,24
Knockout CPZ	144,042921 171,466242 165,980096 275,894048	189,3	29,45

Table 15. Descriptive statistical analyses for MBP Western blot analyses in *GABA_{knockout}* group.

Individual mean values for each mouse. In light grey the mean value of the cohort. In dark grey the SEM value.

MBP			
	Mouse Mean	Cohort Mean	SEM
Genetic Control	1,042141255 1,088030275 0,86982847	1	0,06576
Knockout	0,76152926 0,88825719 0,94016254	0,8633	0,06576
Genetic Control CPZ	0,836963995 0,756788585 0,994718185	0,8628	0,07861
Knockout CPZ	0,95959116 0,812868185 0,70997593	0,8275	0,06861

Table 16. Descriptive statistical analyses for GFAP Western blot analyses in *GABA_{knockout}* group.

Individual mean values for each mouse. In light grey the mean value of the cohort. In dark grey the SEM value.

GFAP			
	Mouse Mean	Cohort Mean	SEM
Genetic Control	1,26109141 0,88411206 0,85479653	1	0,1175
Knockout	0,68490191 0,633460325 0,788579325	0,7023	0,06722
Genetic Control CPZ	1,09297422 0,89455331 0,967430885	0,9850	0,1115
Knockout CPZ	0,82140764 0,633460215 0,75613677	0,7370	0,06767

Table 17. Descriptive statistical analyses for MBP fluorescence intensity in Non-induced_{ctl} group.

Individual mean values for each mouse. In light grey the mean value of the cohort. In dark grey the SEM value.

MBP			
	Mouse Mean	Cohort Mean	SEM
Genetic Control	8,200509907 5,736333307 5,574273877 6,061693147	6,393	0,3266
Genetic control CPZ	7,26659773 5,38570418 5,820370107	6,158	0,2621

Table 18. Descriptive statistical analyses for dMBP fluorescence intensity in Non-induced_{ctl} group.

Individual mean values for each mouse. In light grey the mean value of the cohort. In dark grey the SEM value.

dMBP			
	Mouse Mean	Cohort Mean	SEM
Genetic Control	1,193694243 1,339417513 1,267861567 1,463353607	1,316	0,04724
Genetic control CPZ	1,243886403 1,227184487 1,49470799	1,322	0,03906

Table 19. Descriptive statistical analyses for MBP Western blot analyses in Non-induced_{ctl} group.

Individual mean values for each mouse. In light grey the mean value of the cohort. In dark grey the SEM value.

MBP			
	Mouse Mean	Cohort Mean	SEM
Genetic Control	0,85081127 1,07198878 1,07050983 1,006690125	1,000	0,04648
Genetic control CPZ	1,01360685 1,556495565 1,083449835 1,90195787	1,389	0,1770

Table 20. Descriptive statistical analyses for GFAP Western blot analyses in Non-induced_{ctl} group.

Individual mean values for each mouse. In light grey the mean value of the cohort. In dark grey the SEM value.

GFAP			
	Mouse Mean	Cohort Mean	SEM
Genetic Control	0,698487295 1,222222535 1,21048782 0,86880235	1,000	0,08779
Genetic control CPZ	0,795244455 1,470269845 0,79013786 1,48585088	1,135	0,2005

Table 21. Descriptive statistical analyses of the brain for MBP fluorescence intensity in GABA_{knockout} group.

Individual mean values for each mouse. In light grey the mean value of the cohort. In dark grey the SEM value.

MBP				
		Mouse Mean	Cohort Mean	SEM
Corpus Callosum	Genetic Control	10589,0277 2506,32664 13114,4029 8433,66229	8661	2264
	Knockout	12150,185 3385,89252 6584,01905 10225,3209	8086	1946
	Genetic Control CPZ	1039,74265 4123,28963 3639,81969 10956,4954	4940	2117
	Knockout CPZ	635,133052 8362,53471 799,250208 3516,17958	3328	1803
Cortex	Genetic Control	3980,24628 583,409803 5998,71991 1355,21852	2979	1242
	Knockout	6238,67297 1207,96614 1590,91186 5690,01676	3682	1325
	Genetic Control CPZ	304,56322 2567,96742 909,418946 2848,7148	1658	621,7
	Knockout CPZ	551,386181 6829,68192	2093	1579

		513,575984 476,191362		
Striatum		Mouse Mean	Cohort Mean	SEM
	Genetic Control	6997,83605 1297,61338 8984,16178 3028,03605	5077	1766
	Knockout	13655,2516 2664,88142 4585,82194 7227,78326	7033	2397
	Genetic Control CPZ	1303,33174 4943,34755 2747,37653 4735,26039	3432	865,2
	Knockout CPZ	1967,09441 11940,8197 1521,23902 675,762622	4026	2652
Thalamus	Genetic Control	9079,64814 2874,44767 12776,2946 5740,0177	7618	2136
	Knockout	14005,6551 2716,44259 7459,91792 10037,1425	8555	2366
	Genetic Control CPZ	3217,70997 8941,03362 3537,24665 7700,78198	5849	1451
	Knockout CPZ	2448,99804 1791,25978 3614,6456	2618	533,1

Table 22. Descriptive statistical analyses of the brain for GFAP fluorescence intensity in $GABA_{knockout}$ group.

Individual mean values for each mouse. In light grey the mean value of the cohort. In dark grey the SEM value.

GFAP				
Corpus Callosum		Mouse Mean	Cohort Mean	SEM
	Genetic Control	3359,5976 4433,09503 6336,83991 5645,26197	4944	658,5
	Knockout	5152,46543 3412,67381 2503,48728 2469,29796	3384	628,5
	Genetic Control CPZ	7777,18595 11107,4258 6578,69247 9864,08777	8832	1018

	Knockout CPZ	8510,84633 10186,2309 11068,6474 6471,69933	9059	1013
Cortex		Mouse Mean	Cohort Mean	SEM
	Genetic Control	2554,20296 1830,21112 1873,8747 2774,23777	2258	238,9
	Knockout	3124,63322 1499,19917 862,932504 1203,52841	1673	501,2
	Genetic Control CPZ	5920,37792 7378,33479 4897,62991 3747,62053	5486	771,2
	Knockout CPZ	5267,12632 6208,83841 4598,48169 2807,68819	4721	718,1
Striatum	Genetic Control	2548,41409 2683,82188 1704,3524 3711,48247	2662	411,5
	Knockout	4375,09152 2183,17918 1978,16235 1367,23707	2476	656,3
	Genetic Control CPZ	5062,20478 5512,84671 5493,78529 2334,05898	4601	762,7
	Knockout CPZ	2712,89205 8089,21213 4788,37328 4142,29792	4933	1138
Thalamus	Genetic Control	2035,59526 1659,17576 1384,03465 2816,58225	1974	311,0
	Knockout	3488,78826 1570,14556 1141,5297 1110,53848	1828	563,5
	Genetic Control CPZ	9199,61693 7331,26512 8196,04788 3696,22614	7106	1199
	Knockout CPZ	4466,01005 8343,07412 4445,77743 4901,23944	5539	940,6

Table 23. Descriptive statistical analyses of the brain for Iba1 cell count in GABA_{knockout} group.

Individual mean values for each mouse. In light grey the mean value of the cohort. In dark grey the SEM value.

Iba1				
		Mouse Mean	Cohort Mean	SEM
Corpus Callosum	Genetic Control	6582,12812 6494,38399 6381,41353 9460,75853	7230	744,8
	Knockout	7361,41742 6323,01306 4245,46669 6221,85947	6038	650,6
	Genetic Control CPZ	24218,5908 27470,8841 12182,8284	21291	4650
	Knockout CPZ	30429,0125 36992,3847 14551,5922 15844,8404	24454	5516
Cortex	Genetic Control	7027,10525 6873,75284 5758,3265 8472,715	7033	557,0
	Knockout	7293,32829 6499,72605 4259,4375 5725,48144	5944	646,5
	Genetic Control CPZ	7001,97223 11150,3985 7794,0045 4611,22644	7639	1352
	Knockout CPZ	7874,97464 13219,5379 6592,12318 3979,99754	7917	1945
Striatum	Genetic Control	6255,43784 7079,78506 5279,40216 9848,58204	7116	982,4
	Knockout	8801,25368 10015,5782 4336,79761 4272,58433	6857	1494
	Genetic Control CPZ	7001,97223 7657,03772 7200,1754 4709,30812	6642	658,7
	Knockout CPZ	5048,63559 7135,65703 4376,96084	5021	771,1

		3521,63922		
Thalamus	Genetic Control	7302,46591 7141,25984 5836,35199 9943,51784	7556	860,9
	Knockout	8465,0998 7118,30106 4482,85388 5928,3566	6499	848,5
	Genetic Control CPZ	14980,8434 11045,2487 8675,31423 5773,17658	10119	1946
	Knockout CPZ	6966,48325 7643,41427 5260,35311 4201,28119	6018	786,1

Acknowledgements

Mein Dank gilt insbesondere Prof. Dr. Frank Kirchhoff, dafür dass es mir trotz der weltweiten Pandemiesituation ermöglicht wurde in das Team aufgenommen zu werden und mein Projekt im Labor der AG Kirchhoff zu realisieren. Danke auch für eine sehr engagierte Lehre in der Vorklinik, die mich sehr schnell in den Bann der Physiologie gezogen hat und mich bis heute begeistert.

Ein riesiges Dankeschön geht an meine Hauptbetreuerin Dr. Anja Scheller. Liebe Anja, ohne Deine Unterstützung und Ermutigungen hätte ich diese Arbeit nicht abschließen können. Deine Erreichbarkeit zu jeder Tages- und Nachtzeit und deine Bereitschaft, alle meine Fragen zu beantworten, waren von unschätzbarem Wert. Ich wünsche Dir alles Gute und hoffe, dass Du Dir Deine positive Energie immer bewahren wirst. Mögen die Medizinstudierenden eines Tages aufhören, Dir die Zeit zu stehlen.

Ich möchte mich auch bei meinem Betreuer Phillip Rieder bedanken, dafür dass Du mich in das Labor eingearbeitet und mir beigebracht hast „*How to Science*“ (zumindest ein bisschen). Es war mir eine Freude mit Dir zusammenzuarbeiten und ich schätze sehr Deine Geduld und Ausdauer, eine weitere, ahnungslose Medizinstudentin einzuarbeiten.

Thank you, Eleonora for being by my side on long lab days, answering every single question regarding technical and methodical molecular physiology. Thank you, Anna for spending long cryostat shifts with me and introducing me to the whole process of micro tissue cutting. Thank you, Pascal for sharing not only your antibody knowledge but also many cell counting days together. I wish you guys the best in your scientific careers.

Cai, Lipao, Fei, Qing, Qilin, Davide, Erika, Mariza, Gebhard, Laura, Arne, Ute and Frank, from the very first day you welcomed me warmly to the lab with a really great atmosphere. I am grateful for all the tips and tricks you showed me. You are an amazing team, and I will always carry a great memory of this experience with me.

Danke an meine Saarbrücker Familie Leila, Zaha Karo und Cosi, die mich durch harte Tage begleitet haben und selbst die Lockdownzeiten zu schönen Erinnerungen gemacht haben.

Danke Papa, Danke Mama, für immer an meiner Seite sein.

In Gedenken an Opa Werner und die Kraniche.